DOPPLER-RESILIENT SCHEMES FOR UNDERWATER ACOUSTIC COMMUNICATION CHANNELS

Saed DAOUD

A Thesis

in

The Department

of

Electrical and Computer Engineering

Presented in partial Fulfillment of the Requirements

for the degree of Doctor of Philosophy at

Concordia University

Montreal, Quebec, Canada

January, 2015

CONCORDIA UNIVERSITY
SCHOOL OF GRADUATE STUDIES

This is to certify that the thesis prepared

By: Saed Daoud

Entitled: Doppler-Resilient Schemes for Underwater Acoustic Communication Channels

and submitted in partial fulfillment of the requirements for the degree of

Doctor of Philosophy (Electrical and Computer Engineering)

complies with the regulations of the University and meets the accepted standards with respect to originality and quality.

Signed by the final examining committee:

Dr. M.Y. Chen — Chair

Dr. W. Ajib — External Examiner

Dr. X. Zhou — External to Program

Dr. Y.R. Shayan — Examiner

Dr. M. Reza Soleymani — Examiner

Dr. A. Ghrayeb — Thesis Supervisor

Approved by: Dr. A.R. Sebak, Graduate Program Director

January 13, 2015 Dr. A. Asif, Dean
Faculty of Engineering & Computer Science

ABSTRACT

DOPPLER-RESILIENT SCHEMES FOR UNDERWATER ACOUSTIC COMMUNICATION CHANNELS

Saed DAOUD, PhD

Concordia University, 2015

In this thesis we consider Orthogonal Frequency Division Multiplexing (OFDM) technique by taking into account in the receiver design the fundamental and unique characteristics of Underwater Acoustic (UWA) channels in the context of Relay-Assisted (RA) systems. In particular, OFDM technique is used to combat the problem of Intersymbol Interference (ISI), while to handle the Intercarrier Interference (ICI), a pre-processing unit is used prior to the Minimum Mean Squared Error (MMSE) frequency-domain equalization called Multiple Resampling (MR), which minimizes the effect of time variation. This pre-processor consists of multiple branches, each corresponds to a Doppler scaling factor of a path/user/cluster, and performs of frequency shifting, resampling, and Fast Fourier Transform (FFT) operation. As a suboptimal alternative to MR pre-processing, Single Resampling (SR) pre-processing is also used to reduce the effect of ICI in the system, and it consists of only one branch that performs frequency shifting, resampling, and FFT operation, which corresponds to one approximated resampling factor, that is a function of one or more of the actual Doppler scaling factors. The problem of bandwidth scarcity is considered in the context of Two Way Relaying (TWR) systems in an attempt to increase the bandwidth efficiency of the system, while the problem of fading is considered in the context of Distributed Space-Time Block Coding (D-STBC) to boost the system reliability. Also, joint TWR-D-STBC system is proposed to extract the advantages of both schemes simultaneously.

Second, motivated by the fact that OFDM is extremely sensitive to time variation, which destroys the orthogonality between the subcarriers, we consider another candidate to UWA channels and competitor to OFDM scheme, namely, block-based Single Carrier (SC) modulation with Frequency Domain Equalization (FDE). We start by the Point-to-Point (P2P) systems with path-specific Doppler model and Multiple Access Channel (MAC) system with user-specific

Doppler model. The Maximum Likelihood (ML) receiver in each case is derived, and it is shown that a MR pre-processing stage is necessary to handle the effect of time variation, as it is the case in OFDM. Different from OFDM, however, the structure of this pre-processing stage. Specifically, it consists of multiple branches and each branch corresponds to a Doppler scaling factor per path or per user, and performs frequency shifting, resampling, and followed by and integration. FFT operation is not a part of the pre-processor. The goal of this pre-processing stage is to minimize the level of time variation in the time domain. So, the output of the pre-processor will still be time-varying contaminated by ISI, and hence an equalization stage is required. To avoid the complexity of the optimum Maximum Likelihood Sequence Detector (MLSD), we propose the use of MMSE FDE, where the samples are transformed to the frequency domain by means of FFT operation, and after the FDE transformed back to the time domain, where symbol-by-symbol detection becomes feasible. Also, the channels are approximated such that all paths or all users have the same Doppler scaling factor, and the pre-processing stage in this case consists of only one branch and it is called SR. Having the basic structure of SC-FDE scheme, we then consider the corresponding schemes that are considered for OFDM systems, namely: TWR, D-STBC, and TWR-D-STBC schemes.

A complete complexity analysis, bandwidth efficiency, and extensive Average Bit Error Rate (ABER) simulation results are given. It is shown that MR schemes outperforms its SR counterparts within a given signaling scheme (i.e., OFDM or SC-FDE). However, this superiority in performance comes at the expense of more hardware complexity. Also, for uncoded systems, MR-SC-FDE outperforms its OFDM counterpart with less hardware complexity, because in SC-FDE systems, FFT operation is not part of the MR pre-processor, but rather a part of the equalizer. Finally, under total power constraint, it is shown that TWR-D-STBC scheme serves as a good compromise between bandwidth efficiency and reliability, where it has better bandwidth efficiency with some performance loss compared to D-STBC, while it has better performance and the same bandwidth efficiency compared to TWR.

This dissertation is dedicated to

my parents for their sacrifice, encouragement and help

throughout my life.

ACKNOWLEDGMENTS

First of all, I thank my supervisor prof. Ali Ghrayeb for his guidance and support all the way long during my research, both academically and personally. I sincerely appreciate his patience and kindness with me, and the time he took to read and revise my submitted journals and conferences during my PhD.

I would like to thank the committee members Dr. M. Reza Soleymani, Dr. Yousef R. Shayan, Dr. Xiaowen Zhou, and Dr. Wessam Ajib for their comments and guidance.

I also would like to thank Bahattin Karakaya for his help in providing me the necessary tools and data to generate UWA channels using the Bellhop and VirTEX programs.

Finally, I would like to thank my parents for their sacrifice, encouragement, and help to reach this point, especially my father who has supported me in all possible ways to be where I am now.

TABLE OF CONTENTS

LIST OF TABLES

LIST OF FIGURES

List of Symbols

d	$\triangleq$	The distance between transceivers.
f	$\triangleq$	The frequency.
κ	$\triangleq$	The spreading factor.
$\alpha(f)$	$\triangleq$	The absorption coefficient.
$\mathcal{V}_{\text{Tu}}(f)$	$\triangleq$	PSD of the turbulence noise.
$\mathcal{V}_{\text{s}}(f)$	$\triangleq$	PSD of the shipping noise.
$\mathcal{V}_{\text{w}}(f)$	$\triangleq$	PSD of the wind noise.
$\mathcal{V}_{\text{Th}}(f)$	$\triangleq$	PSD of the thermal noise.
$\mathcal{V}(f)$	$\triangleq$	PSD of the total noise.
s	$\triangleq$	The shipping factor.
w	$\triangleq$	The wind speed.
$\gamma(d, f)$	$\triangleq$	The average Signal-to-Noise Ratio (SNR) for a distance d and frequency f.
$A(d, f)$	$\triangleq$	The distance- and frequency-dependent path loss .
$f_{\text{opt}}(d)$	$\triangleq$	The optimum frequency for a given distance d.
c	$\triangleq$	The sound speed underwater.
v	$\triangleq$	The relative speed between transceivers in m/s.
a	$\triangleq$	The Doppler scaling factor.
h_p	$\triangleq$	The pth path gain.
$h_{XY,p}$	$\triangleq$	The pth path gain between nodes X and Y.
$h_p^{(m,n)}$	$\triangleq$	The pth path gain between the mth user and nth receive antenna.
τ_p	$\triangleq$	The$p$th path delay.
$\tau_{XY,p}$	$\triangleq$	The$p$th path delay between nodes X and Y.

$\tau_p^{(m,n)}$	$\triangleq$	The$p$th path delay between the mth user and nth receive antenna.
a_p	$\triangleq$	The$p$th path Doppler scaling factor.
$a_{XY,p}$	$\triangleq$	The pth path Doppler scaling factor between nodes X and Y.
$a^{(m)}$	$\triangleq$	The Doppler scaling factor of the m user.
a_{SR}	$\triangleq$	The SR factor.
N_p	$\triangleq$	The number of paths.
$N_{XY,p}$	$\triangleq$	The number of paths between nodes X and$Y$.
$N_p^{(m,n)}$	$\triangleq$	The number of paths between user m and receive antenna n.
$\mathcal{A}\}.\|$	$\triangleq$	The real part operator.
K	$\triangleq$	The number of subcarriers.
d_k	$\triangleq$	The kth symbol.
$d_{m,k}$	$\triangleq$	The kth symbol from the m user.
$d_k^{(\mu)}$	$\triangleq$	The kth symbol of the μth block.
$d_{m,k}^{(\mu)}$	$\triangleq$	The kth symbol of the μth block from the mth user.
f_k	$\triangleq$	The kth subcarrier.
f_c	$\triangleq$	The carrier frequency.
$R(t)$	$\triangleq$	A rectangular pulse of duration $T + T_g$.
T	$\triangleq$	The OFDM symbol duration.
T_g	$\triangleq$	The guard interval.
$g(t)$	$\triangleq$	A rectangular pulse of duration T_s.
T_s	$\triangleq$	The symbol duration.
N_0	$\triangleq$	The noise PSD.
$y(t)$	$\triangleq$	The passband received signal.
$v(t)$	$\triangleq$	The baseband received signal.
$w(t)$	$\triangleq$	TheAWGN process.
$\mathbf{v}_{\text{MR}}$	$\triangleq$	The received samples at the output of MR pre-processor.
$\mathcal{W}_{\text{MR}}$	$\triangleq$	The received samples at the output of MR pre-processor in the frequency domain.
$\mathbf{w}_{\text{MR}}$	$\triangleq$	The noise samples at the output of MR pre-processor.

$\mathcal{Z}_{\text{MR}}$	$\triangleq$	The noise samples at the output of MR pre-processor in the frequency domain.
$\mathbf{v}_{\text{SR}}$	$\triangleq$	The received samples at the output of SR pre-processor.
$\mathcal{V}_{\text{SR}}$	$\triangleq$	The received samples at the output of SR pre-processor in the frequency domain.
$\mathbf{w}_{\text{SR}}$	$\triangleq$	The noise samples at the output of SR pre-processor.
$\mathcal{Z}_{\text{SR}}$	$\triangleq$	The noise samples at the output of SR pre-processor in the frequency domain.
$P_k(t)$	$\triangleq$	The channel response for the kth subcarrier.
$f_k(t)$	$\triangleq$	The approximated channel response for the kth subcarrier.
$\Phi_{k,m}$	$\triangleq$	The (k,m)th entry of the equivalent channel at the output of MR pre-processor.
$\Psi_{k,m}$	$\triangleq$	The (k,m)th entry of the equivalent channel at the output of SR pre-processor.
$\mathcal{CN}(\boldsymbol{\mu}, \boldsymbol{\Sigma})$	$\triangleq$	A complex Gaussian with mean $\boldsymbol{\mu}$ and covariance matrix $\boldsymbol{\Sigma}$.
$\|\mathcal{C}\|$	$\triangleq$	The cardinality of a set $\mathcal{C}$.
$\mathcal{G}_K$	$\triangleq$	The K-point FFT matrix.
$\mathcal{G}_K^H$	$\triangleq$	The K-point IFFT matrix.
$\|\mathbf{x}\|^2$	$\triangleq$	The Euclidean distance.
N	$\triangleq$	The number of receive antennas.
M	$\triangleq$	The number of users.
$(.)^*$	$\triangleq$	The complex conjugation operator.
$(.)^H$	$\triangleq$	The complex conjugation transpose operator.
S_m	$\triangleq$	The mth source.
R_j	$\triangleq$	The jth relay.
D	$\triangleq$	The destination.
$[\mathbf{A}]_{k,l}$	$\triangleq$	The (k,l)th element of the matrix $\mathbf{A}$.
$\mathbf{0}_{K\times 1}$	$\triangleq$	The $K \sim 1$ all-zero vector.
$\mathbf{0}_K$	$\triangleq$	The $K \sim K$ all-zero matrix.

List of Acronyms

ABER	Average Bit Error Rate
AF	Amplify-and-Forward
AWGN	Additive White Gaussian Noise
BC	Broadcast
BPSK	Binary Phase Shift Keying
CE	Channel Estimation
CFO	Carrier Frequency Offset
CIR	Channel Impulse Response
CP	Cyclic Prefix
CSI	Channel State Information
DFE	Decision Feedback Equalizer
DoF	Degrees of Freedom
D-STBC	Distributed Space-Time Block Coding
EM	Electromagnetic
FDE	Frequency Domain Equalization
FDTE	Frequency Domain Turbo Equalization
FFT	Fast Fourier Transform
FSK	Frequency Shift Keying
IBI	Interblock Interference
ICI	Intercarrier Interference
IFFT	Inverse FFT
ISI	Intersymbol Interference

IUI	Interuser Interference
Kbps	Kilobits per second
Ksps	Kilo sysmbol per second
LTI	Linear Time-Invariant
MAC	Multiple Access Channel
MIMO	Multiple-Input Multiple-Output
ML	Maximum Likelihood
MLSD	Maximum Likelihood Sequence Detector
MMSE	Minimum Mean Squared Error
MR	Multiple Resampling
MSE	Mean Squared Error
NR	No Resampling
OFDM	Orthogonal Frequency Division Multiplexing
OOK	On Off Keying
PAPR	peak-to-average power ratio
PLL	Phase-Locked Loop
PSD	Power Spectral Density
P2P	Point-to-Point
RA	Relay-Assisted
RF	Radio Frequency
SC	Single Carrier
SNR	Signal-to-Noise Ratio
SR	Single Resampling
SSP	Sound Speed Profile
STBC	Space-Time Block Coding
S/P	Serial-to-Parallel
TDE	Time Domain Equalization
TR	Time Reversal
TWR	Two Way Relaying
UWA	Underwater Acoustic

Chapter 1

Introduction

1.1 Motivation

Our planet is covered by water, about three quarters of its surface, which is in most part under-utilized. Many potential applications in such a vast area of water, both commercial and military, have triggered research efforts towards developing reliable high-data rate Underwater Acoustic (UWA) wireless communication links. A sample of these applications include remote control in offshore oil industry, pollution monitoring in environmental systems, collection of scientific data recorded at ocean-bottom stations and unmanned underwater vehicles, speech transmission between divers, and mapping of the ocean floor for detection of objects and discovery of new resources[1, 2].

Underwater communication networks where nodes are able to communicate in real-time by means of wireless links are preferred over the wire-line networks and the traditional sensor networks usually deployed in underwater environment. In particular, wire-line networks have high cost operation, and limit the flexibility of reconfiguring the network to meet changes in the operation requirements. On the other hand, in traditional sensor networks there is no exchange of information between the sensors themselves or between the sensors and a central unit. Rather, each sensor operates separately by sensing its closed area and store the data in an internal storage until the whole network is recovered back at the end of the mission. The disadvantages of such systems are: real-time applications can not be supported by such networks, the deployment and recovering processes are expensive, such networks are not reconfigurable, any hardware or software failure may result in losing the data collected, and the amount of data that can be collected is limited by the capacity of the internal storage of the sensors.

Among the possible wireless means of transmission in underwater environment, acoustic waves remain the best option so far because of its favorable characteristics over UWA channels. Other options include Radio Frequency (RF) waves and optical waves. However, the propagation of these waves suffer in underwater channels. For example, the absorption of Electromagnetic (EM) waves in sea water is about $45\, f^{0.5}$ dB/Km, where f is the frequency in Hertz [3]. This means that, to use EM waves underwater mandates the use of very low frequencies, which requires large antennas and high transmission power. On the other hand, although optical waves do not suffer from signal attenuation, they suffer from scattering [1, 4].

What is envisioned in the future regarding UWA systems is the so-called "digital ocean", which is a network consisting of stationary and mobile nodes, that exchange information with each others, and with a central control unit at the surface, which can be accessed by an RF link remotely [5]. These nodes will be equipped with multiple sensors, sonars, and video cameras. Different types of signals have different requirements. For example, control signals need low data rate (up to 1 Kilobits per second (Kbps)) but very low Average Bit Error Rate (ABER) transmission, while highly compressed video signals need high data rate (greater than 10 Kbps up to hundreds of Kbps) but moderate ABER transmission [1].

UWA channels are very challenging due to their own unique characteristics that distinguish them from any other single type of channel. The fundamental characteristics of UWA channels are: limited bandwidth, long delay spread, and time variation. Any receiver design should take into account the above mentioned characteristics in order for a system to be efficient and reliable. To this end, Orthogonal Frequency Division Multiplexing (OFDM) and Single Carrier (SC) modulation with Frequency Domain Equalization (FDE) techniques are studied primarily in this thesis in the context of relay-assisted systems where the increased Degrees of Freedom (DoF) of the systems are utilized to improve the bandwidth efficiency and/or the reliability of the systems. In particular, OFDM and SC-FDE are used to counteract the effect of Intersymbol Interference (ISI) in an efficient way, while the existence of one or more relays can be utilized to enhance the throughput of the system and/or its reliability by extracting the available spatial diversity. For time variation, we assume that the relative motion between transceivers is the only source of time variation, and the problem of motion-induced Doppler effect is dealt with using the concept of resampling [6, 7, 8].

1.2 Contributions

The contributions of the thesis can be summarized as follows. Since OFDM systems are highly sensitive to time-variation which destroys the orthogonality between the subcarriers, we propose the use of SC modulation. The optimum ML receiver is derived for path-specific P2P and user-specific MAC systems. The receiver structure is revealed to consist of two stages: MR and equalization. The implementation of the MR stage is shown to consist of multiple branches each branch corresponds to a path/user, and performs frequency shifting, and resampling by the Doppler scaling factor of that path/user, followed by an integration. The output of the resampling stage will be contaminated by time-varying ISI and the noise is colored. Hence the covariance matrix is derived first, and the problem of of frequency selectivity is dealt with by proposing the use of an MMSE equalization in the frequency domain. In particular, the received samples at the output of the MR stage is first transformed to the frequency domain using FFT operation where FDE is performed, and transformed back to the time domain for detection. This sequence in the equalizer, namely, FFT, MMSE FDE and Inverse FFT (IFFT), replaces the need of using MLSD which detects the signals jointly, and hence alleviate its complexity. A suboptimal resampling is also investigated, when the channel is approximated to have a single scaling factor that is common for all paths/users.

To address the problem of bandwidth scarcity and multipath fading, we propose the use of relay-assisted systems over UWA channels for both OFDM and SC-FDE systems. In particular, TWR is used to enhance the bandwidth efficiency, while D-STBC is used to enhance the reliability. Also, a combination of both is used to enhance both the bandwidth efficiency and reliability at the same time. The noise covariance matrix at the relay(s) and the destination(s) are derived for noise whitening at the relays or to be incorporated at the equalizer at the destinations. A comprehensive study in terms of hardware complexity, bandwidth efficiency, and ABER performance is conducted.

1.3 Thesis Outline

The outline of the thesis is is summarized as follows. In Chapter 2, a brief review of UWA channel characteristics are given. In particular, the frequency- and distance-dependent path-loss formula is reviewed, and its effect on the average SNR is revealed through illustrative figures. The characteristics of the additive noise is explained, where it is shown that the PSD

is not constant over the range of interest. Also, it is shown that the effect of ISI and Doppler scaling is severe due to the low propagation speed of sound in underwater. This followed by a comprehensive literature review related to our work.

In Chapter 3, a brief background is given for P2P OFDM systems. The ML receiver is derived for the path-specific Doppler scaling P2P OFDM system, and the structure of the receiver is shown to be consist of two stages: MR and equalization. As a suboptimal resampling, the actual channel is then approximated such that it has a single Doppler scaling factor, and the same derivation is done again.

In Chapter 4, SC-FDE systems are studied in the context of P2P and MAC systems. For the former system we consider path-specific Doppler model, while for the latter user-specific Doppler model is considers. The ML receiver is derived for both cases, and the structure and implementation of the receiver are illustrated. In particular, it is shown that the receiver structure is such that two consecutive stages are required: MR and equalization. For the equalization part, instead of implementing it using the MLSD, we propose the use of an MMSE FDE. Also, a suboptimal resampling is proposed by approximate the channels such that all have a common scaling factor.

In Chapter 5, the P2P OFDM systems are extended to relay-assisted systems. In particular, SR and MR receivers are considered for different techniques employed in relaying systems, namely, TWR, D-STBC, or the combination of both systems. Since the noise after MR pre-processing will be colored, the equivalent noise's covariance matrices are derived at the intermediate relays as well as the final destinations. Because of its simplicity, Amplify-and-Forward (AF) relaying is considered as the relaying scheme. The effect of the resampling technique on the performance and performance of the different systems are illustrated.

In Chapter 6 the corresponding SC-FDE systems of Chapter 5 are derived. The similarities and differences in the corresponding systems structures and their implementations are explained. Also a complexity comparison, bandwidth efficiency, and ABER of both schemes (i.e., OFDM and SC-FDE) are given.

Finally, in Chapter 7, conclusions and some suggested future works are given.

Chapter 2

Background and Literature Review

2.1 Background

2.1.1 UWA Channels Characteristics

UWA channels are recognized as one of the most difficult communication media, because of its unique and challenging characteristics. Three major characteristics that distinguish UWA channels, including frequency and distance dependent path loss, long but sparse time-varying multipath fading, and low speed of sound (about 1500 m/s) [9].

2.1.1.1 Path Loss

The path loss in UWA channels is given by [10]:

$$A(d, f) = d^{\kappa} \left[\alpha(f)\right]^{d} \tag{2.1}$$

where d is the distance between the transmitter and receiver, f is the frequency, κ is the spreading factor, and $\alpha(f)$ is the frequency dependent absorption coefficient. There are two spreading types: cylindrical for which $\kappa = 1$ or spherical for which $\kappa = 2$. However, in practice, κ is taken to be 1.5 as a spreading between cylindrical and spherical. The absorption coefficient is usually calculated empirically using the Thorp's formula as:

$$10 \log_{10}]\alpha(f)\{ = 0.11 \frac{f^2}{1+f^2} + 44 \frac{f^2}{4100+f^2} + 2.75 \sim 10^{-4} f^2 + 0.003, \tag{2.2}$$

measured in dB/Km for f in KHz, which is shown in Fig. 2.1.

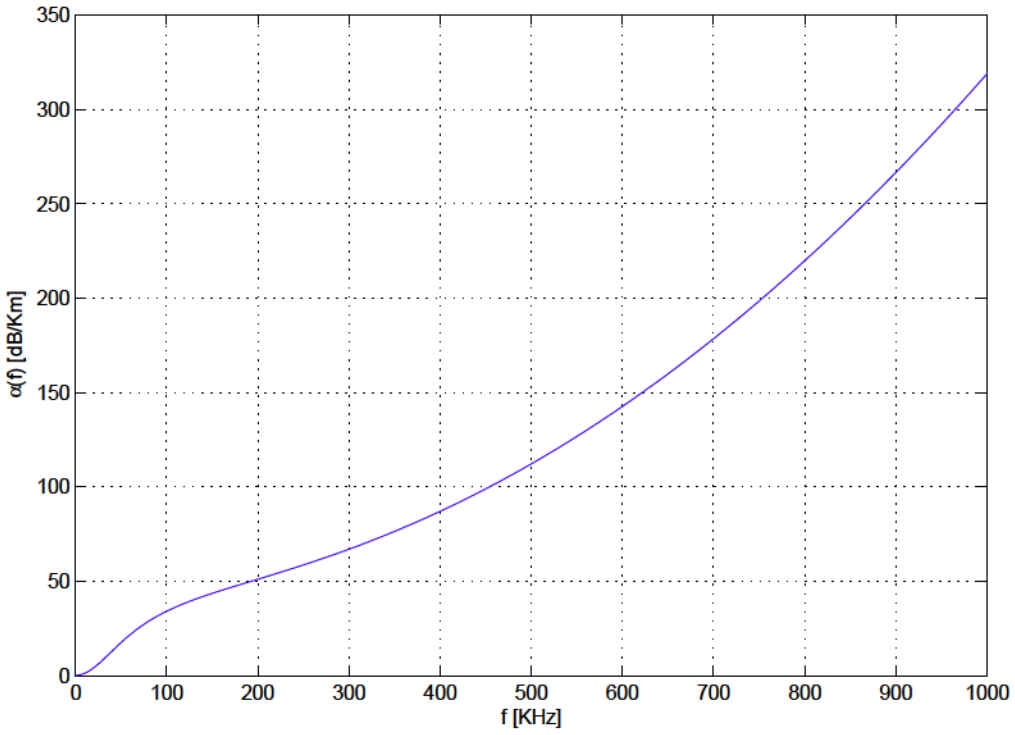

Figure 2.1: Absorption coefficient $\alpha(f)$.

2.1.1.2 Noise

The additive noise in UWA channels is usually modeled as Gaussian but not white as in RF channels where the PSD is constant over the range of frequencies of interest, but rather it is colored and has a decaying PSD with frequency. There are four sources of noise in UWA channels: turbulence, shipping, waves, and thermal noise. The empirical equation of these noises's PSD measured in dB re μ Pa per Hz as a function of f in KHz [10]:

$$10 \log_{10} \mathcal{V}_{\text{Tu}}(f) = 17 \quad 30 \log_{10} f \tag{2.3a}$$

$$10 \log_{10} \mathcal{V}_{s}(f) = 40 + 20(s \quad 0.5) + 26 \log_{10} f \quad 60 \log_{10}(f + 0.03) \tag{2.3b}$$

$$10 \log_{10} \mathcal{V}_{w}(f) = 50 + 7.5\, w^{1/2} + 20 \log_{10} f \quad 40 \log_{10}(f + 0.4) \tag{2.3c}$$

$$10 \log_{10} \mathcal{V}_{\text{Th}}(f) = \quad 15 + 20 \log_{10} f, \tag{2.3d}$$

where $s \ / \ [0, 1]$ is the shipping factor, where $s = 0$ means low shipping activity, and $s = 1$ means high shipping activity, and w is the wind speed in m/s. The total noise's PSD (linear

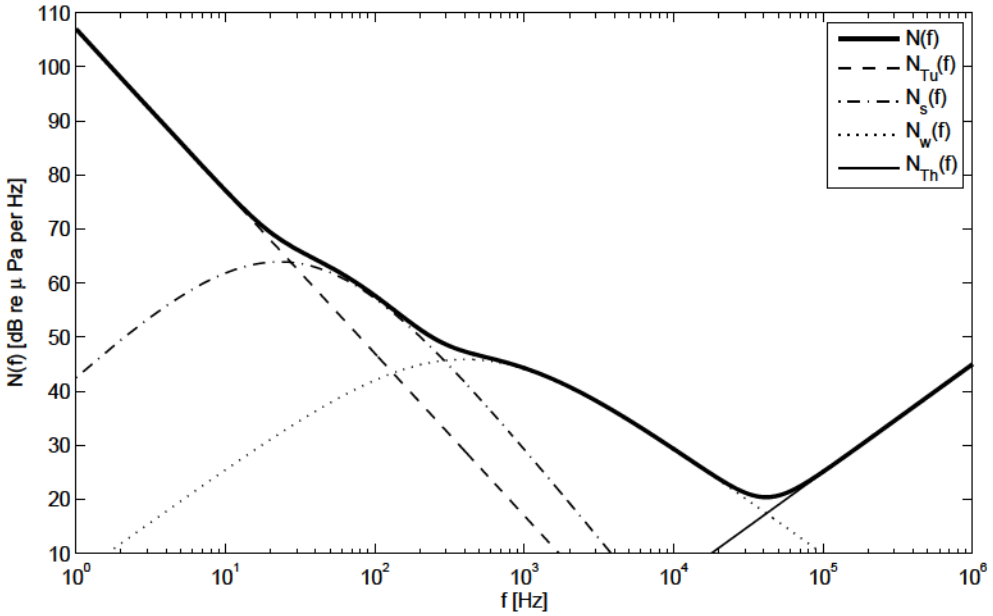

Figure 2.2: Noise PSD for $s = 0$ and $w = 0$ m/s.

scale) is given by

$$\mathcal{V}(f) = \mathcal{V}_{\text{Tu}}(f) + \mathcal{V}_s(f) + \mathcal{V}_w(f) + \mathcal{V}_{\text{Th}}(f). \tag{2.4}$$

Figs. 2.2 and Fig. 2.3 illustrate the PSD of the individual noises as well as the total noise for $(s, w) = (0, 0)$ and $(s, w) = (1, 10)$, respectively. Two observations can be made here: firstly, the PSD of the total noise is not constant, and secondly, each noise type is dominant over a specific range of frequencies.

The path loss and noise determines the average SNR at a given distance and a given frequency. In particular, the received narrow-band SNR for a transmit power P is given by [10]:

$$\gamma(d, f) = \frac{P/A(d, f)}{\mathcal{V}(f)\Delta f}, \tag{2.5}$$

where the factor $]\mathcal{V}(f)A(d, f)\{^{-1}$ is the frequency-and-distance-dependent part of the SNR. So, we can see that there is an optimum frequency $f_{\text{opt}}(d)$ for a given distance d. After determining the optimum carrier frequency for a given distance, 3 dB bandwidth definition could be used to determine the range of frequencies over which the received SNR [dB] lies within 3 dB of the optimum SNR (in dB)[10]. In particular, the frequencies of interest are such that:

$$\gamma(d, f) = \frac{P/A(d, f)}{\mathcal{V}(f)\Delta f} > 0.5\gamma(d, f_{\text{opt}}(d)) = \frac{P/A(d, f_{\text{opt}}(d))}{2\,\mathcal{V}(f_{\text{opt}}(d))\Delta f}, \tag{2.6}$$

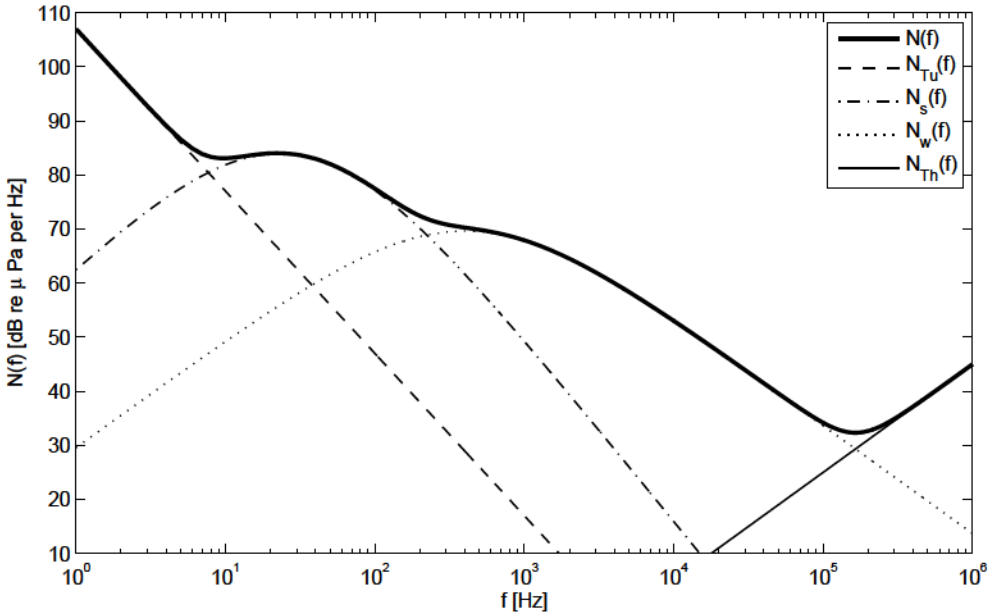

Figure 2.3: Noise PSD for $s = 1$ and $w = 10$ m/s.

which implies that:

$$10\log_{10}\Big]A(d,f)\mathcal{V}\,(f)\Big\{^{-1} > \quad 3 + 10\log_{10}\Big]A(d,f_{\text{opt}}(d))\mathcal{V}\,(f_{\text{opt}}(d))\Big\{^{-1}. \tag{2.7}$$

The range of frequencies that satisfy (2.7) for different distances (in Km) are illustrated in Fig. 2.4 between the intersections of dashed and solid curves. We can see that, as d decreases, the available bandwidth increases, which is more favorable for high data rate transmission. This characteristic makes a strong case for RA systems in UWA channels.

2.1.1.3 Multipath Fading

The signal in UWA channels propagates to the destination over multiple paths because of signal reflections from the surface and bottom, and signal refractions due to spatial variability of the water. The sound speed depends on the salinity, temperature, and pressure of the water, which differ in space. This implies that a signal traveling over a longer path does not necessarily mean that it will arrive at the destination after a signal traveling over shorter path, because the former may travel in higher speed than the latter. However, sound speed can be taken as constant over shallow water channels [9]. Furthermore, these propagation paths are time-varying.

Contrary to RF channels, in UWA channels, there is no consensus regarding the distribution

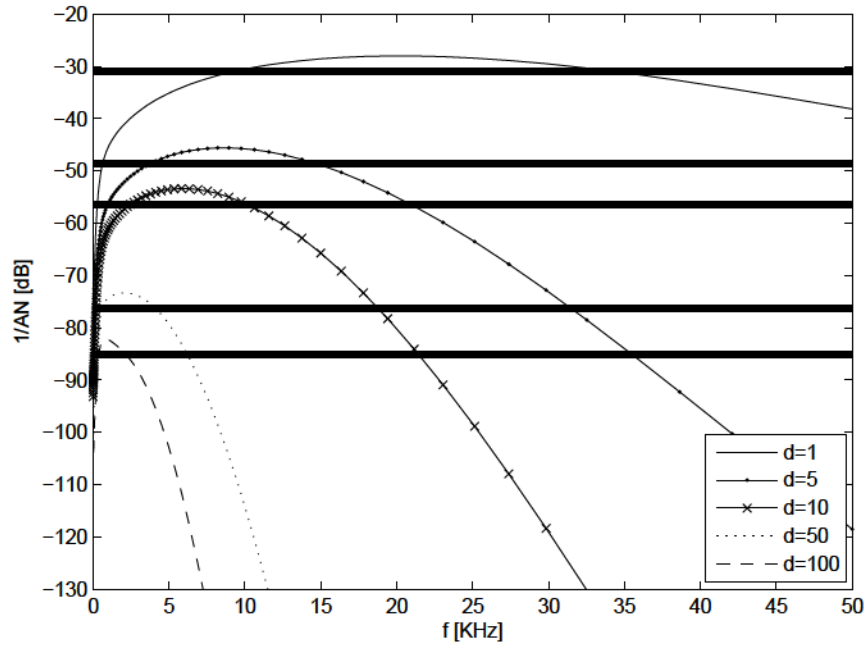

Figure 2.4: $\big)A(d,f)\mathcal{V}\,(f)\big($$^{-1}$ [dB] versus f [KHz].

of the channel taps, where in some channels they are well modeled as deterministic, while in others they can be modeled as Rician or Rayleigh [10]. Most authors consider shallow-water medium range channels as Rayleigh. Also deep water channels are modeled as Rayleigh. However, the available measurements are scarce, making channel modeling controversial [1].

Due to the low propagation speed of sound, multipath delay spread is usually very long, which causes severe ISI, e.g. it is not unusual to have a delay spread of 100 ms, which results in an ISI span of 500 symbols for a transmission rate of 5 Ksps [11]. Also, there are just a small number of significant paths in the Channel Impulse Response (CIR), which makes UWA channels sparse by nature [12].

2.1.1.4 Doppler Effect

The time-variability of UWA channels is attributed to two reasons: inherent changes in the medium, and the relative motion between the transceivers [9]. In shallow water, the main contributor to the time-variability is the surface waves, which cause the displacement of the reflection points. On the other hand, in deep water, internal waves contribute to the time-variability of the medium. Motion of the reflection points causes frequency spreading of the surface-reflected signal. The frequency spreading of a signal component of frequency f and with incidence angle

of θ is $0.0175(f/c)w^{3/2}\cos(\theta)$, where c is the sound speed.

Also, a moving transmitter and/or receiver, either *voluntarily or involuntarily*, causes time-variability, which causes Doppler scaling proportional to the factor $a = v/c$, where v is the relative speed between the transmitter and receiver [1]. Because of the low speed of sound in UWA channels, this factor is significant and can not be safely ignored as it is the case in most RF channels.

In narrow-band systems, where the signal bandwidth is much smaller than the carrier frequency, which is the case in RF channels, the effect of Doppler on a communication system is approximated as a constant Carrier Frequency Offset (CFO), which can be compensated for by adjusting the local carrier frequency oscillator [6]. However, in wide-band signals as in UWA systems, where the the signal bandwidth is comparable to the carrier frequency, each frequency component is affected differently. In this case, it is more accurate to model the Doppler effect as time scaling, i.e., $r(t) = s\ (1+a)t\big[$, where $r(t)$ is the received signal, and $s(t)$ is the transmitted signal, and hence time synchronization is needed in this case as well as frequency synchronization. Sampling $r(t)$ at T_s gives:

$$r[nT_s] = s\Big]n(1+a)T_s\Big\{. \tag{2.8}$$

So, to eliminate the Doppler effect, the sampling time must be adjusted as $nT_s/(1+a)$ [6], which yields

$$r\Big]\Big)\frac{n}{1+a}\Big[\ T_s\Big\{ = s[nT_s]. \tag{2.9}$$

A major design parameter here is the accuracy of the factor a, and the resulting residual Doppler that is tolerated by adaptive equalizers for SC modulation systems, where a residual Doppler of the order 10^{-4} is needed for a Decision Feedback Equalizer (DFE) to track the changes; otherwise, it diverges [6].

For general design purposes, a coherence time in the order of 100 ms may be assumed [10], which makes relative motion between transceivers a common source of time variability in all UWA channels. Because of this we can observe that most of the literature focus on this case of time variability.

2.1.2 Generating UWA Channels

There is no consensus on the characterization of UWA channels because of the scarce measurements available, and hence the best way to test a system over UWA channels is to use experimental data. However, since obtaining experimental data requires expensive equipment, and the available data is not easy to get, the next best option is use a set of software to emulate UWA channels by capturing the most important characteristic taking into account the depths of the sources and receivers, carrier frequency used, the range between transceivers, and the type of environment in which the transmission is virtually done.

As a part of our simulation study, we consider a location in the Arabian Gulf with latitude 26.5^oN and longitude 52.5^oE. For the given location, environmental factors (such as temperature, salinity and acidity of the water) and the morphology of the sea bottom (such as type of sediment and bathymetry) can be found in the databases of US National Oceanic and Atmospheric Administration (NOAA) publicly available at [13].

The geographical-based data along with the system characteristics such as locations and depths of nodes are given as inputs to the Bellhop software. The software produces arrival data which includes the amplitudes, travel times, angles of arrival, and angles of departure associated with each echo. This yields a normalized deterministic raw channel impulse response. To calculate the Doppler scaling factors of the paths in each link, we use the Bellhop output arrival data along with the velocity vector $[\nu_r \ \nu_z]$ for the nodes, as the input parameters of the VirTEX software, where $\nu_r > 0$ corresponds to increasing radial distance, and $\nu_z > 0$ corresponds to motion towards deeper depths.

Environmental File Structure

The input file to the Bellhop software is called the environmental file and it is written using any standard text editor with the extension '.env'. The following '.env'file is used in the simulations to generate UWA channels beside the man-made fixed and Rician channels used.

```
1 'Saed' ! Title
2 16000.00                          ! Frequency (Hz)
3     1                             ! NMedia
4 'CVWT'                    ! Top Option
5     0 0.00   75.00        ! N sigma depth
6             0.00 1548.12   0.00   1.00   0.00   0.00 /    ! z c cs rho
7            10.00 1547.97   0.00   1.00   0.00   0.00 /    ! z c cs rho
```

```
          20.00 1546.67    0.00    1.00    0.00    0.00 /     ! z c cs rho
          30.00 1545.65    0.00    1.00    0.00    0.00 /     ! z c cs rho
          50.00 1544.27    0.00    1.00    0.00    0.00 /     ! z c cs rho
          75.00 1540.39    0.00    1.00    0.00    0.00 /     ! z c cs rho
'A'   0.00                ! Bottom Option, sigma
     75.00 1575.00    0.00    1.70    1.00    0.00 /          ! lower halfspace
   20                                ! NSD
    25.000000
    72.500000   /          ! SD(1)  ... (m)
   20                                ! NRD
    25.000000
    72.500000   /          ! RD(1)  ... (m)
    3                                ! NRR
    2.500000
    3.500000
    6.000000   /           ! RR(1)  ... (km)
'A'                                  ! Run Type
0                                          ! Nbeams
  75.000000 75.000000 /                  ! angles (degrees)
0.000000 80.000000 6.100000              ! deltas (m) Box.z (m) Box.r (km)
```

We give here an explanation of some of the important parameters. The first line corresponds to the file name which can be chosen arbitrarily. The second line corresponds to the carrier frequency used in KHz which is set here to 16 KHz. The third line is always set to one in Bellhop, and it is used as a compatibility parameter with other models in the Acoustic Toolbox. Line four is specified as 'CVWT' which indicates that Bellhop should use C-linear interpolation to calculate the Sound Speed Profile (SSP), the ocean surface is modeled as vacuum, all attenuation values are measured in dB/wavelength, and finally Thorp's column attenuation is used in the water column. In the fifth line, the only parameter that is read by Bellhop is 75 which is the bottom depth and this indicates the last line to be read in the SSP. The lines from 6 11 indicate the depth-sound speed pairs defining the ocean sound speed profile. Line 14 indicates the number of source depths specified which is set to 20, and those 20 depths are uniformly distributed between depths 25 and 75m (specified in the next two lines), which results in a depth step size of 2.5 m. The same thing is specified for the receiver depths in the next three lines. In line 20, the number of horizontal ranges allowed are set to be three, and these three ranges are set in the next three lines to be 2.5, 3.5 and 6 Km.

2.2 Literature Review

UWA channels pose challenges for achieving reliable high data rate transmission. Such channels are characterized as wideband time varying ISI (time- and frequency-selective or doubly selective) channels . Due to their high conductivity to acoustic waves, the corresponding path loss is not just distance-dependent, but also frequency-dependent, which makes the available bandwidth severely limited since the frequencies that travel for long distances are the low frequency ones [9, 12, 14, 15]. Owing to the fact that the propagation speed of sound under water is about $c = 1500$ m/s, ISI becomes severe, especially for high data rate transmission.

Time variation in UWA channels has two main sources: inherent changes in the propagation medium and the relative motion between transceivers. The Doppler effect resulting from the relative motion of the transceivers is extreme, and it is proportional to the ratio v/c, where v is the relative speed between the transceivers. Since the sound speed is very low compared to the EM propagation speed in RF channels, which propagate at the cosmic speed limit, this value in UWA channels is orders of magnitude larger than that in RF channels, and hence it cannot be neglected and should be incorporated into the receiver design. In addition, since UWA channels are wideband by nature, this motion-induced Doppler effect translates different frequencies by different amounts, and this is modeled more accurately as time scaling, compared to RF channels where Doppler effect translates all frequencies roughly by the same amount as that for the carrier frequency, i.e, common CFO, which can be dealt with using frequency synchronization only.

Even though more interest is shown now in UWA channels, its practical beginning can be traced back to the period of World War II [16]. At the beginning, it was though that noncoherent On Off Keying (OOK) and Frequency Shift Keying (FSK) is the only feasible way to communicate over UWA channels because of the rapid phase variation [17, 18]. But noncoherent communication eliminates the need of tracking the phase only, and does't deal with the problem of ISI [19, 20]. So, guard intervals were inserted between successive pulses to ensure that all echos vanish before the next pulse is received. Also, it is desirable to use those frequencies which are separated by more than the coherence bandwidth of the channel [21]. Obviously, noncoherent communication is not bandwidth efficient, and cannot support real time applications that require high data rate.

In [22], the authors demonstrated successful transmission of coherent modulation over UWA channels for the first time. The receiver in their system consisted of an adaptive time-domain DFE with an embedded Phase-Locked Loop (PLL) to track phase variation, where the param-

eters of the receiver were computed jointly to minimize the Mean Squared Error (MSE). The results extended to Multiple-Input Multiple-Output (MIMO) systems in [23, 24]. In [25, 26, 27, 28] the authors employed Time Reversal (TR) technique in the context of collocated and distributed MIMO. However, Time Domain Equalization (TDE) becomes problematically complex as the channel memory grows large. An efficient alternative is OFDM which converts ISI channels into a set of flat subchannels that eliminates the need of complex equalizers [29, 30]. Owning to its success in RF channels in combating long channels efficiently, OFDM systems have been proposed for efficient communication over UWA channels. However, over time varying channels such as UWA channels, the orthogonality between the subcarriers is lost, which introduces ICI [31, 32, 33, 34]. Consequently, the receiver design must take into account this ICI effect, which otherwise degrades the performance significantly.

In [35], the authors considered OFDM systems over *general* UWA channels, where relative motion is not the only source of time variation. Two ICI-mitigation techniques were proposed, one that explicitly estimates the ICI coefficients to be equalized using a MMSE equalizer, and the other does not estimate the ICI coefficients explicitly but rather uses an adaptive DFE equalizer in the frequency domain. To increase the bandwidth efficiency, MIMO-OFDM was considered in [36, 37, 38, 39], where multiple streams are transmitted simultaneously over the same bandwidth, a technique called spatial multiplexing. Post-FFT processing techniques are proposed in [40, 41]. Bit loading or adaptive modulation which is based on channel prediction was proposed and studied in [42].

Even though OFDM is efficient and robust, it still suffers from a number of drawbacks, including being very sensitive to time variation, as well as experiencing a large peak-to-average power ratio (PAPR), which requires very expensive amplifiers. SC modulation with FDE is a good alternative to both time domain equalization and OFDM [43, 44, 45]. In general, less work has been done on SC-FDE over UWA channels. In [46], SC-FDE scheme is studied for MIMO systems over general UWA channels, where Channel Estimation (CE) and equalization is done in the frequency domain. Phase compensation is applied to the equalized signals to counteract the phase rotation effect of time variation. In [47, 48] low complexity Frequency Domain Turbo Equalization (FDTE) is studied for MIMO systems. Others can be found in [49, 50, 51].

However, if the time variation of the channel results only from the relative motion between transceivers, and the channel is assumed fixed over one or more blocks, the received signal will exhibit a structure (i.e, time scaling) that can be utilized by the receiver. Since adaptive time

domain equalizers have a certain threshold with respect to the Doppler effect (the rate of time variation) for them to converge, the authors in [6] introduced the concept of resampling for SC systems over UWA channels that exhibit the same Doppler scaling factor over all paths. In [7], the authors studied OFDM systems over UWA channels where all paths have the same Doppler scaling factor (a model called *user-specific Doppler*), and invoked resampling to completely eliminate the effect of time variation with the assumption of accurate estimation of the Doppler scaling factor, which is translated in the frequency domain as ICI-free communication. The receiver in [7] consisted of only frequency shifting and resampling by the Doppler scaling factor followed by FFT operation, i.e., no further processing is required. In [52, 53], the authors considered OFDM systems over UWA channels while assuming that each path has its own Doppler scaling factor (a model called *path-specific Doppler*). In particular, they studied the optimization of the resampling factor based on different criteria.

In [8], the authors derived the optimum OFDM receiver when the channel exhibits a *cluster-based Doppler* scaling, where the paths are divided into clusters, and each cluster has its own distinct Doppler scaling factor. In this case the receiver consisted of two stages: MR pre-processing stage and an equalization stage. The MR stage consists of different branches, each corresponds to one Doppler scaling factor, and comprises a frequency shifter, a resampler, and a FFT block. In the second stage, MMSE equalization in the frequency domain is used to further reduce the residual interference effect. This is attributed to the fact that, when more than one Doppler scaling factors are present, neither optimized SR [53] nor MR [8] are able to completely eliminate ICI. As such, a stage of equalization is required to take care of the residual interference.

In the next chapter, we give a detailed theoretical background about MR and SR pre-processing techniques in the context of P2P OFDM systems with path-specific Doppler model. This will be useful in the developments in the subsequent chapters.

Chapter 3

P2P OFDM Systems

In this chapter, we study path-specific Doppler P2P UWA channels, and illustrate the optimum MR receiver design and its suboptimal SR receiver design. In particular, the underlying channel is considered to be UWA, and the CIR is given by [53, 54, 55, 56, 57]

$$h(t;\tau) = \sum_{p=1}^{N_p} h_p\, \delta\left(\tau - \tau_p(t)\right), \tag{3.1}$$

where $\tau_p(t) = \tau_p - a_p t$ [7, 58], N_p is the number of paths, and the three-tuple $\{h_p, \tau_p, a_p\}$ describes the pth path's gain, delay, and Doppler scaling factor, respectively. As a means to combat ISI, cyclic-prefixed-OFDM signaling is used, where the passband transmitted signal is given by

$$s(t) = \mathcal{R}\left\{\sum_{k=0}^{K-1} d_k\, e^{j2\pi f_k t}\, R(t)\right\}, \quad t \in [0, T_g, T], \tag{3.2}$$

where $\mathcal{R}\{.\}$ is the real part operator, d_k is the kth symbol drawn from a unit-energy constellation $\mathcal{C}$ modulating the kth subcarrier $f_k = f_c + k/T$ where f_c is the carrier frequency, $R(t)$ is rectangular pulse of duration $T + T_g$, where T is the OFDM symbol duration, and T_g is the Cyclic Prefix (CP) guard interval, which is assumed to be large enough to prevent Interblock Interference (IBI), which allows block-by-block processing. Thus, the passband received signal can be written as

$$y(t) = \sum_{p=1}^{N_p} h_p\, s\left(t[1 + a_p] - \tau_p\right) + n(t), \tag{3.3}$$

where $n(t)$ is an Additive White Gaussian Noise (AWGN) process of zero-mean and PSD $N_0/2$[1]. The equivalent baseband received signal with respect to the carrier frequency f_c can be written as

$$v(t) = \sum_{k=0}^{K-1} d_k \, P_k(t) + w(t), \tag{3.4}$$

where $w(t)$ is an AWGN process of zero-mean and PSD N_0, and

$$P_k(t) = \sum_{p=1}^{N_p} \underbrace{h_p \, e^{-j2\pi f_k \tau_p}}_{H_p(f_k)} \; e^{j2\pi f_0 t a_p} \, e^{j2\pi \frac{k}{T} t[1+a_p]} \, R\left(t[1+a_p] \quad \tau_p\right). \tag{3.5}$$

3.1 MR Receivers

Since the noise in (3.4) is white, the optimum ML receiver finds the sequence that satisfies the following

$$\hat{\mathbf{d}}_{\text{ML}} = \arg \min_{\mathbf{d} \in |\mathcal{A}|^{K \times 1}} \int \left\| v(t) \quad \sum_{k=0}^{K-1} d_k \, P_k(t) \right\|^2 dt, \tag{3.6}$$

where $\mathbf{d} = [d_0 \;\; d_1 \times\times\times d_{K-1}]^T$. This implies that the set of sufficient statistics are given by [8]

$$\begin{aligned} v_{\text{MR},k} &= \int_{-\infty}^{\infty} P_k^*(t) v(t) \, dt \\ &= \sum_{m=0}^{K-1} \Phi_{k,m} \, d_m + w_{\text{MR},k}, \quad k = 0, 1, \ldots, K \quad 1, \end{aligned} \tag{3.7}$$

where

$$\Phi_{k,m} = \int_{-\infty}^{\infty} P_k^*(t) P_m(t) \, dt \tag{3.8a}$$

$$w_{\text{MR},k} = \int_{-\infty}^{\infty} P_k^*(t) w(t) \, dt. \tag{3.8b}$$

In general the channel coefficients $\Phi_{k,m} \neq 0, \forall k \neq m$, which means that the received samples at the output of the matched filters (3.7) are contaminated by ICI, and hence an additional stage of equalization is necessary. Arranging the samples in (3.7) in a vector-matrix form yields

$$\mathbf{v}_{\text{MR}} = \mathbf{\Phi} \, \mathbf{d} + \mathbf{w}_{\text{MR}}, \tag{3.9}$$

[1] In this thesis we follow the convention of assuming that the noise in UWA channels is white rather than colored as it was illustrated in subsection 2.1.1.2. However, it is straightforward to extend the work into colored noise by measuring the noise covariance matrix and incorporating it into the derivations.

where $[\mathbf{\Phi}]_{k,m} = \Phi_{k,m}$, $\mathbf{v}_{\text{MR}} = [v_{\text{MR},0} \;\; v_{\text{MR},1} \times\times\times v_{\text{MR},K-1}]^T$, and $\mathbf{w}_{\text{MR}} \approx \mathcal{DV}\;(\mathbf{0}_{K\times 1},\, N_0\mathbf{\Phi})$. In this case, the optimum detector searches over $\|\mathcal{C}\|^{K\times 1}$ space, where $\|\mathcal{C}\|$ is the cardinality of $\mathcal{C}$, and choose the sequences that has the least Euclidean distance relative to the received vector. This equalizer or detector is called the Maximum Likelihood Sequence Detector (MLSD) [59]. However, this search process grows exponentially with both the constellation size and subcarrier number K, which is prohibitively complex. As a low complexity alternative, MMSE can be used, where the equalizer is given by [60]

$$\begin{aligned} \mathcal{H}_{\text{MR}} &= \arg \min_{\mathcal{G}\in\mathcal{C}^{K\times K}} \mathbb{E}\,\}\;\mathbf{d} \quad \mathcal{H}\mathbf{v}_{\text{MR}}\;^{2}| \\ &= \mathbf{\Phi}^{H} \;\; \mathbf{\Phi}\mathbf{\Phi}^{H} + N_0\mathbf{\Phi}\big[^{-1}\,. \end{aligned} \tag{3.10}$$

Finally, symbol-by-symbol detection is performed on the equalized sequence $\mathbf{z}_{\text{MR}} = \mathcal{H}_{\text{MR}}\mathbf{v}_{\text{MR}}$.

3.1.1 Receiver Implementation

Note that implementing (3.7) directly requires K matched filters, which is very expensive especially for large K. Instead, as shown in [8], the receiver can be efficiently implemented using FFT operations as following. Substituting (3.5) into (3.7) we have

$$\begin{aligned} v_{\text{MR},k} &= \int_{p=1}^{N_p} H_p^*(f_k) \Big[\underbrace{\int_{-\infty}^{\infty} v(t)\, e^{-j2\pi f_0 t a_p}}_{v_{\text{MR}}^{(p)}(t)}\; e^{-j2\pi \frac{k}{T} t[1+a_p]}\, R\left(t[1+a_p] \quad \tau_p\right) dt \\ &= \int_{p=1}^{N_p} \frac{H_p^*(f_k)}{1+a_p} \Big[\underbrace{\int_0^T v_{\text{MR}}^{(p)}\Big)\frac{t}{1+a_p}\Big[\; e^{-j2\pi \frac{k}{T} t}\, dt}_{v_{\text{MR},k}^{(p)}}\,. \end{aligned} \tag{3.11}$$

Note that the samples $\big\}v_{\text{MR},k}^{(p)}\sqrt{}_{k=0}^{K-1}$ are the FFT output of the received signal $v_{\text{MR}}^{(p)}\big)_{\frac{t}{1+a_p}}\big($ in the discrete time, which can be implemented very efficiently [61]. The block diagram of this implementation is shown in Fig. 3.1. We can see that the receiver consists of multiple branches, each branch corresponding to a Doppler scaling factor, and performs the following operations in order: frequency shifting, resampling, Serial-to-Parallel (S/P), and FFT operations. Since the main theme in this implementation is resampling, the receiver is called MR [8].

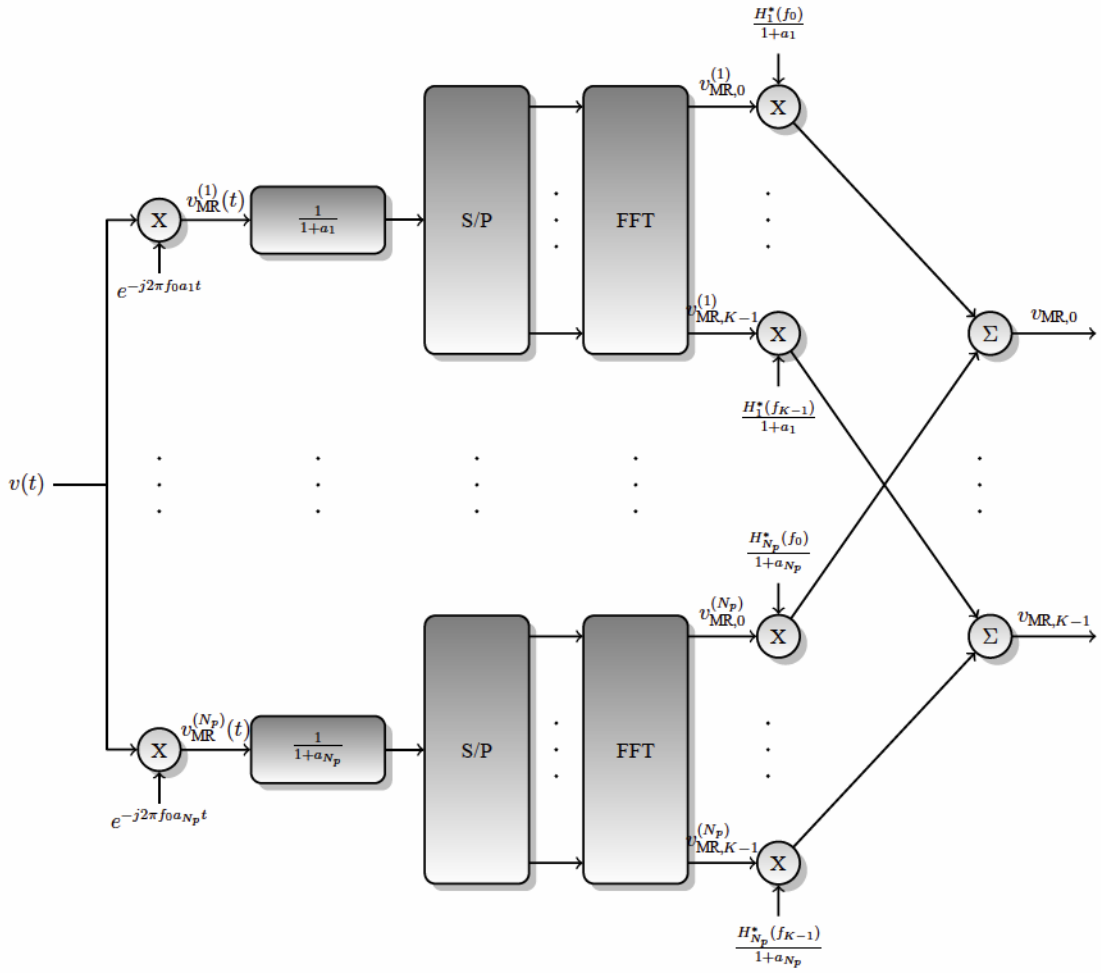

Figure 3.1: MR receiver's block diagram

3.2 SR Receivers

We concluded in Section 3.1 that he optimum pre-processor is the MR one. We also replaced the optimum detector, namely MLSD, by the suboptimal MMSE equalizer followed by symbol-by-symbol detection. In this section, the receiver is further simplified by replacing the optimum pre-processor by a suboptimal one. To this end, the CIR can be approximated with one that has a common Doppler scaling factor, a_{SR}, for all paths. Mathematically speaking,

$$h(t;\tau) \in \int_{p=1}^{N_p} h_p \delta\left(\tau \quad [\tau_p \quad a_{\mathrm{SR}} t]\right), \tag{3.12}$$

In this case, the received samples can be found to be

$$\begin{aligned} v_{\mathrm{SR},k} &= \int_{-\infty}^{\infty} f_k^*(t)\, v(t)\, dt \\ &= \int_{l=0}^{K-1} \Psi_{k,l}\, d_l + w_{\mathrm{SR},k}, \end{aligned} \tag{3.13}$$

where

$$f_k(t) = \int_{p=1}^{N_p} H_p(f_k)\, e^{j2\pi f_0 t a_{\mathrm{SR}}}\, e^{j2\pi \frac{k}{T} t[1+a_{\mathrm{SR}}]}\, R\left(t\left[1+a_{\mathrm{SR}}\right] \quad \tau_p\right) \tag{3.14a}$$

$$\Psi_{k,l} = \int f_k^*(t) P_l(t)\, dt \tag{3.14b}$$

$$w_{\mathrm{SR},k} = \int f_k^*(t)\, w(t)\, dt. \tag{3.14c}$$

Arranging the received samples (3.13) in a vector-matrix form yields

$$\mathbf{v}_{\mathrm{SR}} = \mathbf{\Psi}\, \mathbf{d} + \mathbf{w}_{\mathrm{SR}}, \tag{3.15}$$

where $\mathbf{w}_{\mathrm{SR}} \approx \mathcal{DV}\ (\mathbf{0}_{k\times 1},\ N_0 \mathbf{\Omega}_{\mathrm{SR}})$, where $[\mathbf{\Omega}_{\mathrm{SR}}]_{k,l} = \Omega_{\mathrm{SR},k,l}$ and

$$\Omega_{\mathrm{SR},k,l} = \int f_k^*(t)\, f_l(t)\, dt. \tag{3.16}$$

Again, the optimum detector is the MLSD. However, because it is prohibitively complex, an MMSE equalizer is used, which is given by

$$\mathcal{H}_{\mathrm{SR}} = \mathbf{\Psi}^H \left[\mathbf{\Psi}\mathbf{\Psi}^H + N_0 \mathbf{\Omega}_{\mathrm{SR}}\right]^{-1}, \tag{3.17}$$

and the soft estimates of the transmitted symbols are given by $\mathbf{z}_{\mathrm{SR}} = \mathcal{H}_{\mathrm{SR}} \mathbf{s}_{\mathrm{SR}}$. Finally, symbol-by-symbol detection is performed on $\mathbf{z}_{\mathrm{SR}}$.

3.2.1 Receiver Implementation

Implementing (3.13) directly would result in the same complexity as that of the MR receiver, where they both require K matched filters. However, implementing the receivers indirectly using the approach used in [8] will result in reduction in complexity in terms of the number of branches required in the pre-processing stage. In particular, substituting (3.14a) into (3.13)

yields

$$
\begin{aligned}
v_{\mathrm{SR},k} &= \int_{p=1}^{N_p} H_p^*(f_k) \Big[\int_{-\infty}^{\infty} \underbrace{v(t)\, e^{-j2\pi f_0 t a_{\mathrm{SR}}}}_{v_{\mathrm{SR}}(t)}\; e^{-j2\pi \frac{k}{T} t[1+a_{\mathrm{SR}}]} R\left(t[1+a_{\mathrm{SR}}] \quad \tau_p\right) dt \\
&= \frac{H^*(f_k)}{1+a_{\mathrm{SR}}} \underbrace{\Big[\int_0^T v_{\mathrm{SR}} \Big)\frac{t}{1+a_{\mathrm{SR}}} \Big[e^{-j2\pi \frac{k}{T} t}\, dt}_{v_{\mathrm{SR},k}},
\end{aligned}
\tag{3.18}
$$

where $H(f_k) = \int_{p=1}^{N_p} H_p(f_k)$. Note that the samples $\}v_{\mathrm{SR},k}|_{k=0}^{K-1}$ are the FFT of the received signal $v_{\mathrm{SR}} \Big)\frac{t}{1+a_{\mathrm{SR}}}\Big($ in the discrete time which can be implemented efficiently. The receiver (the pre-processor part of the receiver to be precise) is shown in Fig. 3.2. In this case, the pre-processor is comprised of one branch only that corresponds to a_{SR}. This entails a reduction in hardware complexity compared to MR. However, as we will see in the numerical results, this reduction in complexity translated into worse ABER performance.

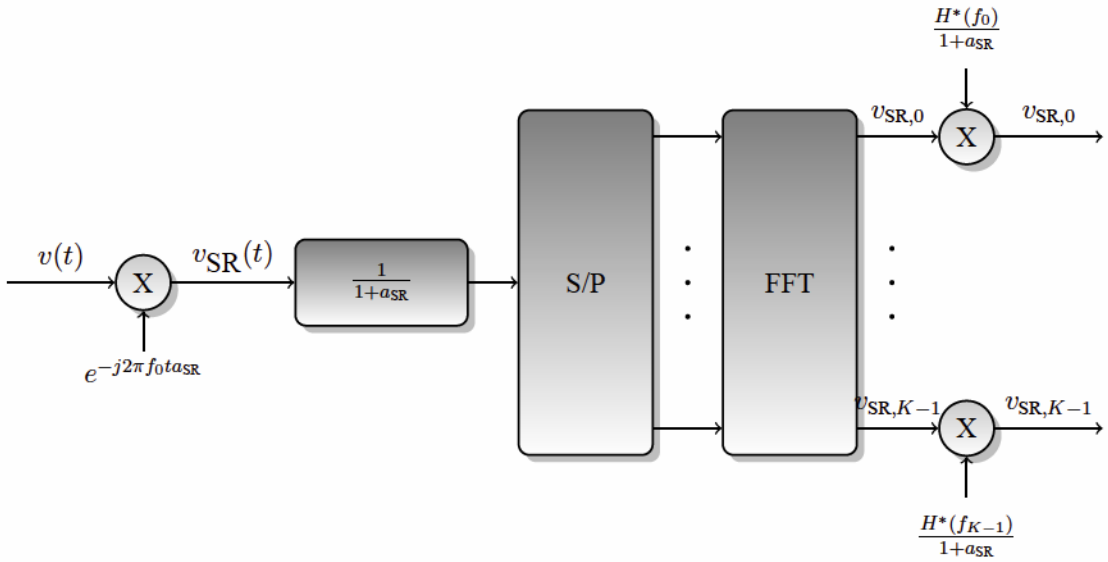

Figure 3.2: SR receiver's block diagram

3.3 Numerical Results

In this section, the ABER of P2P OFDM systems is illustrated. The parameters used in the simulations are: Binary Phase Shift Keying (BPSK) signaling over bandwidth 30 34 KHz, $K = 512$, and the channel's parameters are shown in Fig. 3.3, where each path is labeled by its own Doppler scaling factor.

In Fig. 3.4 the ABER vs. SNR is shown for MR, SR, and No Resampling (NR) pre-processing. For SR, the resampling factor is taken as the arithmetic average of all Doppler scaling factors, since the paths have the same strengths [53]. NR corresponds to the case when no resampling is performed, i.e, the resampling factor is set to zero. We observe that at low SNR, all techniques have almost the same performance. This is because low SNR range corresponds to the noise-limited regime. On the other hand, at high SNR, which is the ICI-limited regime, MR significantly outperforms the corresponding SR and NR techniques. However, this enhancement in performance comes at the expense of more hardware complexity. In particular, six OFDM-branches are required in MR receivers, where an OFDM-branch consists of the following: frequency shifting, resampling, and FFT operations. This is compared to only one OFDM-branch for SR. For NR only a symbol-time sampler and an FFT operation are required. Also, SR outperforms NR, which is expected.

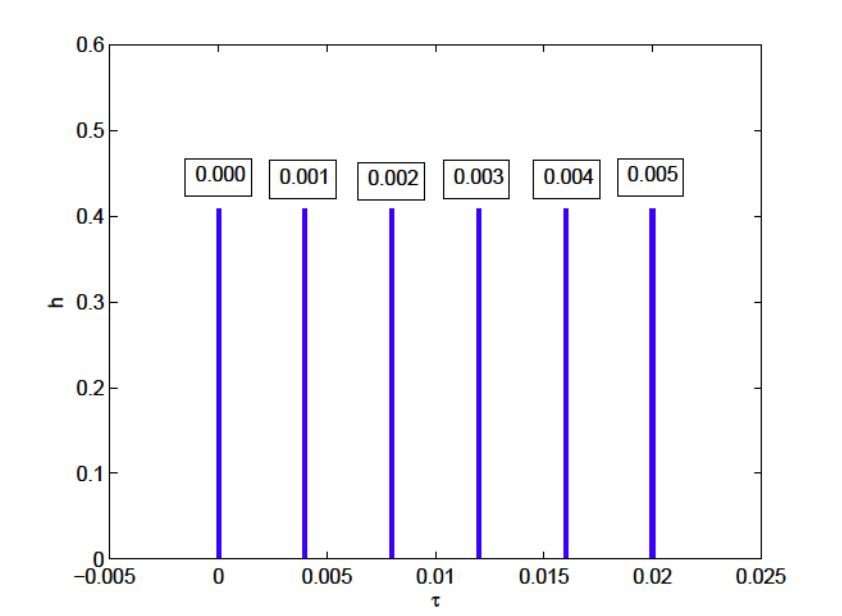

Figure 3.3: P2P OFDM channels' parameters.

In Fig. 3.5 the ABER vs. SNR is shown for P2P OFDM for the same pre-processing techniques shown in Fig. 3.4 but over Rician channels [62], where the mean channels is taken as the vector $\boldsymbol{\mu} = [1 \;\; 1 \;\; 1 \;\; 1]^T$ and the Doppler scaling vector is taken as $\mathbf{a} = [a_0 \;\; a_1 \;\; a_2 \;\; a_3]^T = [0 \;\; 0.0001 \;\; 0.002 \;\; 0.004]^T$. The same observation can be seen, where all pre-processing techniques have the same performance at low SNR because it the noise-limited area, while at high SNR, MR outperforms SR which in turn outperforms NR. Again, the enhanced performance comes at the expense of more hardware complexity.

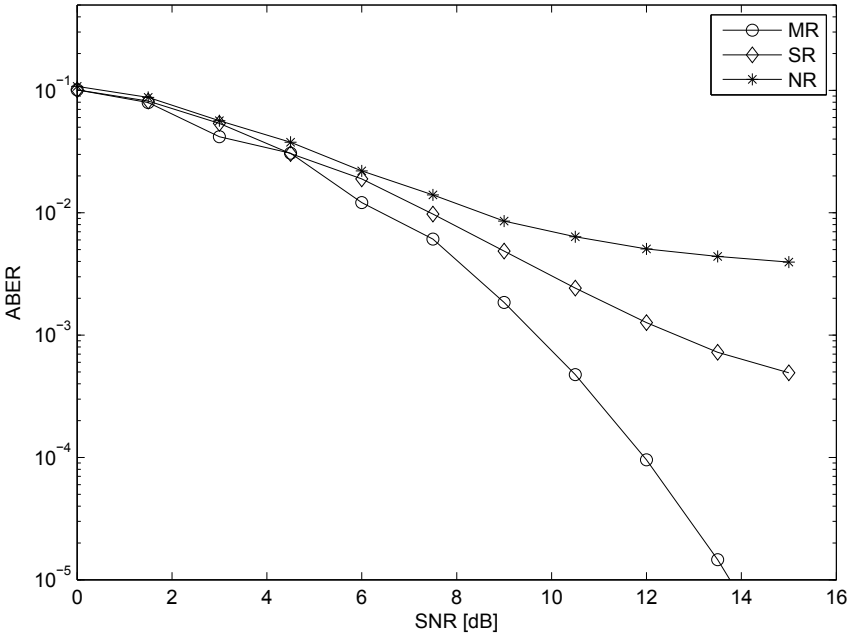

Figure 3.4: ABER of P2P OFDM system for $K = 512$.

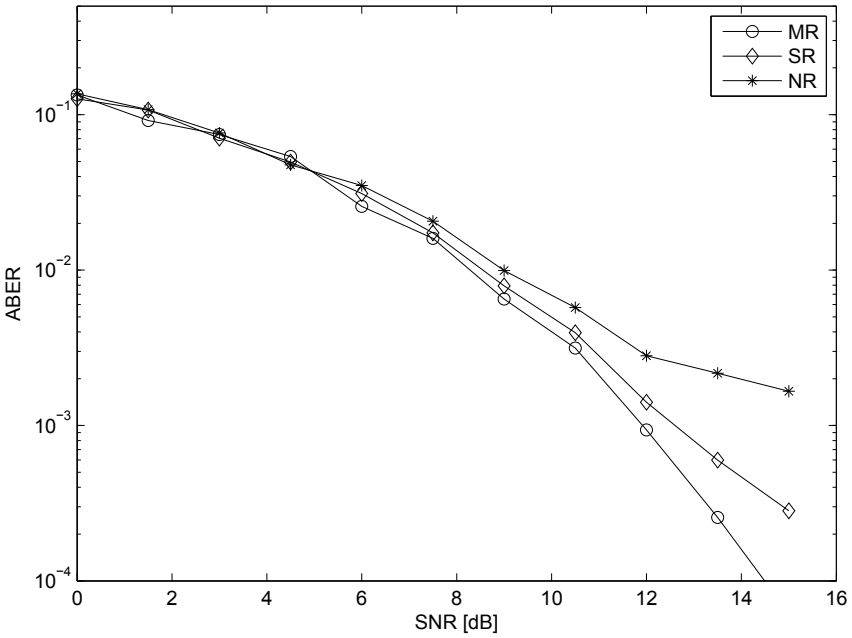

Figure 3.5: ABER of P2P OFDM system for $K = 512$ over Rician Channels.

3.4 Conclusions

In this chapter we reviewed the receiver structure and implementation of P2P OFDM systems over UWA channels with path-specific Doppler model. It was shown that the optimum receiver

consists of two optimum parts: pre-processing and equalization. The optimum pre-processor was shown to be one that consists of multiple branches, and performs frequency shifting, re-sampling, and FFT operations, one for each path. This pre-processor is called MR. On the other hand, the optimum equalizer is MLSD which detects the symbols in each block jointly. Since, MLSD is prohibitively complex to implement, a suboptimal MMSE equalizer is used instead, and symbol-by-symbol detection is performed. To further reduce the complexity of the receiver, a suboptimal pre-processor is illustrated, where the channel is approximated such that all paths have a common Doppler scaling factor. This approximation rendered the pre-processor to consist of only one branch that performs the same sequence of operations as in MR, but for the approximated scaling factor. This suboptimal pre-processor is called SR. Numerical results for uncoded ABER showed that resampling is a necessary component, without which the performance deteriorates significantly. Also they the superiority of MR over SR for both fixed and Rician channels, especially at high SNR, which characterized as the ICI-regime. However, this comes at the expense of more hardware complexity.

Chapter 4

Single Carrier (SC)-Frequency Domain Equalization (FDE) UWA Communication

As mentioned in Chapter Ch. 2, there are a number of drawbacks in OFDM systems like sensitivity to time variation and large PAPR. In [63] the authors showed that SC signaling with FDE significantly outperforms OFDM systems, which requires strong channel coding and frequency interleaving to recover its performance loss. Also, they showed that, when employing channel coding and frequency interleaving, OFDM systems surpass SC-FDE, however, they are more sensitive to carrier synchronization and nonlinear distortions. In terms of hardware complexity, both systems have the same overall complexity. Motivated by these facts, in this chapter we pave the way to use SC signaling with FDE over UWA channels as an efficient and effective means to combat long time varying ISI channels. In the following, we study two SC systems: P2P systems with path-specific Doppler model, and MAC systems with user-specific models.

4.1 P2P SC-FDE

For this scenario, we consider a path-specific Doppler CIR which is given by

$$h(t;\tau) = \int_{p=1}^{N_p} h_p \delta\left(\tau \quad [\tau_p \quad a_p t]\right), \tag{4.1}$$

where N_p is the number of paths, h_p and τ_p are the gain and delay of the pth path, which is characterized by the Doppler scaling factor a_p. We consider a block-based CP-SC transmission.

In particular, the passband transmitted signal is given by

$$s(t) = \mathcal{A}\Big\}e^{j2\pi f_c t}\int_{l=0}^{K-1} d_k\, g\,(t \quad kT_s)\Big(, \quad t \;/\; [\;\; T_g, KT_s], \tag{4.2}$$

where $\mathcal{A}\}.|$ is the real part operator, f_c is the carrier frequency, K is the number of symbols per block, $\}d_k|$ are the equiprobable transmitted symbols drawn from a unit energy complex-valued alphabet $\mathcal{C}$, $g(t)$ is a rectangular pulse of magnitude unity over the interval $[0, T_s)$, where T_s is the symbol duration and T_g is the guard interval, which is assumed to be long enough to prevent IBI and enables block-by-block processing.

Following the same procedure as in section 3.1, the baseband received signal with respect to the carrier frequency, f_c can be shown to be

$$v(t) = \int_{l=0}^{K-1} d_k P_k(t) + w(t), \tag{4.3}$$

where $w(t)$ is an AWGN process of zero-mean and PSD N_0 and

$$P_k(t) = \int_{l=1}^{N_p} \underbrace{h_p\, e^{-j2\pi f_c \tau_p}}_{H_p}\; e^{j2\pi f_c t a_p} g\,(t[1 + a_p] \quad kT_s \quad \tau_p)\,. \tag{4.4}$$

4.1.1 MR Receivers

Since $w(t)$ is AWGN, the ML receiver picks the most probable transmitted sequence such that

$$\hat{\mathbf{d}}_{\text{ML}} = \arg \;\; \min_{\mathbf{d}} \;\; \Big[\;\; \Big\| v(t) \quad \int_{l=0}^{K-1} d_k P_k(t) \Big\|^2 \; dt. \tag{4.5}$$

This implies that the set of sufficient statistics are given by

$$\begin{aligned} v_{\text{MR},k} &= \Big[\;\; P_k^*(t) v(t)\, dt \\ &= \int_{l=0}^{K-1} \Phi_{k,l}\, d_l + w_{\text{MR},k}, \quad k = 0, 1, \ldots, K \quad 1, \end{aligned} \tag{4.6}$$

where

$$\Phi_{k,l} = \int P_k^*(t) P_l(t)\, dt \tag{4.7a}$$

$$w_{\mathrm{MR},k} = \int P_k^*(t) w(t)\, dt. \tag{4.7b}$$

Define $\mathbf{v}_{\mathrm{MR}} \triangleq [v_{\mathrm{MR},0} \;\; v_{\mathrm{MR},1} \times\times\times v_{\mathrm{MR},K-1}]^T$. Consequently, the received samples in (4.6) can be written as

$$\mathbf{v}_{\mathrm{MR}} = \mathbf{\Phi}\, \mathbf{d} + \mathbf{w}_{\mathrm{MR}}, \tag{4.8}$$

where $[\mathbf{\Phi}]_{k,l} = \Phi_{k,l}$, and $\mathbf{w}_{\mathrm{MR}} \approx \mathcal{DV}\ (\mathbf{0}, N_0\mathbf{\Phi})$. Note that if $\mathbf{\Phi}$ is circular, which is the case when the channel is Linear Time-Invariant (LTI), the corresponding matrix in the frequency domain $\mathcal{N}_{\mathrm{MR}}$ will be diagonal. However, the channel matrix $\mathbf{\Phi}$ is not circular because of the residual time variation. (The term "residual" is used here because, as we will see in the receiver implementation, some pre-processing is done at the receiver to minimize the time variation). Furthermore, since $\mathbf{\Phi}$ is not diagonal, the received samples are contaminated by ISI, requiring another stage of equalization. The optimum equalization is implemented using MLSD, which entails $2^{K \log_2 |\mathcal{A}|}$ possibilities, and this is prohibitively complex for practical values of K and alphabet size $\|\mathcal{C}\|$

As an alternative to the MLSD, we propose the use of frequency domain MMSE equalizer followed by symbol-by-symbol detection. To this end, the received samples are transformed to the frequency domain by means of K-point FFT resulting in

$$\mathcal{W}_{\mathrm{MR}} \triangleq \mathcal{G}_K \mathbf{v} = \mathcal{N}_{\mathrm{MR}} \mathcal{F} + \mathcal{Z}_{\mathrm{MR}}, \tag{4.9}$$

where $\mathcal{G}_K$ is the $K \sim K$ discrete Fourier transform (DFT) matrix, and $\mathcal{G}_K^H$ is its inverse, $\mathcal{N}_{\mathrm{MR}} = \mathcal{G}_K \mathbf{\Phi} \mathcal{G}_K^H$, $\mathcal{F} = \mathcal{G}_K \mathbf{d}$, and $\mathcal{Z}_{\mathrm{MR}} = \mathcal{G}_K \mathbf{w}_{\mathrm{MR}}$. The residual time variation in the time domain is translated into ICI in the frequency domain. However, because of the pre-processing stage, the ICI power is concentrated around the main diagonal, which implies that the depth of interference in the frequency domain will be limited. Linear MMSE is used for equalization in the frequency domain as an alternative to the MLSD, which is given by

$$\mathcal{H}_{\mathrm{MR}} = \mathcal{N}_{\mathrm{MR}}^H \left] \mathcal{N}_{\mathrm{MR}} \mathcal{N}_{\mathrm{MR}}^H + N_0 \mathcal{N}_{\mathrm{MR}} \right\{^{-1}. \tag{4.10}$$

Finally, the equalized samples $\{_{\text{MR}} = \mathcal{H}_{\text{MR}}\mathcal{W}_{\text{MR}}$ are transformed back to the time domain as $\mathbf{z}_{\text{MR}} = \mathcal{G}_K^H\{_{\text{MR}}$ where symbol-by-symbol detection is performed.

Receiver Implementation

Substituting (4.4) into (4.6) yields

$$\begin{aligned} v_{\text{MR},k} &= \int_{p=1}^{N_p} H_p^* \Big[\quad v_{\text{MR}}^{(p)}(t)\, g\left(t[1+a_p] \quad kT_s \quad \tau_p\right) dt \\ &= \int_{p=1}^{N_p} \frac{H_p^*}{1+a_p} \int_{kT_s+\tau_p}^{(k+1)T_s+\tau_p} \Big[\quad v_{\text{MR}}^{(p)} \Big) \frac{t}{1+a_p} \Big[\quad dt, \end{aligned} \tag{4.11}$$

where $v_{\text{MR}}^{(p)}(t) = v(t)\, e^{-j2\pi f_c t a_p}$. Note that the MR-SC receiver (see Fig. 4.1) consists of N_p branches, as it is the case in the corresponding OFDM systems, however each performs a frequency shift, and a resampling corresponding to each Doppler scaling factor (hence the name multiple resampling), followed by an integrator. For convenience we term each branch in OFDM systems as an OFDM-branch and each branch in SC systems as SC-branch. The corresponding samples from the different branches are combined and fed to the equalizer. The complexity of both MR-SC-FDE and the corresponding MR-OFDM is shown in Table 4.1. We note that both systems have one IFFT block. In OFDM this block is a part of the transmitter which is used for modulation, whereas in SC-FDE it is a part of the receiver, in particular the equalizer. On the other hand, MR-OFDM requires N_p FFT blocks at the receiver, whereas MR-SC-FDE requires only one FFT block. This is because FFT operation is a part of the preprocessor in OFDM systems, whereas it is part of the equalizer in SC-FDE systems. It is worth mentioning that N_p integrators are introduced in MR-SC-FDE, however integrations are basically summations, whereas FFT operations involve multiplications as well.

4.1.2 SR Receivers

In this section, a suboptimal pre-processing is derived for SC-FDE, where the CIR is approximated as

$$h(t;\tau) \rightarrow \int_{p=1}^{N_p} h_p\, \delta\left(\tau \quad [\tau_p \quad a_{\text{SR}}\, t]\right), \tag{4.12}$$

Table 4.1: Point-to-point SC-FDE vs. OFDM Complexity

	IFFT	FFT	Integrator	Frequency Shifter	Resampler.
SR-OFDM	1	1	0	1	1
MR-OFDM	1	N_p	0	N_p	N_p
SR-SC-FDE	1	1	1	1	1
MR-SC-FDE	1	1	N_p	N_p	N_p

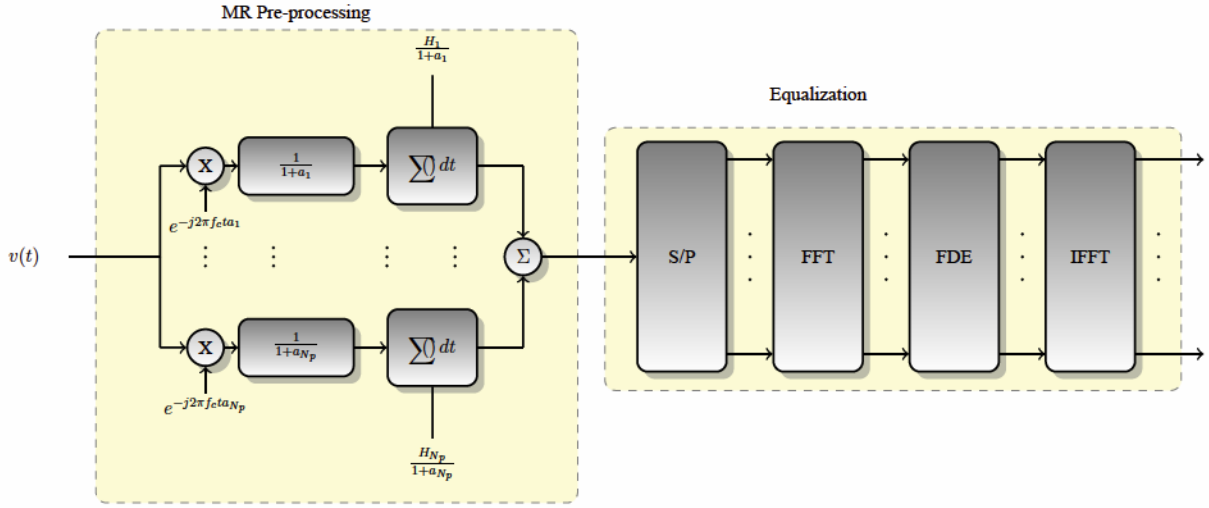

Figure 4.1: Block diagram of MR-SC receiver.

where a_{SR} is an approximate common Doppler scaling factor for all paths, which is similar to the approximate Doppler factor used in [53] for OFDM systems (more on this in the simulation section.) In this case, the received samples are given by

$$\begin{aligned} v_{\text{SR},k} &= \int f_k^*(t) v(t)\, dt \\ &= \int_{l=0}^{K-1} \Psi_{k,l}\, d_l + w_{\text{SR},k}, \end{aligned} \tag{4.13}$$

where

$$f_k(t) = \sum_{p=1}^{N_p} H_p\, e^{j2\pi f_c t\, a_{\text{SR}}}\, g\left(t[1 + a_{\text{SR}}] \quad kT_s \quad \tau_p\right) \tag{4.14a}$$

$$\Psi_{k,l} = \int f_k^*(t) P_l(t)\, dt \tag{4.14b}$$

$$w_{\text{SR},k} = \int f_k^*(t) w(t)\, dt. \tag{4.14c}$$

Writing the time domain samples (4.13) in vector-matrix form we have:

$$\mathbf{v}_{\text{SR}} = \boldsymbol{\Psi}\mathbf{d} + \mathbf{w}_{\text{SR}}, \tag{4.15}$$

where $[\boldsymbol{\Psi}]_{k,l} = \Psi_{k,l}$ and $\mathbf{w}_{\text{SR}} \approx \mathcal{CN}\ (\mathbf{0},\ N_0\boldsymbol{\Omega})$ where $[\boldsymbol{\Omega}]_{k,l} = \Omega_{k,l}$ and

$$\Omega_{k,l} = \int f_k^*(t) f_l(t)\, dt. \tag{4.16}$$

As in MR-SC-FDE, the received samples are transformed to the frequency domain as

$$\mathcal{W}_{\text{SR}} \triangleq \mathcal{G}_K \mathbf{v}_{\text{SR}} = \mathcal{N}_{\text{SR}}\mathcal{F} + \mathcal{Z}_{\text{SR}}, \tag{4.17}$$

where $\mathcal{N}_{\text{SR}} = \mathcal{G}_K \boldsymbol{\Psi} \mathcal{G}_K^H$ and $\mathcal{Z}_{\text{SR}} \approx \mathcal{CN}\ (\mathbf{0},\ N_0\boldsymbol{\Xi})$, where $\boldsymbol{\Xi} = \mathcal{G}_K \boldsymbol{\Omega}\, \mathcal{G}_K^H$. In this case, the MMSE equalizer in the frequency domain is given by

$$\mathcal{H}_{\text{SR}} = \mathcal{N}_{\text{SR}}^H \left[\mathcal{N}_{\text{SR}}\mathcal{N}_{\text{SR}}^H + N_0\boldsymbol{\Xi}\right]^{-1}. \tag{4.18}$$

Finally, the equalized samples are transformed back to the time domain as $\mathbf{z}_{\text{SR}} = \mathcal{G}_K^H \mathcal{H}_{\text{SR}} \mathcal{W}_{\text{SR}}$ where symbol-by-symbol detection takes place.

Receiver Implementation

Substituting (4.14a) into (4.13) yields

$$v_{\text{SR},k} = \sum_{p=1}^{N_p} \frac{H_p^*}{1 + a_{\text{SR}}} \int_{kT_s+\tau_p}^{kT_s+\tau_p} v_{\text{SR}} \left(\frac{t}{1 + a_{\text{SR}}}\right) dt. \tag{4.19}$$

Note that in this case, the pre-processing stage consists only of one SC-branch. The complexity of both SC-FDE and the corresponding OFDM when SR pre-processing is used have almost the same overall complexity (See Table 4.1).

4.2 MAC SC-FDE

In an attempt to increase the bandwidth efficiency, in this section we consider a MAC system, where multiple users are communicating directly with a receiver over the same bandwidth at the same time. In particular, we consider M single-antenna users that are communicating with an N-antenna receiver. The user-specific CIR between the mth user and the nth receive element is given by

$$h^{(m,n)}(t;\tau) = \int_{p=1}^{N_p^{(m,n)}} h_p^{(m,n)}\,\delta\quad\tau\quad\rceil\tau_p^{(m,n)}\quad a^{(m)}t\{\lceil, \tag{4.20}$$

where $N_p^{(m,n)}$ is the number of paths, $h_p^{(m,n)}$, $\tau_p^{(m,n)}$ and $a^{(m)}$ are the pth path gain, delay, and Doppler scaling factor between the mth user and nth receive element, respectively. In this scenario user-specific Doppler scaling model is assumed, where the paths from each user to *all* receiver elements have a common Doppler scaling factor. This assumption is reasonable, since the receive elements are collocated and move as a unit at the same speed and in the same direction. As in the previous section, CP-SC signaling is used, where the passband transmitted signal from the mth user is given by

$$s_m(t) = \mathcal{A}\Big\}e^{j2\pi f_c t}\int_{k=0}^{K-1} d_{m,k}\,g\,(t\quad kT_s)\Big(, \tag{4.21}$$

where $d_{m,k}$ is kth symbol of the mth user, and the rest are as defined previously. The baseband received signal with respect to f_c at the nth receive antenna is given by

$$v^{(n)}(t) = \int_{m=1}^{M}\int_{k=0}^{K-1} d_{m,k}P_k^{(m,n)}(t) + w^{(n)}(t), \tag{4.22}$$

where $w^{(n)}(t)$ is an AWGN process of zero-mean and PSD N_0, and

$$P_k^{(m,n)}(t) = \int_{p=1}^{N_p^{(m,n)}} \underbrace{h_p^{(m,n)}\,e^{-j2\pi f_c\tau_p^{(m,n)}}}_{H_p^{(m,n)}}\; e^{j2\pi f_c t a^{(m)}}\; g\;\; t[1+a^{(m)}]\quad kT_s\quad\tau_p^{(m,n)}\lceil. \tag{4.23}$$

4.2.1 MR Receivers

Arranging the received signals from all antennas in a vector form yields

$$\underbrace{\begin{pmatrix} v^{(1)}(t) \\ v^{(2)}(t) \\ \vdots \\ v^{(N)}(t) \end{pmatrix}}_{\mathbf{v}(t)} = \underbrace{\begin{pmatrix} \mathbf{P}^{(1)}(t) \\ \mathbf{P}^{(2)}(t) \\ \vdots \\ \mathbf{P}^{(N)}(t) \end{pmatrix}}_{\mathbf{P}(t)} \mathbf{d} + \underbrace{\begin{pmatrix} w^{(1)}(t) \\ w^{(2)}(t) \\ \vdots \\ w^{(N)}(t) \end{pmatrix}}_{\mathbf{w}(t)} \tag{4.24}$$

where $\mathbf{d} = [\mathbf{d}_1^T \;\; \mathbf{d}_2^T \;\; \cdots \;\; \mathbf{d}_M^T]^T$, $\mathbf{d}_m = [d_{m,0} \;\; d_{m,1} \;\; \cdots \;\; d_{m,K-1}]^T$ and

$$\mathbf{P}^{(n)}(t) = \big(\mathbf{P}^{(1,n)}(t) \quad \cdots \quad \mathbf{P}^{(M,n)}(t)\big) \tag{4.25a}$$

$$\mathbf{P}^{(m,n)}(t) = \big(P_0^{(m,n)}(t) \quad \cdots \quad P_{K-1}^{(m,n)}(t)\big), \tag{4.25b}$$

for $n = 1, 2, \ldots, N$ and $m = 1, 2, \ldots, M$. The ML receiver will find the sequence $\mathbf{d}$ such that

$$\hat{\mathbf{d}}_{\text{ML}} = \arg \min_{\mathbf{d}} \int \big(\mathbf{v}(t) - \mathbf{P}(t)\mathbf{d}\big)^2 dt, \tag{4.26}$$

where $\mathbf{x} = \sqrt{\int \sum_{n=1}^{N} \|x_n\|^2}$, which leads to the set of sufficient statistics

$$\mathbf{v}_{\text{MR}} = \int \mathbf{P}^H(t)\mathbf{v}(t)\, dt. \tag{4.27}$$

Consequently, the set of sufficient statistics of user m are given by

$$\begin{aligned} \mathbf{v}_{\text{MR}}^{(m)} &= \int_{y=1}^{N} \mathbf{P}^{(m,n)H}(t)\, v^{(n)}(t)\, dt \\ &= \int_{y=1}^{N} \Big] \int_{y=1}^{M} \mathbf{\Phi}^{(m,u)}(n)\, \mathbf{d}^{(u)} + \mathbf{w}_{\text{MR}}^{(m,n)} \Big\{ \\ &= \int_{y=1}^{M} \mathbf{\Phi}^{(m,u)}\, \mathbf{d}^{(u)} + \mathbf{w}_{\text{MR}}^{(m)}, \end{aligned} \tag{4.28}$$

where $\mathbf{\Phi}^{(m,u)} = \int_{n=1}^{N} \mathbf{\Phi}^{(m,u)}(n)$, $\mathbf{w}_{\text{MR}}^{(m)} = \int_{n=1}^{N} \mathbf{w}_{\text{MR}}^{(m,n)}$ and

$$\mathbf{\Phi}^{(m,u)}(n) = \int \mathbf{P}^{(m,n)H}(t)\, \mathbf{P}^{(u,n)}(t)\, dt \tag{4.29a}$$

$$\mathbf{w}_{\text{MR}}^{(m,n)} = \int \mathbf{P}^{(m,n)H}(t)\, w^{(n)}(t)\, dt. \tag{4.29b}$$

It is straightforward to show that $\mathbf{w}_{\text{MR}}^{(m,n)}$ is an AWGN vector of zero-mean and covariance matrix

$$\mathbb{E}\left\{\mathbf{w}_{\text{MR}}^{(m,n)} \mathbf{w}_{\text{MR}}^{(u,n')H}\right\} = \begin{cases} N_0 \mathbf{\Phi}^{(m,u)}(n) & n = n' \\ \mathbf{0}_{K \times K} & n \neq n' \end{cases}, \tag{4.30}$$

and hence $\mathbf{w}_{\text{MR}}^{(m)}$ is an AWGN vector of zero-mean and covariance matrix

$$\mathbb{E}\left\{\mathbf{w}_{\text{MR}}^{(m)} \mathbf{w}_{\text{MR}}^{(u)H}\right\} = N_0 \mathbf{\Phi}^{(m,u)}. \tag{4.31}$$

The samples give by (4.28) can be re-written in a more compact form as

$$\mathbf{v}_{\text{MR}}^{(m)} = \mathbf{\Phi}^{(m)} \mathbf{d} + \mathbf{w}_{\text{MR}}^{(m)}, \tag{4.32}$$

where $\mathbf{\Phi}^{(m)} = \left[\mathbf{\Phi}^{(m,1)} \quad \mathbf{\Phi}^{(m,2)} \quad \cdots \quad \mathbf{\Phi}^{(m,M)}\right]$. Thus, the samples given by (4.27) can be written as

$$\underbrace{\begin{bmatrix} \mathbf{v}_{\text{MR}}^{(1)} \\ \mathbf{v}_{\text{MR}}^{(2)} \\ \vdots \\ \mathbf{v}_{\text{MR}}^{(M)} \end{bmatrix}}_{\mathbf{v}_{\text{MR}}} = \underbrace{\begin{bmatrix} \mathbf{\Phi}^{(1)} \\ \mathbf{\Phi}^{(2)} \\ \vdots \\ \mathbf{\Phi}^{(M)} \end{bmatrix}}_{\mathbf{\Phi}} \mathbf{d} + \underbrace{\begin{bmatrix} \mathbf{w}_{\text{MR}}^{(1)} \\ \mathbf{w}_{\text{MR}}^{(2)} \\ \vdots \\ \mathbf{w}_{\text{MR}}^{(M)} \end{bmatrix}}_{\mathbf{w}_{\text{MR}}} \tag{4.33}$$

where $\mathbf{w}_{\text{MR}} \approx \mathcal{DV}\ (\mathbf{0},\, N_0 \mathbf{\Phi})$. Since the equivalent channel matrix $\mathbf{\Phi}$ is not diagonal, the optimum receiver has to search over all possible valid sequences, which entails $2^{MK \log_2 |\mathcal{A}|}$ possibilities, and this is prohibitively complex. As an alternative, the received samples of each user are first transformed to the frequency domain as

$$\mathcal{W}_{\text{MR}}^{(m)} \triangleq \mathcal{G}_K \mathbf{v}_{\text{MR}}^{(m)} = \int_{u=1}^{M} \mathcal{N}_{\text{MR}}^{(m,u)} \mathcal{F}^{(u)} + \mathcal{Z}_{\text{MR}}^{(m)}, \tag{4.34}$$

where $\mathcal{N}_{\text{MR}}^{(m,u)} = \mathcal{G}_K \mathbf{\Phi}^{(m,u)} \mathcal{G}_K^H$, $\mathcal{F}_u = \mathcal{G}_K \mathbf{d}_u$, and $\mathcal{Z}_{\text{MR}}^{(m)}$ is an AWGN vector of zero-mean and covariance matrix

$$\mathbb{E}\left\{\mathcal{Z}_{\text{MR}}^{(m)} \mathcal{Z}_{\text{MR}}^{(u)H}\right\} = N_0 \mathcal{N}_{\text{MR}}^{(m,u)}. \tag{4.35}$$

Then (4.34) can be conveniently re-written as

$$\mathcal{W}_{\text{MR}}^{(m)} = \mathcal{N}_{\text{MR}}^{(m)} \mathcal{F} + \mathcal{Z}_{\text{MR}}^{(m)}, \tag{4.36}$$

where

$$\mathcal{N}_{\text{MR}}^{(m)} = \left(\mathcal{N}_{\text{MR}}^{(m,1)} \quad \mathcal{N}_{\text{MR}}^{(m,2)} \quad \cdots \quad \mathcal{N}_{\text{MR}}^{(m,M)}\right) \tag{4.37a}$$

$$\mathcal{F} = \left(\mathcal{F}^{(1)T} \quad \mathcal{F}^{(2)T} \quad \cdots \quad \mathcal{F}^{(M)T}\right)^T. \tag{4.37b}$$

Arranging the received samples from all users in the frequency domain in a vector form yields

$$\underbrace{\begin{pmatrix} \mathcal{W}_{\text{MR}}^{(1)} \\ \mathcal{W}_{\text{MR}}^{(2)} \\ \vdots \\ \mathcal{W}_{\text{MR}}^{(M)} \end{pmatrix}}_{\mathcal{W}_{\text{MR}}} = \underbrace{\begin{pmatrix} \mathcal{N}_{\text{MR}}^{(1)} \\ \mathcal{N}_{\text{MR}}^{(2)} \\ \vdots \\ \mathcal{N}_{\text{MR}}^{(M)} \end{pmatrix}}_{\mathcal{H}_{\text{MR}}} \mathcal{F} + \underbrace{\begin{pmatrix} \mathcal{Z}_{\text{MR}}^{(1)} \\ \mathcal{Z}_{\text{MR}}^{(2)} \\ \vdots \\ \mathcal{Z}_{\text{MR}}^{(M)} \end{pmatrix}}_{\mathcal{W}_{\text{MR}}} \tag{4.38}$$

where $\mathcal{Z}_{\text{MR}} \approx \mathcal{CN}(\mathbf{0}, N_0 \mathcal{N}_{\text{MR}})$. Then, the frequency samples from all users are jointly equalized using the MMSE equalizer

$$\mathcal{H}_{\text{MR}} = \mathcal{N}_{\text{MR}}^H \left(\mathcal{N}_{\text{MR}} \mathcal{N}_{\text{MR}}^H + N_0 \mathcal{N}_{\text{MR}}\right)^{-1}. \tag{4.39}$$

The frequency-equalized samples can be written as

$$\begin{aligned} \{_{\text{MR}} &= \mathcal{H}_{\text{MR}} \mathcal{W}_{\text{MR}} \\ &= \left(\{_{\text{MR}}^{(1)T} \quad \{_{\text{MR}}^{(2)T} \quad \cdots \quad \{_{\text{MR}}^{(M)T}\right)^T, \end{aligned} \tag{4.40}$$

where $\{_{\text{MR}}^{(m)}$ corresponds to the frequency-equalized signal of the mth user, for $m = 1, 2, \ldots, M$. Finally, the frequency-equalized signal of each user is transformed back to the time domain as $\mathbf{z}_{\text{MR}}^{(m)} = \mathcal{G}_K^H \{_{\text{MR}}^{(m)}$ where symbol-by-symbol detection takes place.

Table 4.2: Multiple Access SC-FDE vs. OFDM Complexity

	IFFT	FFT	Integrator	Frequency Shifter	Resampler.
SR-OFDM	M	M	0	N	N
MR-OFDM	M	NM	0	NM	NM
SR-SC-FDE	M	M	NM	N	N
MR-SC-FDE	M	M	NM	NM	NM

Receiver Implementation

It can be shown that the kth sample of the mth user at the nth antenna is given by

$$v_{\mathrm{MR},k}^{(m,n)} = \int P_k^{(m,n)*}(t)\, v^{(n)}(t)\, dt. \tag{4.41}$$

Substituting (4.23) into (4.41) gives

$$\begin{aligned} v_{\mathrm{MR},k}^{(m,n)} &= \sum_{p=1}^{N_p^{(m,n)}} H_p^{(m,n)*} \int \Big(v^{(m,n)}(t)\, g\Big) t[1+a^{(m)}] \quad kT_s \quad \tau_p^{(m,n)} \Big(\\ &= \sum_{p=1}^{N_p^{(m,n)}} \frac{H_p^{(m,n)*}}{1+a^{(m)}} \int_{kT_s+\tau_p^{(m,n)}}^{(k+1)T_s+\tau_p^{(m,n)}} v^{(m,n)} \Big) \frac{t}{1+a^{(m)}} \int dt, \end{aligned} \tag{4.42}$$

where $v^{(m,n)}(t) = v^{(n)}(t)\, e^{-j2\pi f_c t a^{(m)}}$. We can see from (4.42) that, for each receive antenna, there is an MR pre-processor consisting of M SC-branches, one for each user (See Fig. 4.2). Each branch performs frequency shifting, resampling, and integration. Even though frequency shifting and resampling are the same among all receive antennas, they are duplicated for each antenna to facilitate parallel processing. On the other hand, in the equalization part, M FFT blocks are required to transform the received samples of all users to the frequency domain, where MMSE equalization is performed, and M IFFT blocks to transform the frequency-equalized samples of each user to the time domain where detection takes place. The complexity comparison with MR-OFDM is shown in Table 4.2. Note that in OFDM [8] , the FFT operation is a part of the pre-precessor and not a part of equalization, which means that MN FFT blocks are required at the receiver side, while one IFFT block is deployed at each user, i.e., a total of M IFFT blocks.

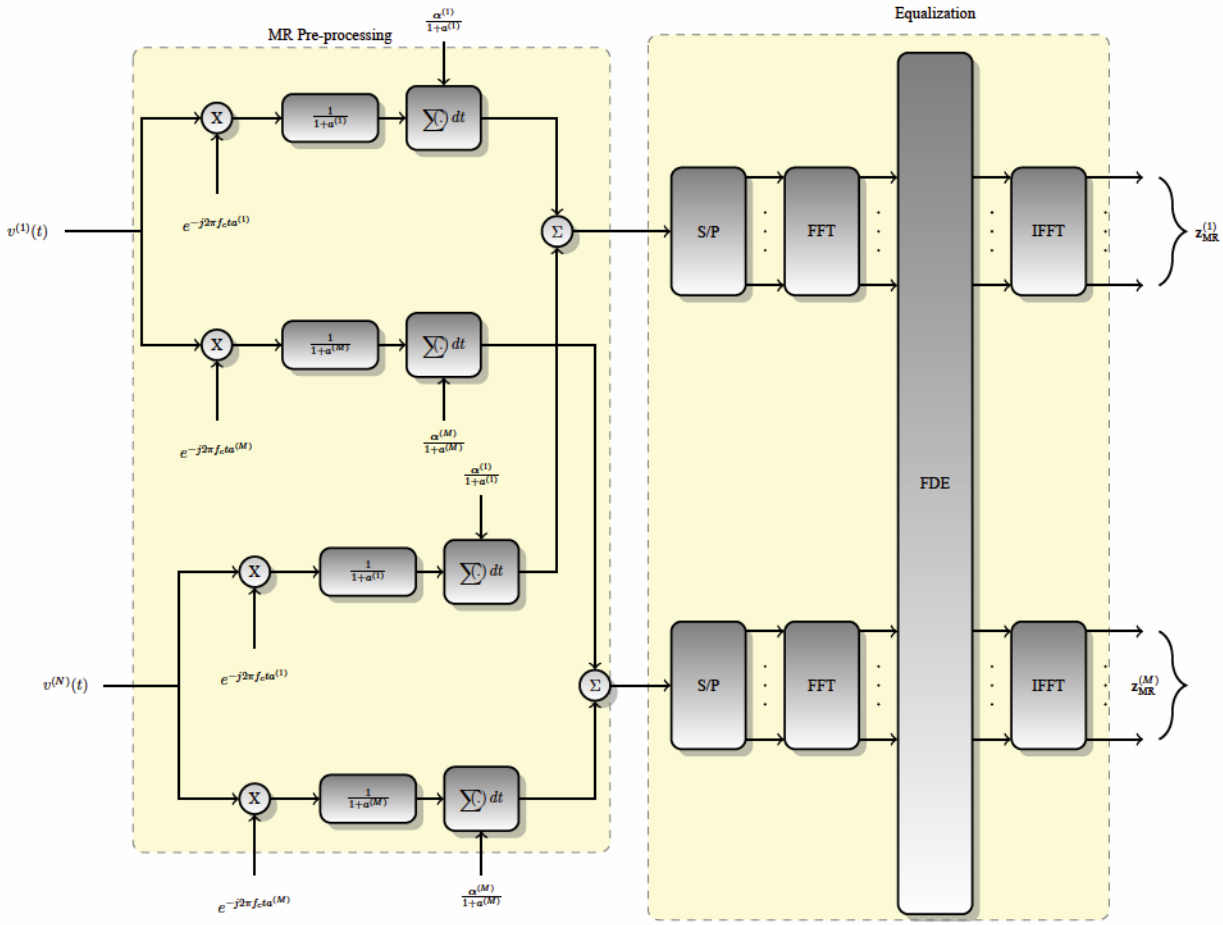

Figure 4.2: Block diagram of MAC MR-SC-FDE receiver.

4.2.2 SR Receivers

To further simplify the receiver structure, the channels of all users are approximated such that all of them have a common Doppler scaling factor, a_{SR}, which is assumed to be the arithmetic average of all Doppler scaling factors. Thus, the received signal at the nth receive antenna is approximated as

$$\begin{aligned} v^{(n)}(t) &\to \int_{m=1}^{M} \int_{k=0}^{K-1} d_k^{(m)} \, f_k^{(m,n)}(t) + w^{(n)}(t) \\ &= \int_{m=1}^{M} \mathbf{f}^{(m,n)}(t) \, \mathbf{d}^{(m)} + w^{(n)}(t) \\ &= \mathbf{f}^{(n)}(t) \, \mathbf{d} + w^{(n)}(t), \end{aligned} \tag{4.43}$$

where

$$\mathbf{f}^{(n)}(t) = \Big)\mathbf{f}^{(1,n)}(t) \quad \times\times\times \quad \mathbf{f}^{(M,n)}(t)\Big(\tag{4.44a}$$

$$\mathbf{f}^{(m,n)}(t) = \Big)f_0^{(m,n)}(t) \quad \times\times\times \quad f_{K-1}^{(m,n)}(t)\Big(, \tag{4.44b}$$

and

$$f_k^{(m,n)}(t) = \int_{p=1}^{N_p^{(m,n)}} H_p^{(m,n)}\, e^{j2\pi f_c a_{\text{SR}}}\, g\ \ t[1+a_{\text{SR}}] \quad kT_s \quad \tau_p^{(m,n)}\big[\,, \tag{4.45}$$

for $n = 1, 2, \ldots, N$ and $m = 1, 2, \ldots, M$. Arranging the received signals from all receive antennas, we have

$$\mathbf{v}(t) \rightarrow \underbrace{\begin{pmatrix} \mathbf{f}^{(1)}(t) \\ \mathbf{f}^{(2)}(t) \\ \vdots \\ \mathbf{f}^{(N)}(t) \end{pmatrix}}_{\mathbf{f}(t)} \mathbf{d} + \mathbf{w}(t). \tag{4.46}$$

The received samples in this case are given by

$$\begin{aligned} \mathbf{v}_{\text{SR}} &= \Big[\ \ \mathbf{f}^H(t)\, \mathbf{v}(t)\, dt \\ &= \boldsymbol{\Psi}\mathbf{d} + \mathbf{w}_{\text{SR}}, \end{aligned} \tag{4.47}$$

where $\mathbf{w}_{\text{SR}} \approx \mathcal{DV}\ \ (\mathbf{0}, N_0\boldsymbol{\Omega}_{\text{SR}})$,

$$\boldsymbol{\Psi} = \Big[\ \ \mathbf{f}^H(t)\, \mathbf{P}(t)\, dt, \tag{4.48}$$

and

$$\boldsymbol{\Omega}_{\text{SR}} = \Big[\ \ \mathbf{f}^H(t)\, \mathbf{f}(t)\, dt. \tag{4.49}$$

The samples given by (4.47) are contaminated by ISI as in the case of MR receivers as well as Interuser Interference (IUI), implying that joint detection of all users' transmitted blocks is required for optimum detection. To alleviate the complexity of this joint detection, an MMSE FDE equalizer is used. To facilitate that, the received samples corresponding to the mth user

can be written as

$$\begin{aligned}\mathbf{v}_{\mathrm{SR}}^{(m)} &= \int_{t=1}^{N} \Big[\; \mathbf{f}^{(m,n)H}(t)\, \mathbf{v}(t)\, dt \\ &= \int_{t=1}^{M} \boldsymbol{\Psi}^{(m,u)}\, \mathbf{d}^{(u)} + \mathbf{w}_{\mathrm{SR}}^{(m)},\end{aligned} \tag{4.50}$$

where $\boldsymbol{\Psi}^{(m,u)} = \int_{n=1}^{N} \boldsymbol{\Psi}^{(m,u)}(n)$, $\mathbf{w}_{\mathrm{SR}}^{(m)} = \int_{n=1}^{N} \mathbf{w}_{\mathrm{SR}}^{(m,n)}$ and

$$\boldsymbol{\Psi}^{(m,u)}(n) = \Big[\; \mathbf{f}^{(m,n)H}(t)\, \mathbf{P}^{(u,n)}(t)\, dt \tag{4.51a}$$

$$\mathbf{w}_{\mathrm{SR}}^{(m,n)} = \Big[\; \mathbf{f}^{(m,n)H}(t)\, \mathbf{w}(t)\, dt. \tag{4.51b}$$

It can be shown that $\mathbf{w}_{\mathrm{SR}}^{(m,n)}$ is an AWGN vector of zero-mean and covariance matrix

$$\mathbb{E}\Big\{\mathbf{w}_{\mathrm{SR}}^{(m,n)} \mathbf{w}_{\mathrm{SR}}^{(u,n')H}\sqrt{} = \begin{cases} N_0 \boldsymbol{\Omega}_{\mathrm{SR}}^{(m,u)}(n) & n = n' \\ \mathbf{0} & n \neq n' \end{cases}, \tag{4.52}$$

where

$$\boldsymbol{\Omega}_{\mathrm{SR}}^{(m,u)}(n) = \Big[\; \mathbf{f}^{(m,n)H}(t)\, \mathbf{f}^{(u,n)}(t)\, dt, \tag{4.53}$$

and thus $\mathbf{w}_{\mathrm{SR}}^{(m)}$ is an AWGN vector of zero-mean and covariance matrix

$$\begin{aligned}\mathbb{E}\Big\{\mathbf{w}_{\mathrm{SR}}^{(m)} \mathbf{w}_{\mathrm{SR}}^{(u)H}\sqrt{} &= N_0 \boldsymbol{\Omega}_{\mathrm{SR}}^{(m,u)} \\ &= N_0 \int_{t=1}^{N} \boldsymbol{\Omega}_{\mathrm{SR}}^{(m,u)}(n).\end{aligned} \tag{4.54}$$

Then the received samples of each user is transformed to the frequency domain as

$$\begin{aligned}\mathcal{W}_{\mathrm{SR}}^{(m)} &\triangleq \mathcal{G}_K \mathbf{v}_{\mathrm{SR}}^{(m)} \\ &= \int_{t=1}^{M} \mathcal{N}_{\mathrm{SR}}^{(m,u)} \mathcal{F}^{(u)} + \mathcal{Z}_{\mathrm{SR}}^{(m)} \\ &= \mathcal{N}_{\mathrm{SR}}^{(m)}\, \mathcal{F} + \mathcal{Z}_{\mathrm{SR}}^{(m)}.\end{aligned} \tag{4.55}$$

It is straightforward to show that $\mathcal{N}_{\text{SR}}^{(m,u)} = \mathcal{G}_K \mathbf{\Psi}^{(m,u)} \mathcal{G}_K^H$, and $\mathcal{Z}_{\text{SR}}^{(m)}$ is an AWGN vector of zero-mean and covariance matrix

$$\mathbb{E}\left\{\mathcal{Z}_{\text{SR}}^{(m)} \mathcal{Z}_{\text{SR}}^{(u)H}\right\} = N_0 \mathbf{\Xi}_{\text{SR}}^{(m,u)}, \tag{4.56}$$

where $\mathbf{\Xi}_{\text{SR}}^{(m,u)} = \mathcal{G}_K \mathbf{\Omega}_{\text{SR}}^{(m,u)} \mathcal{G}_K^H$ and

$$\mathcal{N}_{\text{SR}}^{(m)} = \left[\mathcal{N}_{\text{SR}}^{(m,1)} \cdots \mathcal{N}_{\text{SR}}^{(m,M)}\right]. \tag{4.57}$$

Arranging the frequency domain received samples of all users yields

$$\underbrace{\begin{bmatrix} \mathcal{W}_{\text{SR}}^{(1)} \\ \mathcal{W}_{\text{SR}}^{(2)} \\ \vdots \\ \mathcal{W}_{\text{SR}}^{(M)} \end{bmatrix}}_{\mathcal{V}_{\text{SR}}} = \underbrace{\begin{bmatrix} \mathcal{N}_{\text{SR}}^{(1)} \\ \mathcal{N}_{\text{SR}}^{(2)} \\ \vdots \\ \mathcal{N}_{\text{SR}}^{(M)} \end{bmatrix}}_{\mathcal{H}_{\text{SR}}} \mathcal{F} + \underbrace{\begin{bmatrix} \mathcal{Z}_{\text{SR}}^{(1)} \\ \mathcal{Z}_{\text{SR}}^{(2)} \\ \vdots \\ \mathcal{Z}_{\text{SR}}^{(M)} \end{bmatrix}}_{\mathcal{W}_{\text{SR}}}. \tag{4.58}$$

Here, $\mathcal{Z}_{\text{SR}} \approx \mathcal{CN}(\mathbf{0}, N_0 \mathbf{\Xi}_{\text{SR}})$ such that

$$\mathbf{\Xi}_{\text{SR}} = \begin{bmatrix} \mathbf{\Xi}_{\text{SR}}^{(1,1)} & \mathbf{\Xi}_{\text{SR}}^{(1,2)} & \cdots & \mathbf{\Xi}_{\text{SR}}^{(1,M)} \\ \mathbf{\Xi}_{\text{SR}}^{(2,1)} & \mathbf{\Xi}_{\text{SR}}^{(2,2)} & \cdots & \mathbf{\Xi}_{\text{SR}}^{(2,M)} \\ \vdots & \vdots & \ddots & \vdots \\ \mathbf{\Xi}_{\text{SR}}^{(M,1)} & \mathbf{\Xi}_{\text{SR}}^{(M,2)} & \cdots & \mathbf{\Xi}_{\text{SR}}^{(M,M)} \end{bmatrix}. \tag{4.59}$$

The MMSE FDE in this case is give by

$$\mathcal{H}_{\text{SR}} = \mathcal{N}_{\text{SR}}^H \left[\mathcal{N}_{\text{SR}} \mathcal{N}_{\text{SR}}^H + N_0 \mathbf{\Xi}_{\text{SR}}\right]^{-1}. \tag{4.60}$$

Finally, after jointly equalizing the received signals of all users as $\{_{\text{SR}} = \mathcal{H}_{\text{SR}} \mathcal{W}_{\text{SR}}$, the corresponding equalized samples of the mth user which are denoted by $\{_{\text{SR}}^{(m)}$ are transformed back to the time domain as $\mathbf{z}_{\text{SR}}^{(m)} = \mathcal{G}_K^H \{_{\text{SR}}^{(m)}$ where symbol-by-symbol detection is performed.

Receiver Implementation

It can be shown that the kth sample of the mth user at the nth antenna in this case is given by

$$v_{\mathrm{SR},k}^{(m,n)} = \int f_k^{(m,n)*}(t)\, v^{(n)}(t)\, dt. \tag{4.61}$$

Substituting (4.45) into (4.61) we have

$$\begin{aligned} v_{\mathrm{SR},k}^{(m,n)} &= \sum_{p=1}^{N_p^{(m,n)}} H_p^{(m,n)*} \int v_{\mathrm{SR}}^{(n)}(t)\, g_k \quad t[1+a_{\mathrm{SR}}] \quad kT_s \quad \tau_p^{(m,n)}[\\ &= \sum_{p=1}^{N_p^{(m,n)}} \frac{H_p^{(m,n)*}}{1+a_{\mathrm{SR}}} \int_{kT_s+\tau_p^{(m,n)}}^{(k+1)T_s+\tau_p^{(m,n)}} v_{\mathrm{SR}}^{(n)}\Big) \frac{t}{1+a_{\mathrm{SR}}} \Big[\, dt, \end{aligned} \tag{4.62}$$

where $v_{\mathrm{SR}}^{(n)}(t) = v^{(n)}(t)\, e^{-j2\pi f_c t a_{\mathrm{SR}}}$. Then the received samples corresponding to the mth user are given by

$$v_{\mathrm{SR},k}^{(m)} = \sum_{n=1}^{N} v_{\mathrm{SR},k}^{(m,n)}. \tag{4.63}$$

From (4.62) and (4.63) we can see that for each receive antenna there is one SR pre-processor that performs frequency shifting and resampling by the Doppler scaling factor a_{SR}. Since this is common among all branches, it can be implemented serially (in case one branch is used for all antenna) or in parallel (in case multiple branches are used one for each antenna). On the other hand, in the equalization part, M FFT blocks are required to transform the received samples of all users to the frequency domain, where MMSE equalization is performed, and M IFFT blocks to transform the frequency-equalized samples of each user to the time domain for final detection. The complexity comparison with SR-OFDM is shown in Table 4.2. As shown in the table, both SR-SC-FDE and SR-OFDM have the same complexity in terms of the required number of FFT and IFFT blocks.

4.3 Numerical Results

In this section, we illustrate the performance of the two scenarios discussed above via simulations. The following parameters are assumed: BPSK signaling over the bandwidth 30 34 KHz. The channel parameters for P2P are shown in Fig. 4.3. Each path is labeled by its

Doppler scaling factor. For the MAC scenario, the channel parameters are shown in Fig. 4.7, where $M = N = 2$, and $a^{(1)} = 0.0018$, and $a^{(2)} = \quad 0.0012$.

In Figs. 4.4 and Fig. 4.5, the magnitude of the ICI coefficients at the output of the MR and SR pre-processed SC signals after being transformed to the frequency domain are shown, respectively, for the case of P2P scenario. The SR factor used is set to zero, which is the scaling factor of the strongest path [53]. It can be seen that when MR pre-processing is used in the time domain, the channel power is concentrated around the main diagonal in the frequency domain. This implies that MR pre-processing in the time domain decreases the time variation significantly. In time invariant channels, the channel power is concentrated *exactly* in the main diagonal. On the other hand, when SR pre-processing is used in the time domain, the channel power in scattered, which implies that SR pre-processing is less effective than MR in handling time variation.

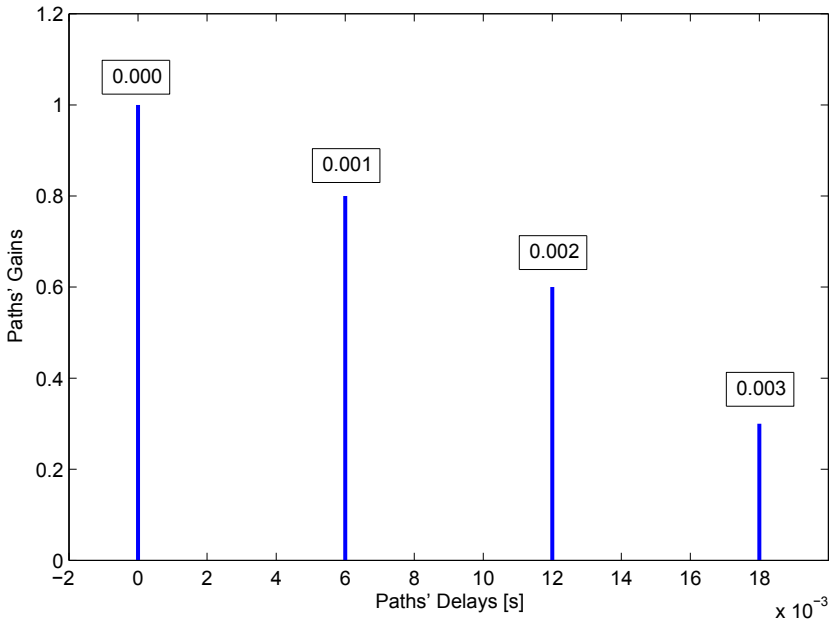

Figure 4.3: The channel parameters of P2P SC-FDE system.

In Fig. 4.6, the uncoded ABER vs. SNR is shown for P2P SR/MR-SC-FDE for $K = 512$. Also, the corresponding curves are shown for OFDM systems. First, we observe that MR-SC-FDE outperforms SR-SC-FDE significantly. However, these improvements come at the expense of more hardware complexity. This improvement in performance can be justified by examining Figs. 4.4 and 4.5 where we can observe that the ICI in the frequency domain after SR is longer in depth and larger in magnitude than that after MR. Also, MR-SC-FDE

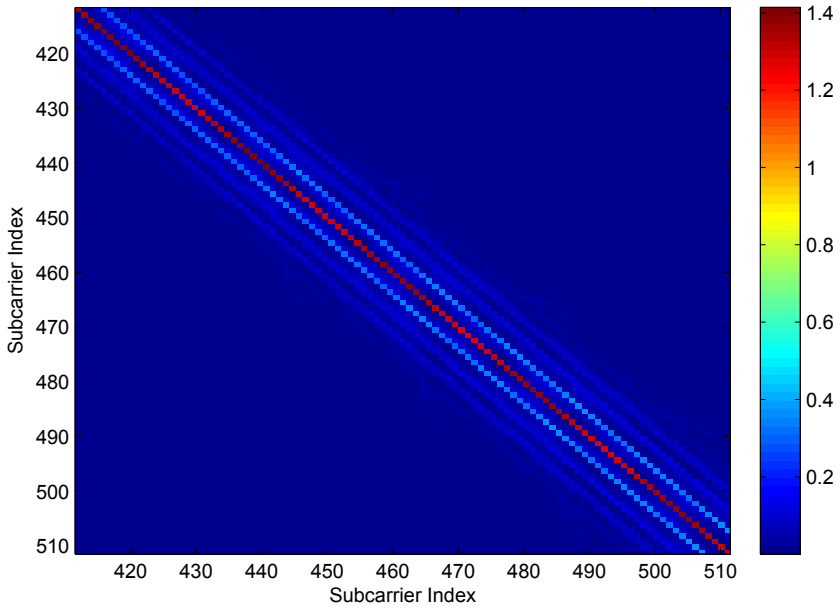

Figure 4.4: Absolute value of the ICI coefficients after transforming the MR pre-processed SC signal to the frequency domain.

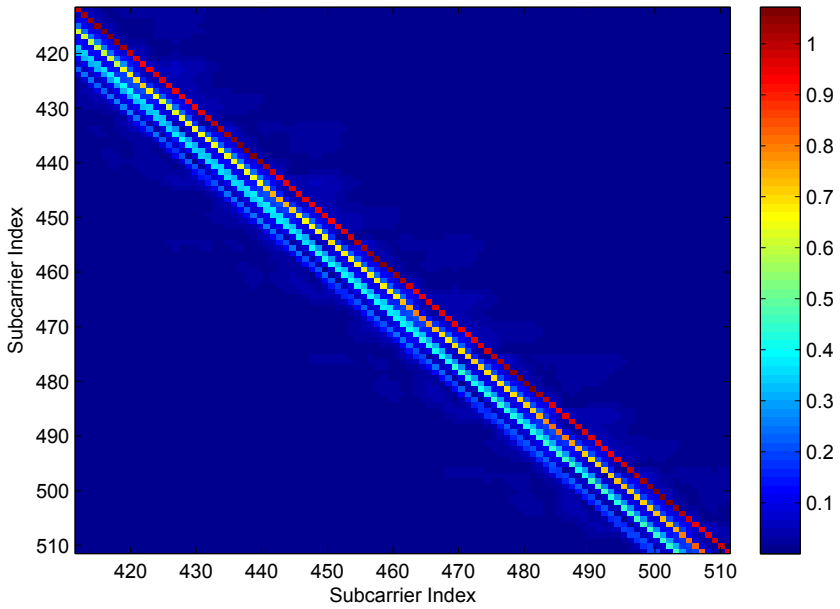

Figure 4.5: Absolute value of the ICI coefficients after transforming the SR pre-processed SC signal to the frequency domain.

outperforms MR-OFDM with lower overall complexity, where N_p FFT block are required in OFDM, whereas just one FFT block is required in MR-SC-FDE. Which makes SC-FDE a strong candidate and competitor to OFDM over UWA channels.

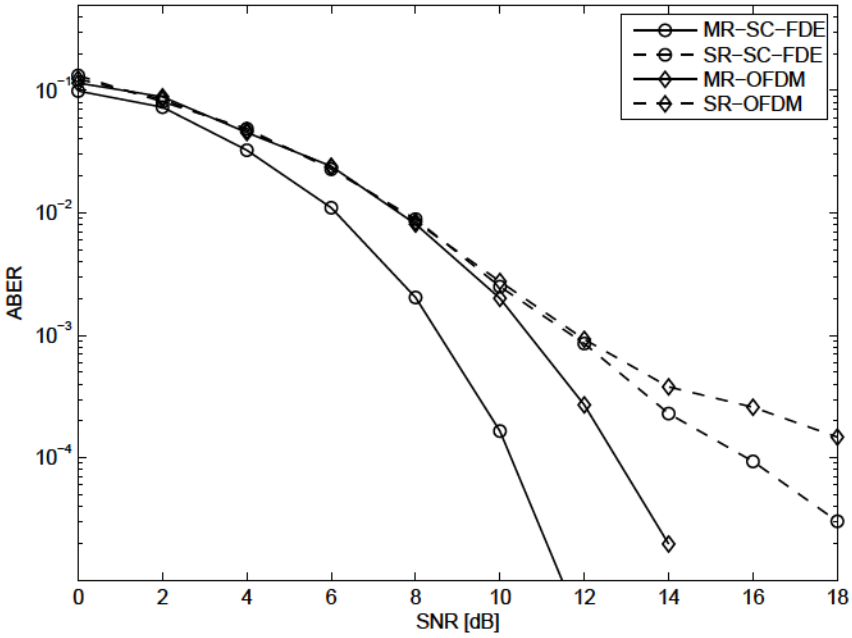

Figure 4.6: ABER of P2P SC-FDE for $K = 512$ and channel parameters shown in Fig. 4.3.

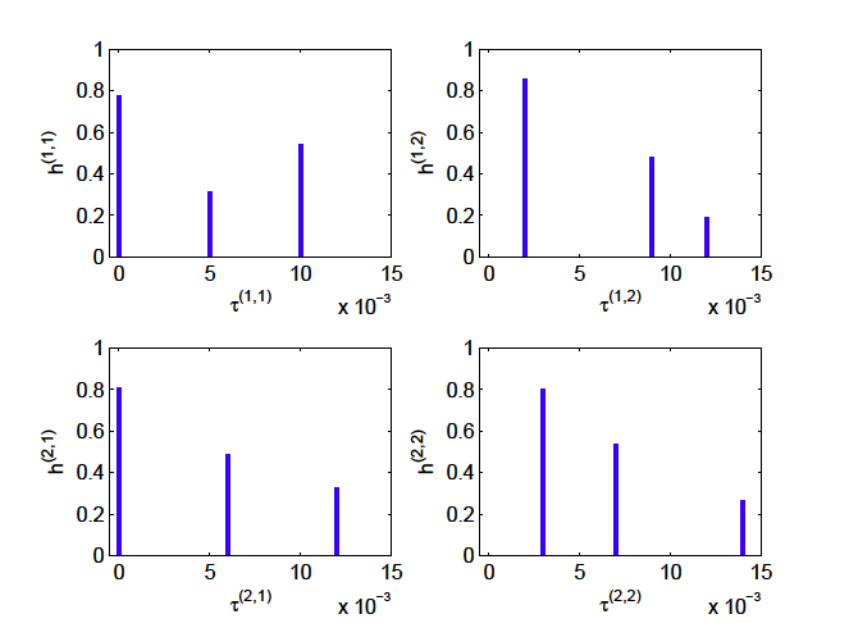

Figure 4.7: The channel parameters of a MA SC-FDE.

In Fig. 4.8, the uncoded ABER vs. SNR is shown for the MAC SR/MR-SC-FDE system for $K = 256$ when the total power is equally divided among the users. The SR factor used, a_{SR}, is the arithmetic average of $a^{(1)}$ and $a^{(2)}$. Also the corresponding curves for OFDM are shown in the same figure. The same observations as in P2P can be made, where MR outperforms SR

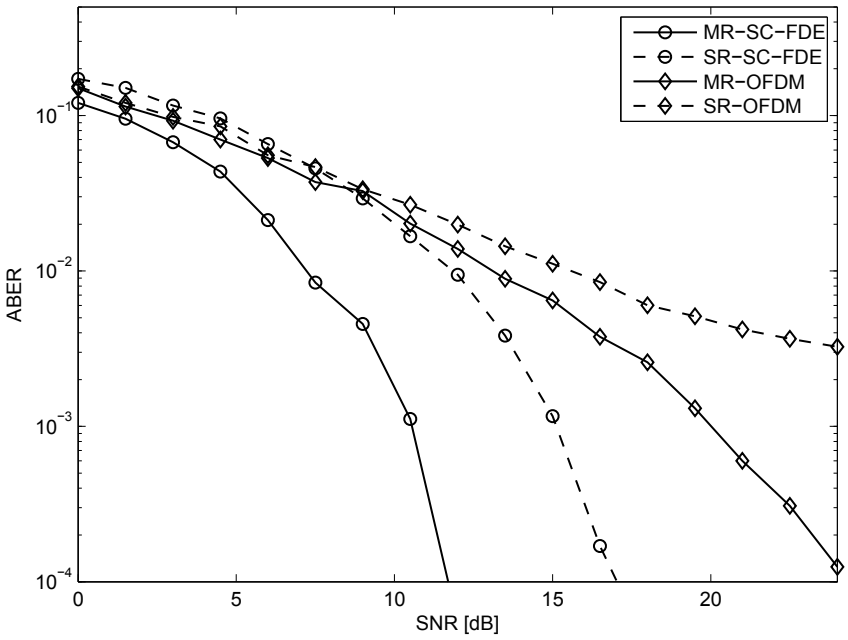

Figure 4.8: ABER of MA SC-FDE with $M = N = 2$, $a^{(1)} = 1.8 \sim 10^{-3}$, $a^{(2)} = \quad 1.2 \sim 10^{-3}$, and $a^{(0)} = \frac{a^{(1)}+a^{(2)}}{2}$. The channels's gains and delays are shown in Fig. 4.7.

in SC-FDE, and MR-SC-FDE outperforms MR-OFDM when uncoded transmission is used. Also, in this scenario, the hardware complexity of MR-SC-FDE is less than that of MR-OFDM, where $M = 2$ FFT blocks are required for the former while $MN = 4$ FFT blocks are required for the latter, while both SR-SC-FDE and SR-OFDM have the same overall complexity in terms of FFT and IFFT blocks required in the system.

4.4 Conclusions

In this chapter we proposed the use of SC signaling as an alternative to OFDM over UWA channels, since it was shown in the literature that the former is better in handling time variation than the latter. We studied two scenarios for SC signaling. The first one is a P2P system over path-specific Doppler scaling model, and the second is a MAC (or multi-user MIMO) system where multiple single-antenna users communicate with a multiple-antenna common receiver. In both cases, the optimum receiver is derived, and the structure and implementation of the receiver was revealed. In particular, it was shown that, as it is the case in OFDM, the optimum receiver consists of two components: MR and MLSD. Different from OFDM, however, is the structure of the MR pre-processor. In particular, it was shown that a MR consist of multiple

branched, and each branch performs frequency shifting, resampling, and integration for each path/user. In other words, FFT operation is no longer a part of the pe-processor. To alleviate the complexity problem of the optimum equalizer, we proposed to use MMSE in the frequency domain. To facilitate this, the samples at the output of the pre-processor were first transformed to the frequency domain by means of FFT operation, where joint MMSE FDE is done, and then transformed back to the time domain by means of IFFT operation where symbol-by-symbol detection became feasible. Also, SR pre-processor was proposed to further reduce the complexity of the receiver. Numerical studies for uncoded ABER showed that MR outperforms SR in both scenarios, as expected, at higher complexity requirement. It was shown that the ICI at the output of the MR pre-processor in the frequency-domain is concentrated around the main diagonal, unlike the case for SR where ICI is dispersed, indicating that the residual time variation at the output of SR is higher than that of MR. Also, a comparison with OFDM was shown, which revealed that SC-FDE is more Doppler-resilient at lower complexity requirement. This reduction in complexity comes from the fact that FFT is not a part of the pre-processor, but a part of the equalizer.

Chapter 5

Relay-Assisted OFDM UWA Communication

In this chapter we consider relay-assisted OFDM systems, where one or more AF relays deployed between the transmitter and the receiver in order to increase the bandwidth efficiency and/or reliability of the system. To address the problem of bandwidth scarcity in UWA channels, we study TWR system [64, 65, 66], where two sources exchange their information via one AF relays. Since UWA channels are multipath channels, we consider D-STBC system to enhance the reliability, where one source communicated with one destination via the help of two AF relays, and Alamouti's Space-Time Block Coding (STBC) [67, 68] in distributed fashion is used in the second hop between the relays and the destination. Finally, we combine TWR and D-STBC schemes to extract both schemes' advantages simultaneously. In all cases, path-specific Doppler model is assumed for the underlying channels.

5.1 TWR OFDM Systems

A TWR system consists of two sources S_1 and S_2 that exchange information via the help of one AF relay R. The CIR between node X and node Y is given by

$$h_{XY}(t;\tau) = \int_{p=1}^{N_{XY}} h_{XY,p}\,\delta\left(\tau \quad \tau_{XY,p}(t)\right) \tag{5.1}$$

where N_{XY} is the number of paths, $\tau_{XY,p}(t) = \tau_{XY,p} \quad a_{XY,p}t$ [7], and $a_{XY,p}$, $h_{XY,p}$ and $\tau_{XY,p}$ are the the pth path's Doppler scaling factor, gain and delay, respectively, and any node could

be a transmitter and receiver, i.e, $\}X, Y|\ \ /\ \}S_1, S_2, R|$, where $X \neq Y$[1]. The transmission is divided into two phases: MAC phase in which S_1 and S_2 transmit their respective signals simultaneously over the same bandwidth to R, and Broadcast (BC) phase in which R broadcasts the processed received signal from the MAC phase to both destinations (the sources of the MAC phase). We consider CP-OFDM transmission, where the passband transmitted signal froth the mth source is given by

$$s_m(t) = \mathcal{A}\Big\}\int_{k=0}^{K-1} d_{m,k}\, e^{j2\pi f_k t}\, R\,(t)\Big(, \tag{5.2}$$

where $d_{m,k}$ is the kth symbol of the OFDM block transmitted from the mth source. The operators, other parameters and functions are defined as in Section 3.

The passband received signal at R is given by

$$y_R(t) = \mathcal{A}\Big\}\int_{m=1}^{2}\int_{k=0}^{K-1} d_{m,k}\int_{p=1}^{N_{S_mR}} h_{S_mR}\, e^{j2\pi f_k([1+a_{S_mR}]t-\tau_{S_mR})}\, R\,([1+a_{S_mR}]t \quad \tau_{S_mR})\Big(+ n_{R(t)}, \tag{5.3}$$

where $n_R(t)$ is an AWGN process of zero mean and PSD $N_0/2$. The equivalent baseband received signal at R can be written as

$$v_R(t) = \int_{m=1}^{2}\int_{k=0}^{K-1} d_{m,k}\, P_{S_mR,k}(t) + w_R(t), \tag{5.4}$$

where $w_R(t)$ is an AWGN process of zero mean and PSD N_0 and

$$P_{S_mR,k}(t) = \int_{p=1}^{N_{S_mR}} H_{S_mR,p}\,(f_k)\; e^{j2\pi f_c t a_{S_mR}}\, e^{j2\pi \frac{k}{T} t[1+a_{S_mR}]}\, R\,(t[1+a_{S_mR}] \quad \tau_{S_mR,p})\,, \tag{5.5}$$

where $H_{XY,p}\,(f_k) = h_{XY,p}\, e^{-j2\pi f_k \tau_{XY,p}}$. The received samples corresponding to the mth source at R are given by

$$\begin{aligned} v_{S_mR,k} &= \Big[\ \ P^*_{S_mR,k}(t)\, v_R(t)\, dt \\ &= \int_{l=1}^{2}\int_{l=0}^{K-1} d_{u,l}\Phi^{S_mR,k}_{S_uR,l} + w_{S_mR,k},\ \ k = 0,\, 1\ldots, K \quad 1, \end{aligned} \tag{5.6}$$

where

[1]In this and subsequent systems, it is assumed that the channel parameters remain fixed until the transmission from the source to the destination is completed. Also, it is assume that the Channel State Information (CSI) is perfectly known at each node to perform the necessary processing.

$$\Phi_{WZ,l}^{XY,k} = \int P_{XY,k}^{*}(t)\, P_{WZ,l}(t)\, dt \tag{5.7a}$$

$$w_{XY,k} = \int P_{XY,k}^{*}(t)\, w_Y(t)\, dt. \tag{5.7b}$$

Arranging the samples (5.6) in vector-matrix form we have

$$\mathbf{v}_{S_mR} = \sum_{u=1}^{2} \mathbf{\Phi}_{S_uR}^{S_mR}\mathbf{d}_u + \mathbf{w}_{S_uR}, \quad i = 1, 2, \tag{5.8}$$

where $\left[\mathbf{\Phi}_{S_uR}^{S_mR}\right]_{k,l} = \Phi_{S_uR,l}^{S_mR,k}$, $\mathbf{d}_u = [d_{u,0}\ \ d_{u,1} \cdots d_{u,K-1}]^T$ and $\mathbf{w}_{S_mR}$ is an AWGN vector of zero-mean and covariance matrix

$$\mathbb{E}\left\{\mathbf{w}_{S_mR}\mathbf{w}_{S_uR}^{H}\right\} = N_0\mathbf{\Phi}_{S_uR}^{S_mR}. \tag{5.9}$$

Then R adds the received samples of both sources together as

$$\begin{aligned}\mathbf{v}_R &= \sum_{u=1}^{2} \mathbf{v}_{S_mR} \\ &= \sum_{u=1}^{2} \mathbf{\Phi}_{S_uR}\mathbf{d}_u + \mathbf{w}_R,\end{aligned} \tag{5.10}$$

where $\mathbf{\Phi}_{S_uR} = \sum_{m=1}^{2} \mathbf{\Phi}_{S_uR}^{S_mR}$, $\mathbf{w}_R \approx \mathcal{DV}\ (\mathbf{0}, N_0\mathbf{\Omega}_R)$ and $\mathbf{\Omega}_R = \sum_{u=1}^{2} \mathbf{\Phi}_{S_uR}$. To whiten the noise, (5.10) is left-multiplied by $\mathbf{\Omega}_R^{-1/2}$ results in

$$\tilde{\mathbf{v}}_R = \sum_{u=1}^{2} \tilde{\mathbf{\Phi}}_{S_uR}\mathbf{d}_u + \tilde{\mathbf{w}}_R, \tag{5.11}$$

where $\tilde{\mathbf{\Phi}}_{S_uR} = \mathbf{\Omega}_R^{-1/2}\mathbf{\Phi}_{S_uR}$ and $\tilde{\mathbf{w}}_R \approx \mathcal{DV}\ (\mathbf{0}, N_0\mathbf{I}_K)$. Then the received signal (5.11) is left multiplied by the amplification matrix $\boldsymbol{\beta} = \text{diag}\,(\beta_0\, \beta_1, \ldots \beta_{K-1})$ to normalize the power where

$$\beta_k = \left[\sum_{u=1}^{2} \tilde{\mathbf{\Phi}}_{S_uR}\tilde{\mathbf{\Phi}}_{S_uR}^{H} + N_0\mathbf{I}_K\right]_{k,k}^{-1/2}. \tag{5.12}$$

Define $\mathbf{d}_R = \boldsymbol{\beta}\tilde{\mathbf{v}}_R = [d_{R,0}\ \ d_{R,1} \cdots d_{R,K-1}]^T$. In the BC phase, the baseband received signal

at S_m is then given by

$$v_{S_m}(t) = \int_{l=0}^{K-1} d_{R,k} P_{RS_m,k}(t) + w_{S_m}(t), \quad m = 1, 2, \tag{5.13}$$

and the corresponding received samples by

$$\begin{aligned} v_{RS_m,k} &= \Big[\; P^*_{RS_m,k}(t)\, v_{S_m}(t)\, dt \\ &= \int_{l=0}^{K-1} d_{R,l} \Phi^{RS_m,k}_{RS_m,l} + w_{RS_m,k}, \quad k = 0,\, 1 \ldots, K \quad 1. \end{aligned} \tag{5.14}$$

Arranging the samples (5.14) in vector-matrix form yields

$$\begin{aligned} \mathbf{v}_{RS_m} &= \mathbf{\Phi}^{RS_m}_{RS_m} \mathbf{d}_R + \mathbf{w}_{RS_m} \\ &= \int_{l=1}^{2} \mathbf{H}^{(m,u)} \mathbf{d}_u + \mathbf{w}_{S_m,\text{eq}}, \end{aligned} \tag{5.15}$$

where $\mathbf{H}^{(m,u)} = \mathbf{\Phi}^{RS_m}_{RS_m} \boldsymbol{\beta} \tilde{\mathbf{\Phi}}_{S_u R}$ and $\mathbf{w}_{S_m,\text{eq}} = \mathbf{\Phi}^{RS_m}_{RS_m} \boldsymbol{\beta} \tilde{\mathbf{w}}_R + \mathbf{w}_{RS_m}$. It is straightforward to show that $\mathbf{w}_{S_m,\text{eq}} \approx \mathcal{DV}\ (\mathbf{0}, N_0 \mathbf{\Omega}_{S_m})$ where $\mathbf{\Omega}_{S_m} = \mathbf{\Phi}^{RS_m}_{RS_m} \boldsymbol{\beta}\ \ \mathbf{\Phi}^{RS_m}_{RS_m} \boldsymbol{\beta} \big[^H + \mathbf{\Phi}^{RS_m}_{RS_m}$. Assuming perfect CSI is available at S_m, it then subtracts its own signal resulting in

$$\tilde{\mathbf{v}}_{RS_m} = \mathbf{H}^{(m,u)} \mathbf{d}_u + \mathbf{w}_{S_m,\text{eq}}, \text{ for } m, u = 1, 2 \text{ and } m \not\forall u. \tag{5.16}$$

The equivalent channel matrix $\mathbf{H}^{(m,u)}$ is, in general, not diagonal, and hence the optimal detector is the MLSD. Since the complexity of MLSD is prohibitive for practical scenarios, linear MMSE equalizer is used as an alternative, where it is given by

$$\mathbf{G}_{S_m} = \mathbf{H}^{(m,u)H} \big] \mathbf{H}^{(m,u)} \mathbf{H}^{(m,u)H} + N_0 \mathbf{\Omega}_{S_m} \big\{^{-1}. \tag{5.17}$$

Finally, symbol-by-symbol detection is performed on the equalized samples.

5.2 D-STBC OFDM System

In this section we consider D-STBC over UWA channels, where a source S communicates with D via the help of two AF relays R_1 and R_2. The CIR between nodes X and Y is given as in

(6.1), for $X \ / \ \}S, R_1, R_2|$ and $Y \ / \ \}R_1, R_2, D|$, and $X \nVdash Y$. The transmission is divided into two phases: in the first phase, S transmits two signals sequentially to both relays, and in the second phase the relays cooperate together to form STBC in distributed fashion. This implies that each phase consists of two time slots, where each time slot is the time necessary to transmit one OFDM symbol. In total, we are transmitting two signals over four time slots, which results in a bandwidth efficiency of $1/2$.

As previously, CP-OFDM is used to combat ISI, and the μth passband transmitted signal from S is given by

$$s^{(\mu)}(t) = \mathcal{A}\Re\left\{\sum_{k=0}^{K-1} d_k^{(\mu)}\, e^{j2\pi f_k t}\, R(t)\right\}, \quad t \ / \ \} \ \ T_g, T|\,, \tag{5.18}$$

where $d_k^{(\mu)}$ is the kth symbol of the μth block, for $k = 0, 1, \ldots, K \quad 1$, and $\mu = 1, 2$. The remaining parameters were defined previously.

The baseband received signal due to $s^{(\mu)}(t)$ at R_j is given by

$$v_{R_j}^{(\mu)}(t) = \sum_{k=0}^{K-1} d_k^{(\mu)}\, P_{SR_j,k}(t) + w_{R_j}^{(\mu)}(t), \tag{5.19}$$

and the noise-whitened received samples due to $s^{(\mu)}(t)$ at R_j are given by

$$\tilde{\mathbf{v}}_{R_j}^{(\mu)} = \tilde{\mathbf{\Phi}}_{SR_j}^{SR_j}\mathbf{d}^{(\mu)} + \tilde{\mathbf{w}}_{R_j}^{(\mu)}, \tag{5.20}$$

where $\tilde{\mathbf{w}}_{R_j}^{(\mu)} \approx \mathcal{CN}\ (\mathbf{0}, N_0\mathbf{I}_K)$, $\tilde{\mathbf{\Phi}}_{SR_j}^{SR_j} = \left(\mathbf{\Phi}_{SR_j}^{SR_j}\right)^{1/2}$, $\left]\mathbf{\Phi}_{SR_j}^{SR_j}\right\{_{k,l} = \Phi_{SR_j,l}^{SR_j,k}$. Then the samples (5.20) are left multiplied by the matrix $\boldsymbol{\beta}_{R_j} = \text{diag}\ \ \beta_{R_j,0}\ \ \beta_{R_j,1} \times\times\beta_{R_j,K-1}\big[$ to form the signal $\mathbf{d}_{R_j}^{(\mu)} = \boldsymbol{\beta}_{R_j}\tilde{\mathbf{v}}_{R_j}^{(\mu)} = [d_{R_j,0}^{(\mu)}\ \ d_{R_j,1}^{(\mu)} \ldots d_{R_j,K-1}^{(\mu)}]^T$ where

$$\beta_{R_j,k} = \left]\tilde{\mathbf{\Phi}}_{SR_j}^{SR_j}\right)^{H}\tilde{\mathbf{\Phi}}_{SR_j}^{SR_j} + N_0\mathbf{I}_K\Big[_{k,k}^{-1/2}. \tag{5.21}$$

Define the μth passband signal transmitted from R_j as[2]

$$s_{R_j}^{(\mu)*}(t) = \mathcal{A}\Re\left\{\sum_{k=0}^{K-1} d_{R_j,k}^{(\mu)*}\, e^{j2\pi f_k t}\, R\,(t)\right\}. \tag{5.22}$$

[2]Here we define the signal with the complex conjugation $(.)^*$ to indicate that conjugation affects only the transmitted symbols.

The two passband received signals at D due to D-STBC transmission from the relays are then given by

$$y_D^{(1)}(t) = h_{R_1D}(t;\tau) \star s_{R_1}^{(1)}(t) + h_{R_2D}(t;\tau) \star s_{R_2}^{(2)*}(t) + n_D^{(1)}(t) \tag{5.23a}$$

$$y_D^{(2)}(t) = \quad h_{R_1D}(t;\tau) \star s_{R_1}^{(2)}(t) + h_{R_2D}(t;\tau) \star s_{R_2}^{(1)*}(t) + n_D^{(2)}(t), \tag{5.23b}$$

where $n_D^{(\mu)}(t)$ is an AWGN of zero-mean and PSD $N_0/2$ for $\mu = 1, 2$. The corresponding baseband signals can be shown to be

$$v_D^{(1)}(t) = \int_{k=0}^{K-1} \Big] d_{R_1,k}^{(1)} P_{R_1D,k}(t) + d_{R_2,k}^{(2)*} P_{R_2D,k}(t) \Big\{ + w_D^{(1)}(t) \tag{5.24a}$$

$$v_D^{(2)}(t) = \int_{k=0}^{K-1} \Big] \quad d_{R_1,k}^{(2)} P_{R_1D,k}(t) + d_{R_2,k}^{(1)*} P_{R_2D,k}(t) \Big\{ + w_D^{(2)}(t), \tag{5.24b}$$

where $w_D^{(\mu)}(t)$ is an AWGN of zero-mean and PSD N_0 for $\mu = 1, 2$.

The received samples corresponding to R_j from the received signal $v_D^{(1)}(t)$ are given by

$$\begin{aligned} v_{R_jD,k}^{(1)} &= \Big[\quad P_{R_jD,k}^*(t)\, v_D^{(1)}(t)\, dt \\ &= \int_{l=0}^{K-1} \Big] \Phi_{R_1D,l}^{R_jD,k}\, d_{R_1,l}^{(1)} + \Phi_{R_2D,l}^{R_jD,k}\, d_{R_2,l}^{(2)*} \Big\{ + w_{R_jD,k}^{(1)}, \end{aligned} \tag{5.25}$$

where

$$w_{R_jD,k}^{(\mu)} = \Big[\quad P_{R_jD,k}^*(t) w_D^{(\mu)}(t), \;\; i, j, \mu = 1, 2. \tag{5.26}$$

Arranging the samples (5.25) in a vector-matrix form yields

$$\mathbf{v}_{R_jD}^{(1)} = \mathbf{\Phi}_{R_1D}^{R_jD}\, \mathbf{d}_{R_1}^{(1)} + \mathbf{\Phi}_{R_2D}^{R_jD}\, \mathbf{d}_{R_2}^{(2)*} + \mathbf{w}_{R_jD}^{(1)}. \tag{5.27}$$

Similarly, the received samples corresponding to R_j from the received signal $v_D^{(2)}(t)$ can be shown to be

$$\mathbf{v}_{R_jD}^{(2)} = \quad \mathbf{\Phi}_{R_1D}^{R_jD}\, \mathbf{d}_{R_1}^{(2)} + \mathbf{\Phi}_{R_2D}^{R_jD}\, \mathbf{d}_{R_2}^{(1)*} + \mathbf{w}_{R_jD}^{(2)}, \;\; j = 1, 2. \tag{5.28}$$

Define $\mathbf{H}_{1j} = \mathbf{\Phi}_{R_1D}^{R_jD} \boldsymbol{\beta}_{R_1} \tilde{\mathbf{\Phi}}_{SR_1}^{SR_1}$, $\mathbf{H}_{2j} = \mathbf{\Phi}_{R_2D}^{R_jD} \boldsymbol{\beta}_{R_2}^* \tilde{\mathbf{\Phi}}_{SR_2}^{SR_2*}$, $\mathbf{G}_{1j} = \mathbf{\Phi}_{R_1D}^{R_jD} \boldsymbol{\beta}_{R_1}$ and $\mathbf{G}_{2j} = \mathbf{\Phi}_{R_2D}^{R_jD} \boldsymbol{\beta}_{R_2}^*$,

the destination D then arrange the received sample as

$$\underbrace{\begin{pmatrix} \mathbf{v}^{(1)}_{R_1D,k} \\ \mathbf{v}^{(1)}_{R_2D,k} \\ \mathbf{v}^{(2)*}_{R_1D,k} \\ \mathbf{v}^{(2)*}_{R_2D,k} \end{pmatrix}}_{\mathbf{v}} = \underbrace{\begin{pmatrix} \mathbf{H}_{11} & \mathbf{H}_{21} \\ \mathbf{H}_{12} & \mathbf{H}_{22} \\ \mathbf{H}^*_{21} & \mathbf{H}^*_{11} \\ \mathbf{H}^*_{22} & \mathbf{H}^*_{12} \end{pmatrix}}_{\mathbf{\Phi}} \underbrace{\begin{pmatrix} \mathbf{d}^{(1)} \\ \mathbf{d}^{(2)*} \end{pmatrix}}_{\mathbf{d}} + \mathbf{w}, \tag{5.29}$$

where

$$\mathbf{w} = \begin{pmatrix} \mathbf{G}_{11}\tilde{\mathbf{w}}^{(1)}_{R_1} + \mathbf{G}_{21}\tilde{\mathbf{w}}^{(2)*}_{R_2} + \mathbf{w}^{(1)}_{R_1D} \\ \mathbf{G}_{12}\tilde{\mathbf{w}}^{(1)}_{R_1} + \mathbf{G}_{22}\tilde{\mathbf{w}}^{(2)*}_{R_2} + \mathbf{w}^{(1)}_{R_2D} \\ \mathbf{G}^*_{11}\tilde{\mathbf{w}}^{(2)*}_{R_1} + \mathbf{G}^*_{21}\tilde{\mathbf{w}}^{(1)}_{R_2} + \mathbf{w}^{(2)*}_{R_1D} \\ \mathbf{G}^*_{12}\tilde{\mathbf{w}}^{(2)*}_{R_1} + \mathbf{G}^*_{22}\tilde{\mathbf{w}}^{(1)}_{R_2} + \mathbf{w}^{(2)*}_{R_2D}. \end{pmatrix} \tag{5.30}$$

It can be shown that $\mathbf{w}$ is an AWGN vector of zero-mean and covariance matrix

$$\mathbb{E}\{\mathbf{w}\mathbf{w}^H\} = N_0 \underbrace{\begin{pmatrix} \mathbf{\Omega}_{1,1} & \mathbf{\Omega}_{1,2} & \mathbf{0}_K & \mathbf{0}_K \\ \mathbf{\Omega}_{2,1} & \mathbf{\Omega}_{2,2} & \mathbf{0}_K & \mathbf{0}_K \\ \mathbf{0}_K & \mathbf{0}_K & \mathbf{\Omega}^*_{1,1} & \mathbf{\Omega}^*_{1,2} \\ \mathbf{0}_K & \mathbf{0}_K & \mathbf{\Omega}^*_{2,1} & \mathbf{\Omega}^*_{2,2} \end{pmatrix}}_{\mathbf{\Omega}} \tag{5.31}$$

where $\mathbf{0}_K$ is the all-zero $K \sim K$ matrix and

$$\mathbf{\Omega}_{i,j} = \mathbf{G}_{1i}\mathbf{G}^H_{1j} + \mathbf{G}_{2i}\mathbf{G}^H_{2j} + \mathbf{\Phi}^{R_iD}_{R_jD}. \tag{5.32}$$

Finally, the signal (5.28) is equalized using the MMSE equalizer

$$\mathbf{G} = \mathbf{\Phi}^H\left[\mathbf{\Phi}\mathbf{\Phi}^H + N_0\mathbf{\Omega}\right]^{-1}, \tag{5.33}$$

before symbol-by-symbol detection as

$$\hat{\mathbf{d}}^{(1)} = \text{Dec}\{\mathbf{z}(0:K \quad 1)\} \tag{5.34a}$$

$$\hat{\mathbf{d}}^{(2)} = \text{Dec}\{\mathbf{z}^*(K:2K \quad 1)\}, \tag{5.34b}$$

where Dec(.) denotes the decoding operation.

5.3 TWR-D-STBC OFDM Systems

In this section TWR and D-STBC techniques are combined together, in an attempt to increase the bandwidth efficiency using the former and the reliability using the latter. The system consists of two sources S_1 and S_2 that exchange information via the help of two AF relays R_1 and R_2. The CIR between nodes X and Y is given by (6.1) for $\}X, Y|\ /\ \}S_1, S_2, R_1, R_2|$ and $X \nVdash Y$. The transmission is divided into two phases: TWR phase, and D-STBC phase. In TWR phase, each source transmits two signals sequentially, and the two sources transmit simultaneously over the same bandwidth. In D-STBC the two relays cooperate to realize STBC from the received signals in distributed fashion.

The μth passband transmitted signal from S_m is given by

$$s_m^{(\mu)}(t) = \mathcal{A} \Big\} \int_{k=0}^{K-1} d_{S_m,k}^{(\mu)} \, e^{j2\pi f_k t} \, R\,(t) \Big(, \tag{5.35}$$

where $d_{S_m,k}^{(\mu)}$ is the kth transmitted symbol of the μth block from the mth source, for $m, \mu = 1, 2$.

Following the same procedure as in Section 5.1, it can be shown that the noise-whitened received samples at R_j due to the transmission of the μth signal from both sources simultaneously are given by

$$\tilde{\mathbf{v}}_{R_j}^{(\mu)} = \int_{u=1}^{2} \tilde{\mathbf{\Phi}}_{S_u R_j} \mathbf{d}_u^{(\mu)} + \tilde{\mathbf{w}}_{R_j}^{(\mu)}, \tag{5.36}$$

where $\tilde{\mathbf{w}}_{R_j}^{(\mu)} \approx \mathcal{DV}\ (\mathbf{0}, N_0 \mathbf{I}_K)$, $\tilde{\mathbf{\Phi}}_{S_u R_j} = \mathbf{\Omega}_{R_j}^{-1/2} \mathbf{\Phi}_{S_u R_j}$, $\mathbf{\Omega}_{R_j} = \int_{u=1}^{2} \mathbf{\Phi}_{S_u R_j}$, $\mathbf{\Phi}_{S_u R_j} = \int_{m=1}^{2} \mathbf{\Phi}_{S_u R_j}^{S_m R_j}$, where $\Big] \mathbf{\Phi}_{S_u R_j}^{S_m R_j} \Big\{_{k,l} = \Phi_{S_u R_j, l}^{S_m R_j, k}$.

Then R_j normalizes the power of the received signals as $\mathbf{d}_{R_j}^{(\mu)} = \boldsymbol{\beta}_{R_j} \tilde{\mathbf{v}}_{R_j}^{(\mu)}$ where $\boldsymbol{\beta}_{R_j} = \text{diag}\ \ \beta_{R_j,0}\ \ \beta_{R_j,1} \ldots \beta_{R_j,K-1} \big[$ and

$$\beta_{R_j,k} = \Big] \int_{u=1}^{2} \tilde{\mathbf{\Phi}}_{S_u R_j} \tilde{\mathbf{\Phi}}_{S_u R_j}^H + N_0 \mathbf{I}_K \Big\{_{k,k}^{-1/2} . \tag{5.37}$$

The μth passband transmitted signal from R_j is given by

$$s_{R_j}^{(\mu)*}(t) = \mathcal{A} \Big\} \int_{k=0}^{K-1} d_{R_j,k}^{(\mu)*} \, e^{j2\pi f_k t} \, R\,(t) \Big(, \tag{5.38}$$

where $d_{R_j,k}^{(\mu)}$ is the kth symbol of the vector $\mathbf{d}_{R_j}^{(\mu)}$. Following the same procedure as in Section

5.2, the received samples at S_m corresponding to R_j are given by

$$\mathbf{v}^{(1)}_{R_jS_m} = \mathbf{\Phi}^{R_jS_m}_{R_1S_m}\mathbf{d}^{(1)}_{R_1} + \mathbf{\Phi}^{R_jS_m}_{R_2S_m}\mathbf{d}^{(2)*}_{R_2} + \mathbf{w}^{(1)}_{R_jS_m} \tag{5.39a}$$

$$\mathbf{v}^{(2)}_{R_jS_m} = \mathbf{\Phi}^{R_jS_m}_{R_1S_m}\mathbf{d}^{(2)}_{R_1} + \mathbf{\Phi}^{R_jS_m}_{R_2S_m}\mathbf{d}^{(2)*}_{R_2} + \mathbf{w}^{(2)}_{R_jS_m}. \tag{5.39b}$$

Substituting for $\mathbf{d}^{(\mu)}_{R_j}$, and arranging the received samples as the following

$$\underbrace{\begin{pmatrix}\mathbf{v}^{(1)}_{R_1S_m}\\ \mathbf{v}^{(1)}_{R_2S_m}\\ \mathbf{v}^{(2)*}_{R_1S_m}\\ \mathbf{v}^{(2)*}_{R_1S_m}\end{pmatrix}}_{\mathbf{v}_{S_m}} = \sum_{u=1}^{2} \underbrace{\begin{pmatrix}\mathbf{H}^{(m,u)}_{11} & \mathbf{H}^{(m,u)}_{21}\\ \mathbf{H}^{(m,u)}_{12} & \mathbf{H}^{(m,u)}_{22}\\ \mathbf{H}^{(m,u)*}_{21} & \mathbf{H}^{(m,u)*}_{11}\\ \mathbf{H}^{(m,u)*}_{22} & \mathbf{H}^{(m,u)*}_{12}\end{pmatrix}}_{\mathbf{\Phi}^{(m,u)}} \underbrace{\begin{pmatrix}\mathbf{d}^{(1)}_{u}\\ \mathbf{d}^{(2)*}_{u}\end{pmatrix}}_{\mathbf{d}_u} + \underbrace{\begin{pmatrix}\mathbf{w}^{(1)}_{R_1S_m,\text{eq}}\\ \mathbf{w}^{(1)}_{R_2S_m,\text{eq}}\\ \mathbf{w}^{(2)*}_{R_1S_m,\text{eq}}\\ \mathbf{w}^{(2)*}_{R_2S_m,\text{eq}}\end{pmatrix}}_{\mathbf{w}_{S_m}} \tag{5.40}$$

where

$$\mathbf{H}^{(m,u)}_{1j} = \underbrace{\mathbf{\Phi}^{R_jS_m}_{R_1S_m}\beta_{R_1}}_{\mathbf{G}^{(m)}_{1j}}\tilde{\mathbf{\Phi}}_{S_uR_1} \tag{5.41a}$$

$$\mathbf{H}^{(m,u)}_{2j} = \underbrace{\mathbf{\Phi}^{R_jS_m}_{R_2S_m}\beta^*_{R_2}}_{\mathbf{G}^{(m)}_{2j}}\tilde{\mathbf{\Phi}}^{*}_{S_uR_2}. \tag{5.41b}$$

It can be shown that $\mathbf{w}_{S_m} \approx \mathcal{DN}\left(\mathbf{0}, N_0\mathbf{\Omega}^{(m)}\right)$ where

$$\mathbf{\Omega}^{(m)} = \begin{pmatrix}\mathbf{\Omega}^{(m)}_{1,1} & \mathbf{\Omega}^{(m)}_{1,2} & \mathbf{0}_K & \mathbf{0}_K\\ \mathbf{\Omega}^{(m)}_{2,1} & \mathbf{\Omega}^{(m)}_{2,2} & \mathbf{0}_K & \mathbf{0}_K\\ \mathbf{0}_K & \mathbf{0}_K & \mathbf{\Omega}^{(m)*}_{1,1} & \mathbf{\Omega}^{(m)*}_{1,2}\\ \mathbf{0}_K & \mathbf{0}_K & \mathbf{\Omega}^{(m)*}_{2,1} & \mathbf{\Omega}^{(m)*}_{2,2}\end{pmatrix} \tag{5.42}$$

and

$$\mathbf{\Omega}^{(m)}_{ij} = \mathbf{G}^{(m)}_{1i}\mathbf{G}^{(m)H}_{1j} + \mathbf{G}^{(m)}_{2i}\mathbf{G}^{(m)H}_{2j} + \mathbf{\Phi}^{R_iS_m}_{R_jS_m}. \tag{5.43}$$

Assuming perfect CSI is available at S_m, it then subtracts its own signal as

$$\begin{aligned}\tilde{\mathbf{v}}_{S_m} =& \mathbf{v}_{S_m} - \mathbf{\Phi}^{(m,m)}\mathbf{d}_m\\ =& \mathbf{\Phi}^{(m,u)}\mathbf{d}_u + \mathbf{w}_{S_m}, \quad m,u = 1,2 \text{ and } m \neq u,\end{aligned} \tag{5.44}$$

which is then equalized using the MMSE equalizer

$$\mathbf{G}_{S_m} = \mathbf{\Phi}^{(m,u)H} \Big] \mathbf{\Phi}^{(m,u)} \mathbf{\Phi}^{(m,u)H} + N_0 \mathbf{\Omega}^{(m)} \Big\{^{-1}, \tag{5.45}$$

before symbol-by-symbol detection is performed.

5.4 Numerical Results

In this section the ABER performance of the above discussed systems is illustrated for the following parameters: BPSK signaling over the bandwidth 30 34 KHz, $K = 512$ and the channel parameters are shown in Figs. 6.1 and 6.2. Each path is labeled by its own Doppler scaling factor. For the reciprocal channels[3], the channel parameters are assumed to remain the same except for the Doppler scaling factor, where the sign is reversed. Also, for comparison reasons, a total power constraint in each system is assumed, where this power is uniformly distributed among all transmitting nodes.

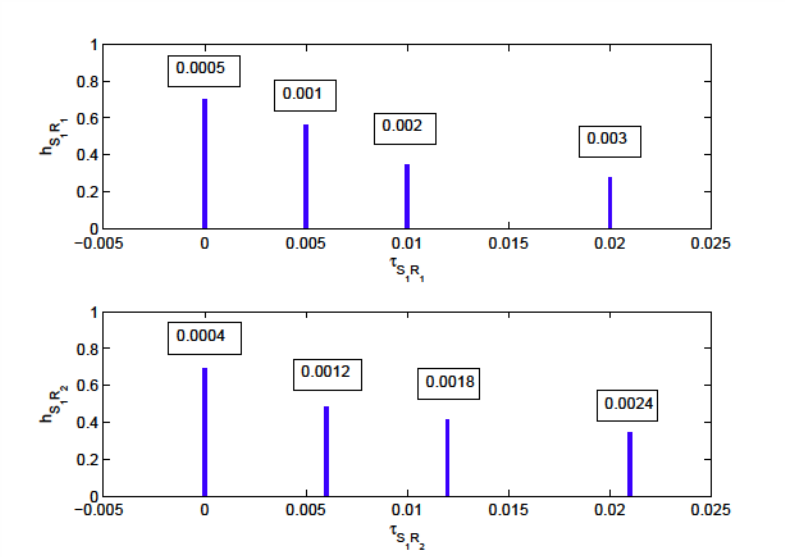

Figure 5.1: The $S_1 \simeq R_1, R_2$ channels' parameters.

In Figs. 5.3 and 5.4 the ABER vs. SNR is shown for MR/SR-TWR-OFDM systems through R_1 and R_2, respectively, at S_1. The SR factor at R_j is taken as $a_{R_j} = \frac{a_{S_1R_j}(1)+a_{S_2R_j}(1)}{2}$, while at S_m as $a_{S_m} = a_{R_jS_m}(1)$, for $j, m = 1, 2$. We observe that both techniques have the nearly the same performance at low SNRs, this is because this range of SNR is the noise limited range. On

[3]The reciprocal channel between X and Y is the channel between Y and X.

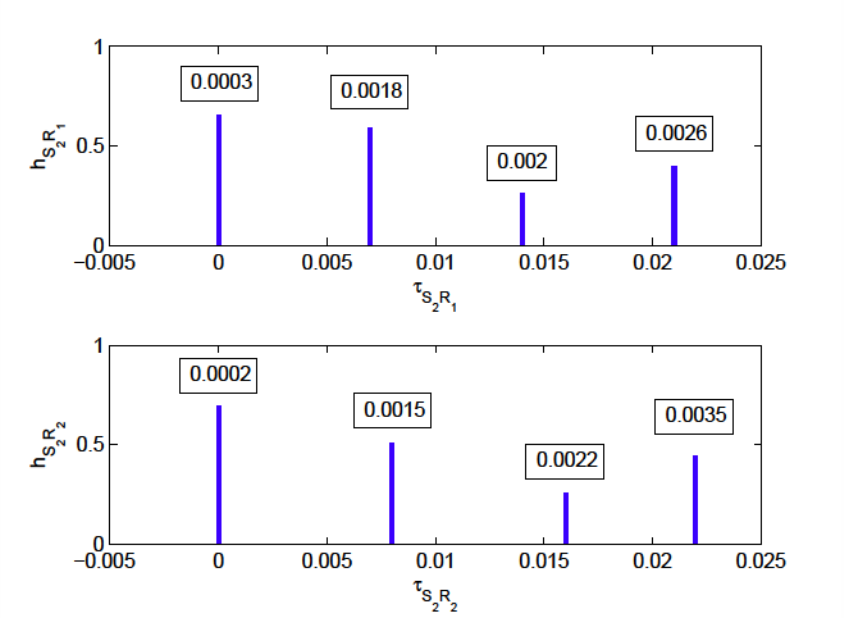

Figure 5.2: The $S_2 \simeq R_1, R_2$ channels' parameters.

the other hand, at high SNRs, which is described as ICI-limited area, MR receivers significantly outperform their SR counterparts, which means that MR receivers are better in handling the ICI effect of the time variation of the channels. However, this gain in performance comes at the expense of more hardware complexity.

In Fig. 5.5 the ABER vs. SNR is shown for MR/SR-D-STBC-OFDM systems at S_1, i.e., the source node is S_2. In this case the SR factor at R_j is taken as $a_{R_j} = a_{S_2R_j}(1)$ and at D as $a_D = \frac{a_{R_1S_1}(1)+a_{R_2S_1}(1)}{2}$. The same observations as in the TWR case can be noticed. However, compared to MR-TWR, the MR-ABER of D-STBC is better. In particular, the ABER of 10^{-4} is achieved at 33.5 dB and 29.5 dB through R_1 and R_2, respectively, while it is achieved at about 24 dB for D-STBC. This performance gain comes at the expense of decreased bandwidth efficiency, where it is one in the case of of TWR while it is $1/2$ in the case of D-STBC.

In Fig. 5.6 the ABER vs. SNR is shown for MR/SR-TWR-D-STBC-OFDM systems at S_1. The SR factors at R_j and S_m in this case are taken as $a_{R_j} = \frac{a_{S_1R_j}(1)+a_{S_2R_j}(1)}{2}$ and $a_{S_m} = \frac{a_{R_1S_m}(1)+a_{R_2S_m}(1)}{2}$, respectively, for $j, m = 1, 2$. In this case the discrepancy between MR and SR occurs from the very beginning, which implies that the ICI is very severe. May be this is because that there are intra-block (from within the same block) and inter-block (from the other block) interference in both phases: in the TWR at the relays, and in the D-STBC at the destinations, where as in TWR and D-STBC systems we have intra-block and inter-block interferences in one phase, while in the other phase there is only inter-block interference. Compared to both

TWR and D-STBC, TWR-D-STBC outperforms the former while it is outperformed by the latter in terms of ABER. In terms of bandwidth efficiency, TWR-D-STBC has the same bandwidth efficiency as TWR which is double the bandwidth efficiency of D-STBC. However, this joint enhanced performance and bandwidth efficiency comes at the expense of more hardware complexity.

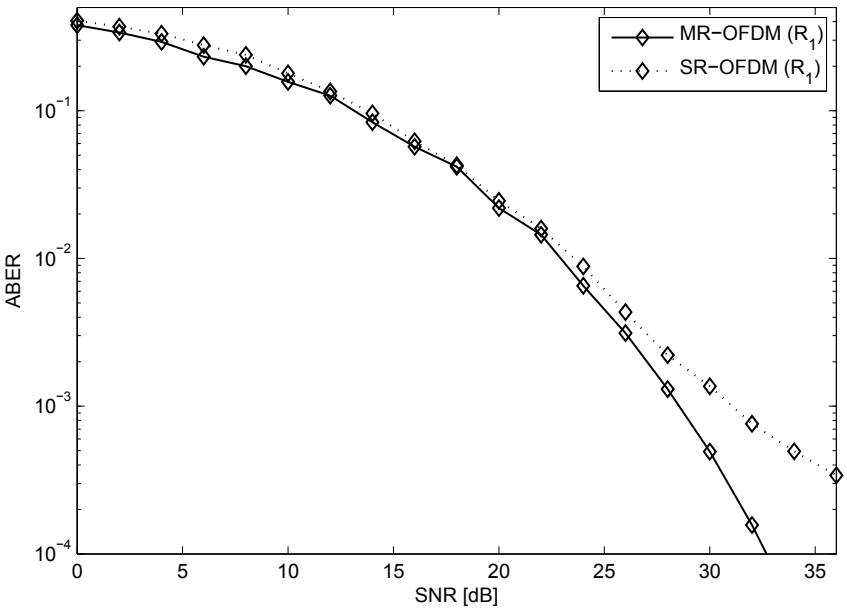

Figure 5.3: ABER of TWR OFDM for $K = 512$ through R_1.

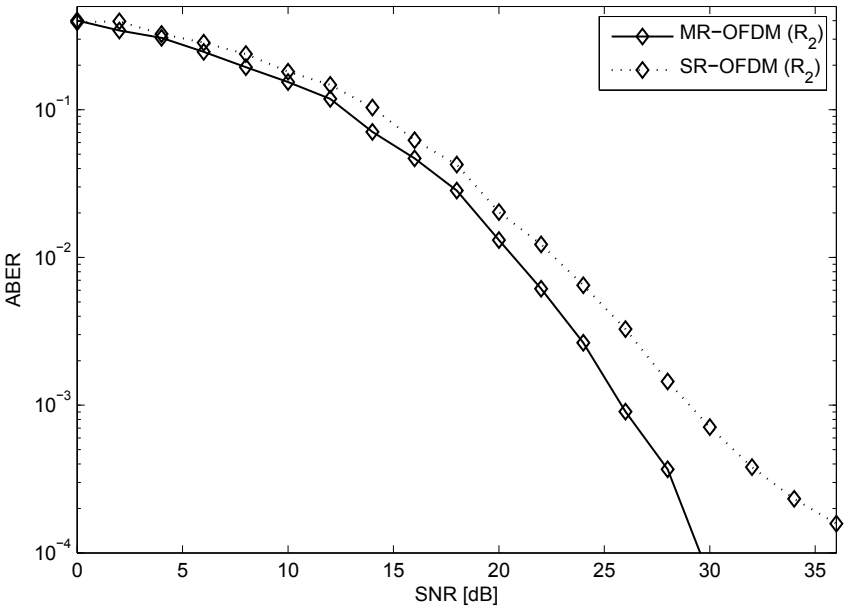

Figure 5.4: ABER of TWR OFDM for $K = 512$ through R_2.

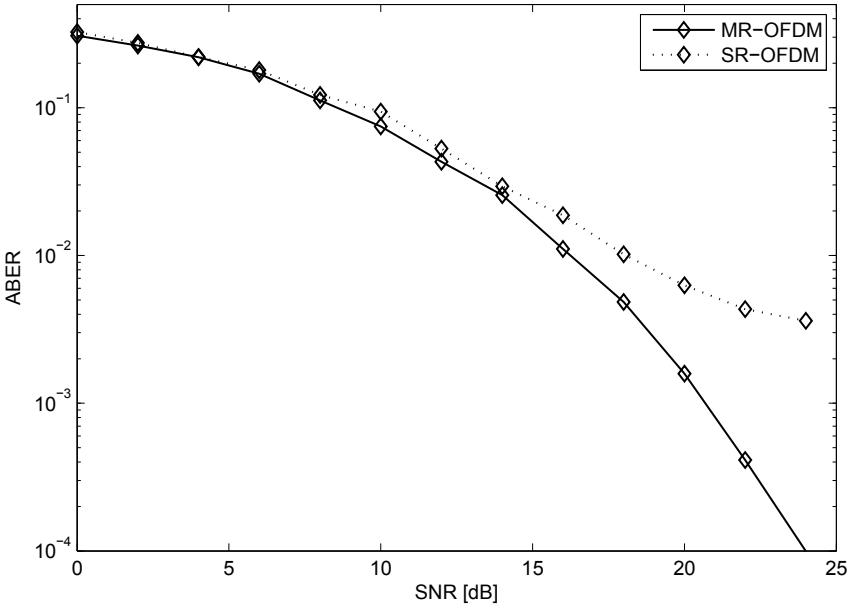

Figure 5.5: ABER of D-STBC OFDM for $K = 512$.

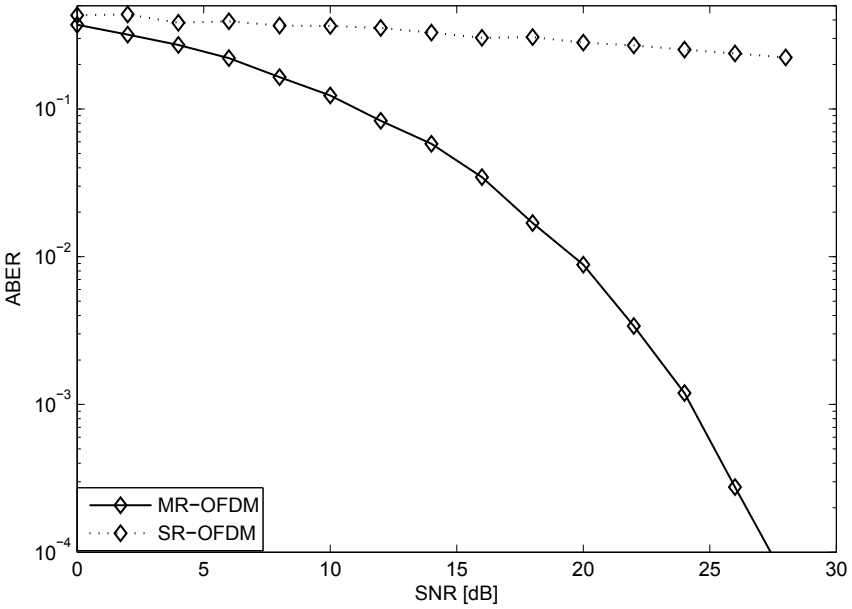

Figure 5.6: ABER of TWR-D-STBC OFDM for $K = 512$.

Table 5.1: Simulation Parameters for the Rician Channels

Channel Parameters	$S_1 \quad R_1$	$S1 \quad R_2$	$S_2 \quad R_1$	$S_2 \quad R_2$
Paths' Delays (ms)	$[0 \;\; 5 \;\; 10]$	$[0 \;\; 6 \;\; 12]$	$[0 \;\; 7 \;\; 14]$	$[0 \;\; 8 \;\; 16]$
Doppler Scales ($\sim 10^{-3}$)	$[0 \;\; 1 \;\; 12]$	$[0 \;\; 1.2 \;\; 1.8]$	$[0 \;\; 1.2 \;\; 2]$	$[0 \;\; 1.1 \;\; 1.7]$

Next we test the proposed techniques over Rician channels, where the parameters are given as in Table 5.1 for $K = 256$. The channel coefficients are generated as in [62]. The mean vector of all links is taken as $\boldsymbol{\mu} = [1 \;\; 0.5 \;\; 0.1]^T$, and the Rician factor is 20 dB. The SR factor at each node is taken as the arithmetic average of all scaling factors from the transmitters to that node. For the reciprocal channels only the sign of the scaling factors are reversed. We can seen again in Figs. 5.7, 5.8, 5.9, and 5.10 that MR outperforms SR at higher complexity. Also, deploying one more relay and using D-STBC is still beneficial in both D-STBC and TWR-D-STBC systems, where some spatial diversity can be extracted as seen in Fig. 5.11 where a comparison of all techniques are depicted when MR is employed.

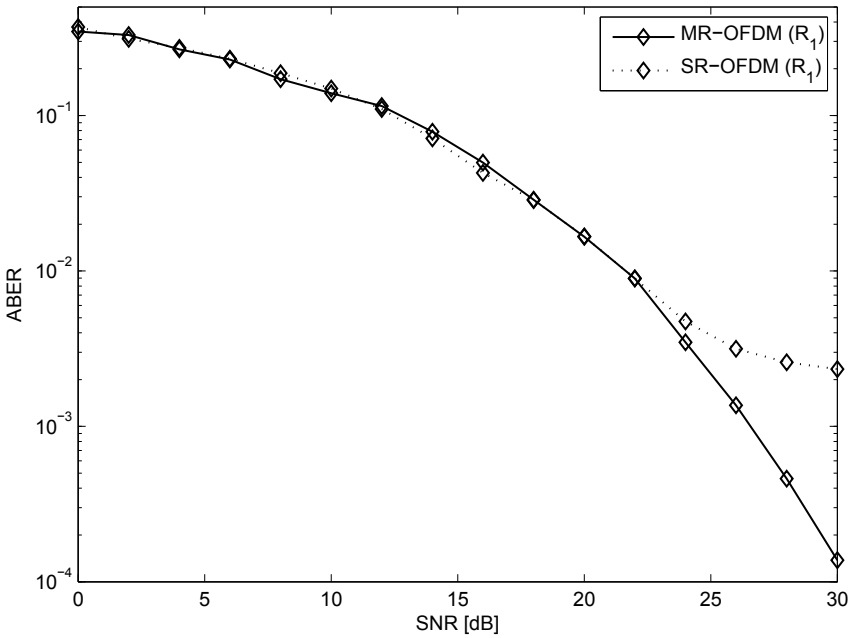

Figure 5.7: ABER of TWR OFDM for $K = 256$ through R_1 over Rician channels.

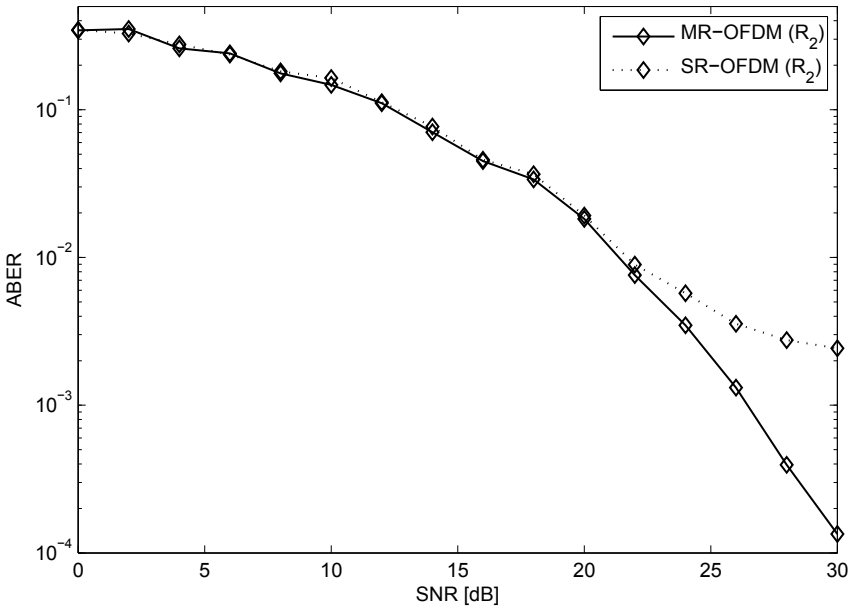

Figure 5.8: ABER of TWR OFDM for $K = 256$ through R_2 over Rician channels.

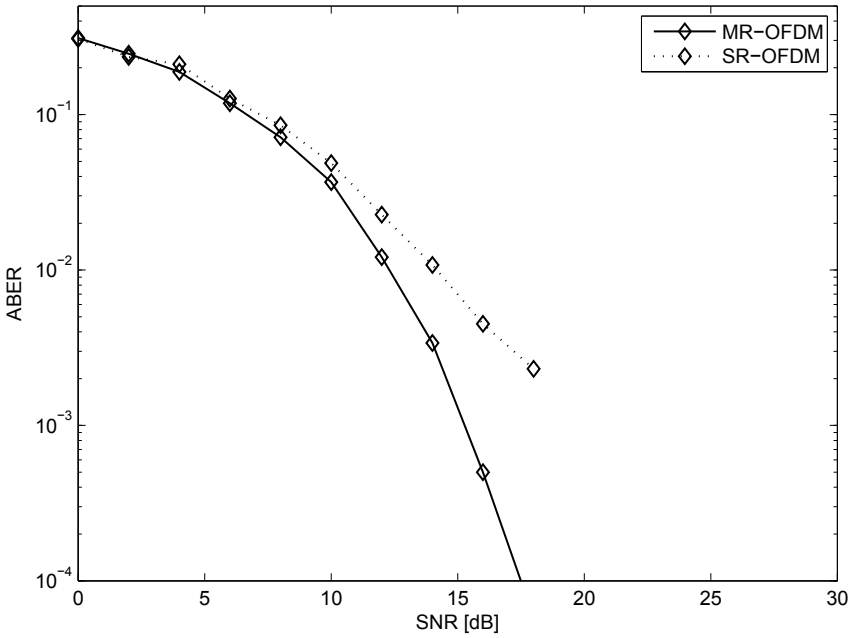

Figure 5.9: ABER of D-STBC OFDM for $K = 256$ over Rician channels.

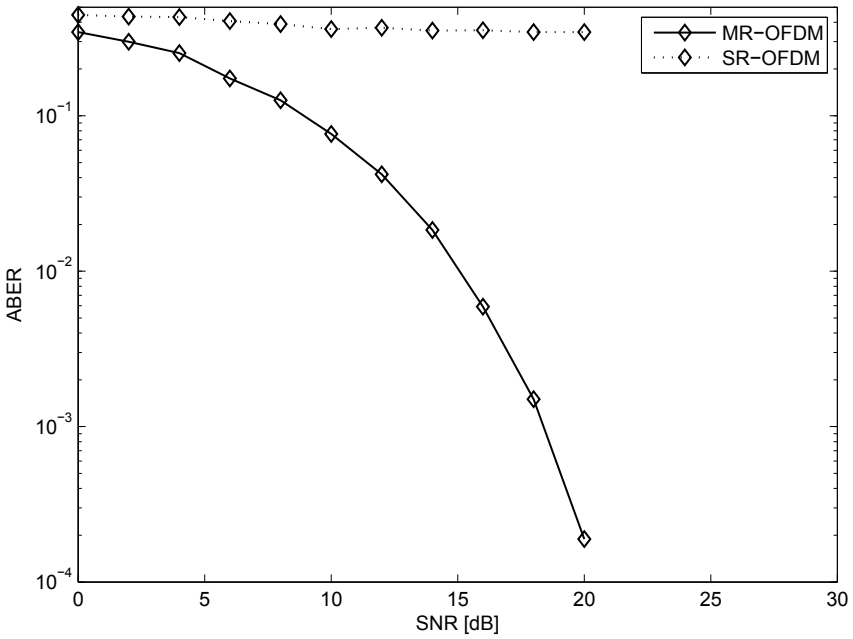

Figure 5.10: ABER of TWR-D-STBC OFDM for $K = 256$ over Rician channels.

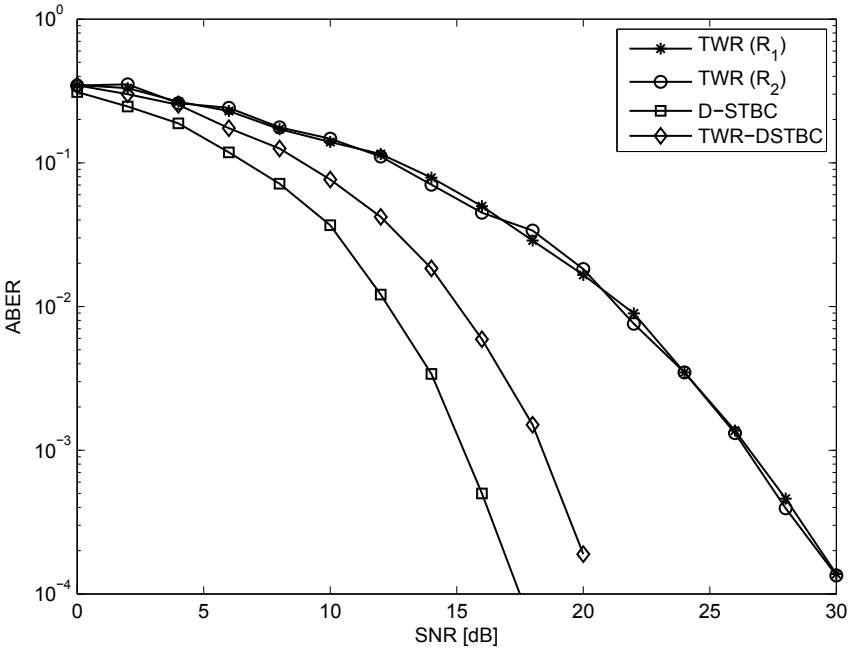

Figure 5.11: ABER comparison of all OFDM schemes with MR for $K = 256$ over Rician channels.

5.5 Conclusions

In this chapter we studied the performance of relay-assisted OFDM systems over path-specific Doppler scaling UWA channels. In particular, since the bandwidth is severely limited in UWA channels as it was shown in Fig. 2.4, we proposed to employ one AF relay that enabled two sources to exchange information, a scheme that is known as TWR. In the first time slot both source transmit to the relay, and in the second time slot the relay forwards a processed version of the received signals. On the other hand, to enhance the reliability of the system, we proposed employing two AF relays, and use D-STBC. Finally, to extract the benefits of both schemes, namely, TWR and D-STBC, two AF relays are deployed between two sources, where in the first phase each source transmitted two consecutive signals, and the sources transmitted at the same time over the same bandwidth. This phase was called TWR phase. In the second phase, the relays cooperated to transmit a D-STBC signal to both destinations. The structure and implementation of both MR and SR were used at all nodes. The The noise covariance matrix is derived at the relay and at the destinations. At the relay, the noise was first whitened, and then the noise-whitened signal is normalized in power before forwarding. At the destinations, given perfect CSI is available, each subtracts its signal if applicable, and the other source's signal was equalized using MMSE in the frequency domain. Numerical results for uncoded ABER over both fixed and Rician channels revealed that MR outperforms SR, and this performance gap was huge in the case of TWR-D-STBC because of the accumulated interference of both phases. Also, under total power constraint, and uniform distribution of power among the transmitting node, it was shown that TWR-D-STBC is a good set up that has a better bandwidth efficiency than D-STBC and better performance than TWR.

Chapter 6

Relay-Assisted SC-FDE UWA Communication

In this chapter we extend P2P SC-FDE systems to relay-assisted systems as was done for the case of OFDM systems. We begin with TWR systems through D-STBC to TWR-D-STBC systems. The underlying channels are assumed to be path-specific Doppler scaling UWA channels. The ML receivers are derived, and the necessary operations at each node is detailed. Also, the receiver's implementation for both MR and SR pre-processing techniques are illustrated.

6.1 TWR SC-FDE Systems

In TWR SC-FDE, the systems consists of two sources S_1 and S_2 which exchange information via the help of one AF relay, R. The CIR between nodes X and Y is given by

$$h_{XY}(t;\tau) = \int_{p=1}^{N_{XY}} h_{XY,p}\,\delta\left(\tau \quad [\tau_{XY,p} \quad a_{XY,p}t]\right), \tag{6.1}$$

where N_{XY} is the number of paths, and the three-tuple $\}h_{XY,p}, \tau_{XY,p}, a_{XY,p}|$ captures the pth path's gain, delay, and Doppler scaling factor between nodes X and Y, for $X, Y \ / \ \}S_1, S_2, R|$.

As a transmission scheme, block-based CP SC signaling is used, where the passband signal from the mth source is given by

$$s_m(t) = \mathcal{A}\Big\}e^{j2\pi f_c t}\int_{k=0}^{K-1} d_{m,k}\,g(t \quad kT_s)\Big(, \ \ t \ / \} \ \ T_g, KT_s|, \tag{6.2}$$

where K is the number of symbols per block, $d_{m,k}$ is the kth symbol of the mth source, $g(t)$ is a rectangular pulse of duration T_s, where T_s is the symbol duration, and T_g is the CP interval which is assumed to be large enough to prevent IBI which enables block-by-block processing.

The transmission in TWR SC-FDE systems is divided into two phases: MAC, and BC. In the MAC phase both users access R at the same time and over the same bandwidth. In the BC phase, R broadcasts a processed version of the received signals from the MAC phase to both sources. Finally, assuming perfect CSI, each source subtracts its own signal before processing the other source's signal.

Hence, the passband received signal at R in the MAC phase can be written as

$$y_R(t) = \mathcal{A} \Big\} \int_{m=1}^{2} \int_{k=0}^{K-1} d_{m,k} \int_{p=1}^{N_{S_m R}} h_{S_m R,p}\, e^{j2\pi f_c \left(t[1+a_{S_m R,p}]-\tau_{S_m R,p}\right)} \Big(+ n_R(t), \tag{6.3}$$

where $n_R(t)$ is an AWGN noise process of zeros-mean and PSD $N_0/2$. The corresponding baseband signal with respect to the carrier frequency f_c can be shown to be

$$v_R(t) = \int_{m=1}^{2} \int_{k=0}^{K-1} d_{m,k}\, P_{S_m R,k}(t) + w_R(t), \tag{6.4}$$

where $w_R(t)$ is an AWGN process of zero-mean and PSD N_0 and

$$P_{XY,k}(t) = \int_{p=1}^{N_{XY}} \underbrace{h_{XY,p}\, e^{-j2\pi f_c \tau_{XY,p}}}_{H_{XY,p}}\; e^{j2\pi f_c t a_{XY,p}}\, g\left(t[1+a_{XY,p}] \quad kT_s \quad \tau_{XY,p}\right), \tag{6.5}$$

for $X, Y \;/\; \}S_1, S_2, R|$ and $X \nexists Y$.

The set of sufficient statistics at R that correspond to $s_m(t)$ are given by

$$\begin{aligned} v_{S_m R,k} &= \Big[\quad P^*_{S_m R,k}(t) v_R(t)\, dt \\ &= \int_{u=1}^{2} \int_{l=0}^{K-1} \Phi^{S_m R,k}_{S_u R,l}\, d_{u,l} + w_{S_i R,k}, \quad k = 0, 1, \ldots, K \quad 1, \end{aligned} \tag{6.6}$$

where

$$\Phi^{XY,k}_{WZ,l} = \Big[\quad P^*_{XY,k}(t) P_{WZ,l}(t)\, dt \tag{6.7a}$$

$$w_{XY,k} = \Big[\quad P^*_{XY,k}(t) w_Y(t)\, dt. \tag{6.7b}$$

Arranging the received samples in (6.6) in a vector form yields

$$\mathbf{v}_{S_m R} = \sum_{u=1}^{2} \mathbf{\Phi}_{S_u R}^{S_m R} \mathbf{d}_u + \mathbf{w}_{S_m R}, \tag{6.8}$$

where $\left[\mathbf{\Phi}_{S_u R}^{S_m R}\right]_{k,l} = \Phi_{S_u R,l}^{S_m R,k}$, $\mathbf{d}_u = [d_{u,0} \;\; d_{u,1} \cdots d_{u,K-1}]^T$ and $\mathbf{w}_{S_m R}$ is an AWGN vector of zero-mean and covariance matrix

$$\mathbb{E}\left\{\mathbf{w}_{S_m R}\mathbf{w}_{S_u R}^H\right\} = N_0 \mathbf{\Phi}_{S_u R}^{S_m R}. \tag{6.9}$$

Next, since R has two soft-information received signals, it combines them as

$$\begin{aligned} \mathbf{v}_R &= \sum_{m=1}^{2} \mathbf{v}_{S_m R} \\ &= \sum_{u=1}^{2} \underbrace{\left[\sum_{m=1}^{2} \mathbf{\Phi}_{S_u R}^{S_m R}\right]}_{\mathbf{\Phi}_{S_u R}} \left\{ \mathbf{d}_u + \underbrace{\sum_{m=1}^{2} \mathbf{w}_{S_m R}}_{\mathbf{w}_R} \right\}. \end{aligned} \tag{6.10}$$

It can be shown that $\mathbf{w}_R \approx \mathcal{CN}(\mathbf{0}, N_0 \mathbf{\Omega}_R)$, where $\mathbf{\Omega}_R = \sum_{u=1}^{2} \mathbf{\Phi}_{S_u R}$. To whiten the noise, the signal in (6.10) is left-multiplied by $\mathbf{\Omega}_R^{-1/2}$ which yields to

$$\tilde{\mathbf{v}}_R = \sum_{u=1}^{2} \tilde{\mathbf{\Phi}}_{S_u R} \mathbf{d}_u + \tilde{\mathbf{w}}_R, \tag{6.11}$$

where $\tilde{\mathbf{\Phi}}_{S_u R} = \mathbf{\Omega}_R^{-1/2} \mathbf{\Phi}_{S_u R}$ and $\tilde{\mathbf{w}}_R \approx \mathcal{CN}(\mathbf{0}, N_0 \mathbf{I}_K)$.

The next step is power normalization, where R multiplies the signal in (6.11) by $\boldsymbol{\beta} = \text{diag}\,(\beta_0, \beta_1, \ldots, \beta_{K-1})$ results in $\mathbf{d}_R = \boldsymbol{\beta} \tilde{\mathbf{v}}_R = [d_{R,0} \;\; d_{R,1} \cdots d_{R,K-1}]^T$ such that

$$\beta_k = \left[\sum_{u=1}^{2} \tilde{\mathbf{\Phi}}_{S_u R} \tilde{\mathbf{\Phi}}_{S_u R}^H + N_0 \mathbf{I}_K \right]_{k,k}^{-1/2}. \tag{6.12}$$

In the BC phase, R forms the passband signal

$$s_R(t) = \mathcal{A}\left\{ e^{j2\pi f_c t} \sum_{k=0}^{K-1} d_{R,k}\, g(t - kT_s) \right\}, \tag{6.13}$$

and broadcasts it to both sources. Following the same procedures as in the MAC phase, the

baseband received signal at S_m can be written as

$$v_{S_m}(t) = \int_{k=0}^{K-1} d_{R,k} P_{RS_m}(t) + w_{S_m}(t), \tag{6.14}$$

where $w_{S_m}(t)$ is an AWGN process of zero-mean and PSD N_0. The received samples can be shown to be

$$\begin{aligned} \mathbf{v}_{S_m} =& \mathbf{\Phi}_{RS_m}^{RS_m} \mathbf{d}_R + \mathbf{w}_{S_m} \\ =& \int_{u=1}^{2} \underbrace{\mathbf{\Phi}_{RS_m}^{RS_m} \beta \tilde{\mathbf{\Phi}}_{S_u R}}_{\mathbf{H}^{(m,u)}} \mathbf{d}_u + \underbrace{\mathbf{\Phi}_{RS_m}^{RS_m} \beta \tilde{\mathbf{w}}_R + \mathbf{w}_{S_m}}_{\mathbf{w}_{S_m,\text{eq}}}, \end{aligned} \tag{6.15}$$

where $\mathbf{w}_{S_m,\text{eq}} \approx \mathcal{DV}\ (\mathbf{0}, N_0 \mathbf{\Omega}_{S_m})$ and $\mathbf{\Omega}_{S_m} = \mathbf{\Phi}_{RS_m}^{RS_m} \beta\ \ \mathbf{\Phi}_{RS_m}^{RS_m} \beta \big[^H + \mathbf{\Phi}_{RS_m}^{RS_m}$. Before proceeding any further, S_m subtracts its own signal a process that yields to

$$\begin{aligned} \tilde{\mathbf{v}}_{S_m} =& \tilde{\mathbf{v}}_{S_m} \quad \mathbf{H}^{(m,m)} \mathbf{d}_m \\ =& \mathbf{H}^{(m,u)} \mathbf{d}_u + \mathbf{w}_{S_m,\text{eq}}, \quad m, u = 1, 2 \text{ and } m \neq u. \end{aligned} \tag{6.16}$$

Note that since the channel matrix $\mathbf{H}^{(m,u)}$ is not diagonal a further equalization process is needed. To avoid the complexity burden of the optimum MLSD, MMSE equalization in the frequency domain is used instead. To that end, S_m transforms the received signal in (6.15) to the frequency domain as

$$\mathcal{W}_{S_m} = \mathcal{N}^{(m,u)} \mathcal{F}_u + \mathcal{Z}_{S_m}, \tag{6.17}$$

where $\mathcal{N}^{(m,u)} = \mathcal{G}_K \mathbf{H}^{(m,u)} \mathcal{G}_K^H$, $\mathcal{F}_u = \mathcal{G}_K \mathbf{d}_u$, $\mathcal{Z}_{S_m} \approx \mathcal{DV}\ (\mathbf{0}, N_0 \mathbf{\Xi}_{S_m})$ and $\mathbf{\Xi}_{S_m} = \mathcal{G}_K \mathbf{\Omega}_{S_m} \mathcal{G}_K^H$. So, the signal in (6.17) is equalized using the MMSE FDE equalizer

$$\mathcal{H}_{S_m} = \mathcal{N}^{(m,u)H} \quad \mathcal{N}^{(m,u)} \mathcal{N}^{(m,u)H} + N_0 \mathbf{\Xi}_{S_m} \big[^{-1}, \tag{6.18}$$

before transformed back to the time domain where symbol-by-symbol detection takes place.

6.2 D-STBC SC-FDE Systems

We consider D-STBC SC-FDE systems where a source S communicates with a destination D via the help of two AF relays R_1 and R_2 only, i.e, there is no direct link between S and D. The

Table 6.1: TWR SC-FDE vs. OFDM Complexity

	IFFT	FFT	Integrator	Frequency Shifter	Resampler.
SR-OFDM	3	3	0	3	3
MR-OFDM	3	N_{TWR}	0	N_{TWR}	N_{TWR}
SR-SC-FDE	2	2	3	3	3
MR-SC-FDE	2	2	N_{TWR}	N_{TWR}	N_{TWR}

CIR between nodes X and Y is given as in (6.1) for $X \ / \ \}S, R_1, R_2|$ and $Y \ / \ \}R_1, R_2, D|$ and $X \nVdash Y$. The transmission is divided into two phases: In Phase I, S broadcasts two signals sequentially to both relays, and in Phase II the two relays cooperate to transmit the received signals from Phase I to D using distributed Alamouti's STBC.

In phase I, S forms the μth passband transmitted signal as

$$s^{(\mu)}(t) = \mathcal{A}\Big\}e^{j2\pi f_c t}\int_{\not}^{K-1} d_k^{(\mu)} g(t \quad kT_s)\Big(, \quad \mu = 1, 2, \tag{6.19}$$

where $d_k^{(\mu)}$ is the kth transmitted signal of the μth transmitted block. The baseband received signal at R_j due to the μth signal can be shown to be given by

$$v_{R_j}^{(\mu)}(t) = \int_{\not}^{K-1} d_k^{(\mu)} P_{SR_j}(t) + w_{R_j}^{(\mu)}(t), \tag{6.20}$$

where $w_{R_j}^{(\mu)}(t)$ is an AWGN with zero-mean and PSD N_0, and $P_{SR_j}(t)$ is as given in (6.5) for $X = S$ and $Y = R_j$.

The set of sufficient statistics in case of D-STBC due to $s^{(\mu)}(t)$ at R_j are given by

$$\begin{aligned} v_{SR_j,k}^{(\mu)} &= \Big[\quad P_{SR_j}^*(t) v_{R_j}^{(\mu)}(t)\, dt \\ &= \int_{\not}^{K-1} \Phi_{SR_j,l}^{SR_j,k}\, d_k^{(\mu)} + w_{SR_j,k}^{(\mu)}, \quad k = 0, 1, \ldots, K \quad 1, \end{aligned} \tag{6.21}$$

where

$$w_{XY,k}^{(\mu)} = \Big[\quad P_{XY,k}^*(t) w_Y^{(\mu)}(t)\, dt. \tag{6.22}$$

Arranging the samples in (6.21) in a vector form yields

$$\mathbf{v}_{SR_j}^{(\mu)} = \mathbf{\Phi}_{SR_j}^{SR_j}\,\mathbf{d}^{(\mu)} + \mathbf{w}_{SR_j}^{(\mu)}, \tag{6.23}$$

where $\mathbf{\Phi}_{SR_j}^{SR_j} = \Phi_{SR_j,l}^{SR_j,k}$, $\mathbf{d}^{(\mu)} = [d_0^{(\mu)}\ d_1^{(\mu)}\ \cdots\ d_{K-1}^{(\mu)}]^T$, and $\mathbf{w}_{SR_j}^{(\mu)} \approx \mathcal{CN}(\mathbf{0}, N_0\mathbf{\Phi}_{SR_j}^{SR_j})$. To whiten the noise, (6.23) is left multiples by $(\mathbf{\Phi}_{SR_j}^{SR_j})^{-1/2}$ which yields to

$$\tilde{\mathbf{v}}_{SR_j}^{(\mu)} = \tilde{\mathbf{\Phi}}_{SR_j}^{SR_j}\,\tilde{\mathbf{d}}^{(\mu)} + \tilde{\mathbf{w}}_{SR_j}^{(\mu)}, \tag{6.24}$$

such that $\tilde{\mathbf{\Phi}}_{SR_j}^{SR_j} = (\mathbf{\Phi}_{SR_j}^{SR_j})^{1/2}$ and $\tilde{\mathbf{w}}_{SR_j}^{(\mu)} \approx \mathcal{CN}(\mathbf{0}, N_0\mathbf{I}_K)$. After whitening the noise, R_j normalizes the received power as $\mathbf{d}_{R_j}^{(\mu)} = \beta_{R_j}\tilde{\mathbf{v}}_{SR_j}^{(\mu)} = [d_{R_j,0}^{(\mu)}\ d_{R_j,1}^{(\mu)}\ \cdots\ d_{R_j,K-1}^{(\mu)}]^T$ where $\beta_{R_j} = \text{diag}[\beta_{R_j,0}\ \beta_{R_j,1}\ \cdots\ \beta_{R_j,K-1}]$ and

$$\beta_{R_j,k} = \left[\tilde{\mathbf{\Phi}}_{SR_j}^{SR_j}(\tilde{\mathbf{\Phi}}_{SR_j}^{SR_j})^H + N_0\mathbf{I}_K\right]_{k,k}^{-1/2}. \tag{6.25}$$

Then R_2 creates the new signals $\mathbf{x}_{R_2}^{(\mu)} = \mathbf{P}\mathbf{d}_{R_2}^{(\mu)} = [d_{R_2,0}^{(\mu)}\ d_{R_2,K-1}^{(\mu)}\ \cdots\ d_{R_2,1}^{(\mu)}]^T$ for $\mu = 1, 2$, where $\mathbf{P}$ is a permutation matrix given by [69]

$$\mathbf{P} = \begin{pmatrix} 1 & 0 & 0 & \cdots & 0 \\ 0 & 0 & 0 & \cdots & 1 \\ \vdots & \vdots & \vdots & \ddots & \vdots \\ 0 & 1 & 0 & \cdots & 0 \end{pmatrix}, \tag{6.26}$$

with the property that $\mathbf{P}\mathbf{P} = \mathbf{I}_K$.

In Phase II, the transmitted signals from R_1 and R_2 in the first time slot are $\mathbf{d}_{R_1}^{(1)}$ and $\mathbf{x}_{R_2}^{(2)*}$, respectively, while in the second time slot they are $\mathbf{d}_{R_1}^{(2)}$ and $\mathbf{x}_{R_2}^{(1)*}$, respectively. This transmitting protocol translates to the following baseband received signals

$$v_D^{(1)}(t) = \int_{l=0}^{K-1} d_{R_1,k}^{(1)}P_{R_1D,k}(t) + x_{R_2,k}^{(2)*}P_{R_2D,k}(t) + w_D^{(1)}(t) \tag{6.27a}$$

$$v_D^{(2)}(t) = \int_{l=0}^{K-1} d_{R_1,k}^{(2)}P_{R_1D,k}(t) + x_{R_2,k}^{(1)*}P_{R_2D,k}(t) + w_D^{(2)}(t), \tag{6.27b}$$

and the received samples corresponding to R_j are

$$v^{(1)}_{R_jD,k} = \int_{l=0}^{K-1} \Phi^{R_jD,k}_{R_1D,l}\, d^{(1)}_{R_1,l} + \Phi^{R_jD,k}_{R_2D,l}\, x^{(2)*}_{R_2,l} + w^{(1)}_{R_jD,k} \tag{6.28a}$$

$$v^{(2)}_{R_jD,k} = \int_{l=0}^{K-1} \Phi^{R_jD,k}_{R_1D,l}\, d^{(2)}_{R_1,l} + \Phi^{R_jD,k}_{R_2D,l}\, x^{(1)*}_{R_2,l} + w^{(2)}_{R_jD,k}, \tag{6.28b}$$

where

$$v^{(\mu)}_{R_jD,k} = \int P^{*}_{R_jD,k}(t)\, v^{(\mu)}_{D}(t)\, dt, \tag{6.29}$$

for $k = 0, 1, \ldots, K$ 1. Arranging the samples in (6.28a) and (6.28b) into a vector and substituting for $\mathbf{d}^{(\mu)}_{R_j}$ and $\mathbf{x}^{(\mu)}_{R_j}$ yields

$$\mathbf{v}^{(1)}_{R_jD} = \mathbf{H}_{1j}\mathbf{d}^{(1)} + \mathbf{H}_{2j}\ \mathbf{P}\mathbf{d}^{(2)}\big[^{*} + \boldsymbol{\eta}^{(1)}_{R_jD} \tag{6.30a}$$

$$\mathbf{v}^{(2)}_{R_jD} = \ \ \mathbf{H}_{1j}\mathbf{d}^{(2)} + \mathbf{H}_{2j}\ \mathbf{P}\mathbf{d}^{(1)}\big[^{*} + \boldsymbol{\eta}^{(2)}_{R_jD}, \tag{6.30b}$$

where $\mathbf{H}_{1j} = \boldsymbol{\Phi}^{R_jD}_{R_1D}\boldsymbol{\beta}_{R_1}\tilde{\boldsymbol{\Phi}}^{SR_1}_{SR_1}$, $\mathbf{H}_{2j} = \boldsymbol{\Phi}^{R_jD}_{R_1D}\boldsymbol{\Gamma}^{*}_{R_2}\boldsymbol{\Psi}^{SR_2*}_{SR_2}$, $\boldsymbol{\Gamma}_{R_2} = \mathbf{P}\boldsymbol{\beta}_{R_2}\mathbf{P}$ and $\boldsymbol{\Psi}^{SR_2}_{SR_2} = \mathbf{P}\tilde{\boldsymbol{\Phi}}^{SR_2}_{SR_2}\mathbf{P}$. For the noise terms $\boldsymbol{\eta}^{(\mu)}_{R_jD}$ for $j, \mu = 1, 2$ it can be shown that each is an AWGN vector of zero mean covariance matrix

$$\mathbb{E}\Big\{\boldsymbol{\eta}^{(\mu)}_{R_iD}\boldsymbol{\eta}^{(\mu')H}_{R_jD}\Big\surd = N_0\Big]\mathbf{G}_{1i}\mathbf{G}^{H}_{1j} + \mathbf{G}_{2i}\mathbf{G}^{H}_{2j} + \boldsymbol{\Phi}^{R_iD}_{R_jD}\Big\{ = N_0\boldsymbol{\Omega}_{ij}\boldsymbol{\delta}(\mu \quad \mu'), \tag{6.31}$$

where $\mathbf{G}_{1j} = \boldsymbol{\Phi}^{R_jD}_{R_1D}\boldsymbol{\beta}_{R_1}$, $\mathbf{G}_{2j} = \boldsymbol{\Phi}^{R_jD}_{R_2D}\boldsymbol{\Gamma}^{*}_{R_2}$ and

$$\boldsymbol{\delta}(\mu \quad \mu') = \begin{cases} \mathbf{I}_K & \mu = \mu' \\ \mathbf{0}_{K\times 1} & \mu \not\forall \mu' \end{cases}, \tag{6.32}$$

for $i, j, \mu, \mu' = 1, 2$. Then the received signals in (6.30a) and (6.30b) are transformed to the frequency domain by mean of K-point FFT which yields to

$$\mathcal{W}^{(1)}_{R_jD} = \mathcal{N}_{1j}\mathcal{F}^{(1)} + \mathcal{N}_{2j}\mathcal{F}^{(2)*} + \boldsymbol{\xi}^{(1)}_{R_jD} \tag{6.33a}$$

$$\mathcal{W}^{(2)}_{R_jD} = \ \ \mathcal{N}_{1j}\mathcal{F}^{(2)} + \mathcal{N}_{2j}\mathcal{F}^{(1)*} + \boldsymbol{\xi}^{(2)}_{R_jD}, \tag{6.33b}$$

where $\mathcal{N}_{ij} = \mathcal{G}_K\mathbf{H}_{ij}\mathcal{G}^{H}_{K}$, $\mathcal{F}^{(\mu)} = \mathcal{G}_K\mathbf{d}^{(\mu)}$ and $\boldsymbol{\xi}^{(\mu)}_{R_jD}$ is an AWGN with zero-mean and covariance

Table 6.2: D-STBC SC-FDE vs. OFDM Complexity

	IFFT	FFT	Integrator	Frequency Shifter	Resampler.
SR-OFDM	3	4	0	4	4
MR-OFDM	3	$N_{\text{D-STBC}}$	0	$N_{\text{D-STBC}}$	$N_{\text{D-STBC}}$
SR-SC-FDE	2	2	4	4	4
MR-SC-FDE	2	2	$N_{\text{D-STBC}}$	$N_{\text{D-STBC}}$	$N_{\text{D-STBC}}$

matrix

$$\mathbb{E}\left\{\boldsymbol{\xi}_{R_iD}^{(\mu)}\boldsymbol{\xi}_{R_jD}^{(\mu')H}\right\} = N_0\boldsymbol{\Xi}_{ij}\delta(\mu - \mu'), \tag{6.34}$$

and $\boldsymbol{\Xi}_{ij} = \mathcal{G}_K\boldsymbol{\Omega}_{ij}\mathcal{G}_K^H$. Then the received samples in the frequency domain are arranged as

$$\underbrace{\begin{bmatrix}\mathcal{W}_{R_1D}^{(1)}\\ \mathcal{W}_{R_2D}^{(1)}\\ \mathcal{W}_{R_1D}^{(2)*}\\ \mathcal{W}_{R_2D}^{(2)*}\end{bmatrix}}_{\mathcal{V}} = \underbrace{\begin{bmatrix}\mathcal{N}_{11} & \mathcal{N}_{21}\\ \mathcal{N}_{12} & \mathcal{N}_{22}\\ \mathcal{N}_{21}^* & \mathcal{N}_{11}^*\\ \mathcal{N}_{22}^* & \mathcal{N}_{12}^*\end{bmatrix}}_{\mathcal{H}}\underbrace{\begin{bmatrix}\mathcal{F}^{(1)}\\ \mathcal{F}^{(2)*}\end{bmatrix}}_{\mathcal{D}} + \underbrace{\begin{bmatrix}\xi_{R_1D}^{(1)}\\ \xi_{R_2D}^{(1)}\\ \xi_{R_1D}^{(2)*}\\ \xi_{R_2D}^{(2)*}\end{bmatrix}}_{\xi}. \tag{6.35}$$

It is straightforward to show that the noise vector $\boldsymbol{\xi}$ is an AWGN noise with zero mean and covariance matrix

$$\mathbb{E}\{\boldsymbol{\xi}\boldsymbol{\xi}^H\} = N_0\underbrace{\begin{bmatrix}\boldsymbol{\Xi}_{11} & \boldsymbol{\Xi}_{12} & \mathbf{0} & \mathbf{0}\\ \boldsymbol{\Xi}_{21} & \boldsymbol{\Xi}_{22} & \mathbf{0} & \mathbf{0}\\ \mathbf{0} & \mathbf{0} & \boldsymbol{\Xi}_{11}^* & \boldsymbol{\Xi}_{12*}\\ \mathbf{0} & \mathbf{0} & \boldsymbol{\Xi}_{21}^* & \boldsymbol{\Xi}_{22*}\end{bmatrix}}_{\boldsymbol{\Xi}}. \tag{6.36}$$

Then, the frequency domain samples are jointly equalized using the MMSE equalizer

$$\mathcal{H} = \mathcal{N}\left[\mathcal{N}\mathcal{N}^H + N_0\boldsymbol{\Xi}\right]^{-1}, \tag{6.37}$$

as $\{ = \mathcal{H}\mathcal{W} = [\{^{(1)T} \{^{(2)H}]^T$, where $\{^{(\mu)}$ are the frequency-equalized samples that correspond to the μth signal. Finally, the equalized samples are transformed back to the time domain as $\mathbf{z}^{(\mu)} = \mathcal{G}_K^H\{^{(\mu)}$ where symbol-by-symbol detection takes place.

6.3 TWR D-STBC SC-FDE Systems

In an attempt to extract the advantages of both of the above systems, namely, TWR and D-STBC systems, in this section they are combined in one system. In particular, two sources S_1 and S_2 exchange information via the help of two AF relays R_1 and R_2. The CIR between nodes X and Y is give as in (6.1) for $\}X, Y|\ \ / \ \}S_1, S_2, R_1, R_2|$ and $X \nVdash Y$. The transmission is divided into two phases: TWR-phase at which each source transmits two signals sequentially while both sources transmit simultaneously, and D-STBC-phase at which the two relays cooperate to realize Alamouti's STBC in distributed fashion at the block level.

As previously, block-based SC modulation is considered, where the μth signal from the mth source is given by

$$s_m^{(\mu)}(t) = \mathcal{A} \Big\} e^{j2\pi f_c t} \int_{l=0}^{K-1} d_{m,k}^{(\mu)}\, g(t \quad kT_s) \Big(, \tag{6.38}$$

where $d_{m,k}^{(\mu)}$ is the kth transmitted signal in the μth signal from the mth source, for $k = 0, 1, \ldots, K$ 1, and $m, \mu = 1, 2$. The μth baseband received signal at R_j is given by

$$v_{R_j}^{(\mu)}(t) = \int_{m=1}^{2} \int_{l=0}^{K-1} d_{m,k}^{(\mu)}\, P_{S_m R_j,k}(t) + w_{R_j}^{(\mu)}(t), \quad j, \mu = 1, 2, \tag{6.39}$$

where $w_{R_j}^{(\mu)}(t)$ is an AWGN noise process of zero-mean and PSD N_0 and $P_{S_m R_j,k}(t)$ is given as in (6.5) for $X = S_m$ and $Y = R_j$. The received samples corresponding to $s_m^{(\mu)}(t)$ at R_j can be shown to be given by

$$\begin{aligned} v_{S_m R_j,k}^{(\mu)} &= \Big[\ \ P_{S_m R_j,k}^{*}(t) v_{R_j}^{(\mu)}(t)\, dt \\ &= \int_{u=1}^{2} \int_{l=0}^{K-1} \Phi_{S_u R_j,l}^{S_m R_j,k}\, d_{u,l}^{(\mu)} + w_{S_m R_j,k}^{(\mu)}, \end{aligned} \tag{6.40}$$

where $\Phi_{S_u R_j,l}^{S_m R_j,k}$ and $w_{S_m R_j,k}^{(\mu)}$ are given as in (6.7a) and (6.22). Stack the samples in (6.40) in a a vector yields

$$\mathbf{v}_{S_m R_j}^{(\mu)} = \int_{u=1}^{2} \mathbf{\Phi}_{S_u R_j}^{S_m R_j} \mathbf{d}_u^{(\mu)} + \mathbf{w}_{S_m R_j}^{(\mu)}. \tag{6.41}$$

It can be shown that $\mathbf{w}_{S_m R_j}^{(\mu)}$ is an AWGN vector of zero-mean and covariance matrix

$$\mathbb{E} \Big\} \mathbf{w}_{S_m R_j}^{(\mu)} \mathbf{w}_{S_u R_{j'}}^{(\mu')} \sqrt{} = N_0 \mathbf{\Phi}_{S_u R_{j'}}^{S_m R_j} \boldsymbol{\delta} \left((\mu \quad \mu')(j \quad j') \right), \tag{6.42}$$

where

$$\boldsymbol{\delta}\left((\mu \quad \mu')(j \quad j')\right) = \begin{cases} \mathbf{I}_K & \mu = \mu' \text{ and } j = j' \\ \mathbf{0}_{K\times 1} & \text{Otherwise} \end{cases}. \tag{6.43}$$

After that R_j adds the signals corresponding to both sources as

$$\begin{aligned} \mathbf{v}_{R_j}^{(\mu)} &= \sum_{m=1}^{2} \mathbf{v}_{S_m R_j}^{(\mu)} \\ &= \sum_{u=1}^{2} \boldsymbol{\Phi}_{S_u R_j} \mathbf{d}_u^{(\mu)} + \mathbf{w}_{R_j}^{(\mu)}, \end{aligned} \tag{6.44}$$

such that $\boldsymbol{\Phi}_{S_u R_j} \mathbf{d}_u^{(\mu)} = \sum_{m=1}^{2} \boldsymbol{\Phi}_{S_u R_j}^{S_m R_j}$, $\mathbf{w}_{R_j}^{(\mu)} \approx \mathcal{DN}\left(\mathbf{0}, N_0 \boldsymbol{\Omega}_{R_j}\right)$, and $\boldsymbol{\Omega}_{R_j} = \sum_{u=1}^{2} \boldsymbol{\Phi}_{S_u R_j}$. To whiten the noise, the signal in (6.44) is left multiplied by $\boldsymbol{\Omega}_{R_j}^{-1/2}$ which results in

$$\tilde{\mathbf{v}}_{R_j}^{(\mu)} = \sum_{u=1}^{2} \tilde{\boldsymbol{\Phi}}_{S_u R_j} \mathbf{d}_u^{(\mu)} + \tilde{\mathbf{w}}_{R_j}^{(\mu)}, \tag{6.45}$$

where $\tilde{\boldsymbol{\Phi}}_{S_u R_j} = \boldsymbol{\Omega}_{R_j}^{-1/2} \boldsymbol{\Phi}_{S_u R_j}$, $\tilde{\mathbf{w}}_{R_j}^{(\mu)} \approx \mathcal{DN}\left(\mathbf{0}, N_0 \mathbf{I}_K\right)$. Then the relays form the signals $\mathbf{d}_{R_j}^{(\mu)} = \boldsymbol{\beta}_{R_j} \tilde{\mathbf{v}}_{R_j}^{(\mu)} = [d_{R_j,0}^{(\mu)} \; d_{R_j,1}^{(\mu)} \times\times\times d_{R_j,K-1}^{(\mu)}]^T$ and $\mathbf{x}_{R_j}^{(\mu)} = \mathbf{P}\mathbf{d}_{R_j}^{(\mu)} = [x_{R_j,0}^{(\mu)} \; x_{R_j,1}^{(\mu)} \times\times\times x_{R_j,K-1}^{(\mu)}]^T = [d_{R_j,0}^{(\mu)} \; d_{R_j,K-1}^{(\mu)} \times\times\times d_{R_j,1}^{(\mu)}$ where $\boldsymbol{\beta}_{R_j} = \text{diag}\left[\beta_{R_j,0}, \beta_{R_j,1}, \ldots, \beta_{R_j,K-1}\right]$ and

$$\beta_{R_j,k} = \left[\sum_{u=1}^{2} \tilde{\boldsymbol{\Phi}}_{S_u R_j} \tilde{\boldsymbol{\Phi}}_{S_u R_j}^{H} + N_0 \mathbf{I}_K\right]_{k,k}^{-1/2}. \tag{6.46}$$

Following the same transmission protocol as in the D-STBC systems, the received signals in the D-STBC-phase at S_m are given by

$$v_{S_m}^{(1)}(t) = \sum_{u=0}^{K-1} \left[d_{R_1,k}^{(1)} P_{R_1 S_m,k}(t) + x_{R_2,k}^{(2)*} P_{R_2 S_m,k}(t)\right] + w_{S_m}^{(1)}(t) \tag{6.47a}$$

$$v_{S_m}^{(2)}(t) = \sum_{u=0}^{K-1} \left[d_{R_1,k}^{(2)} P_{R_1 S_m,k}(t) + x_{R_2,k}^{(1)*} P_{R_2 S_m,k}(t)\right] + w_{S_m}^{(2)}(t), \tag{6.47b}$$

and samples corresponding to R_j in both received signals can be shown to be

$$v^{(1)}_{R_jS_m,k} = \int P^*_{R_jS_m,k}(t) v^{(1)}_{S_m}(t)\, dt \tag{6.48a}$$
$$= \sum_{l=0}^{K-1} \Phi^{R_jS_m,k}_{R_1S_m,l} d^{(1)}_{R_1,l} + \Phi^{R_jS_m,k}_{R_2S_m,l} x^{(2)*}_{R_2,l} + w^{(1)}_{R_jS_m,k}$$

$$v^{(2)}_{R_jS_m,k} = \int P^*_{R_jS_m,k}(t) v^{(2)}_{S_m}(t)\, dt \tag{6.48b}$$
$$= \sum_{l=0}^{K-1} \Phi^{R_jS_m,k}_{R_1S_m,l} d^{(2)}_{R_1,l} + \Phi^{R_jS_m,k}_{R_2S_m,l} x^{(1)*}_{R_2,l} + w^{(2)}_{R_jS_m,k}.$$

Arranging the samples in (6.48a) and (6.48b) in a vector-matrix form yields

$$\mathbf{v}^{(1)}_{R_jS_m} = \sum_{u=1}^{2} \mathbf{H}^{(m,u)}_{1j} \mathbf{d}^{(1)}_u + \mathbf{H}^{(m,u)}_{2j} \mathbf{P} \mathbf{d}^{(2)}_u + \boldsymbol{\eta}^{(1)}_{R_jS_m} \tag{6.49a}$$

$$\mathbf{v}^{(2)}_{R_jS_m} = \sum_{u=1}^{2} \mathbf{H}^{(m,u)}_{1j} \mathbf{d}^{(2)}_u + \mathbf{H}^{(m,u)}_{2j} \mathbf{P} \mathbf{d}^{(1)}_u + \boldsymbol{\eta}^{(2)}_{R_jS_m}, \tag{6.49b}$$

such that

$$\mathbf{H}^{(m,u)}_{1j} = \underbrace{\boldsymbol{\Phi}^{R_jS_m}_{R_1S_m} \boldsymbol{\beta}_{R_1}}_{\mathbf{G}^{(m)}_{1j}} \tilde{\boldsymbol{\Phi}}_{S_uR_1} \tag{6.50a}$$

$$\mathbf{H}^{(m,u)}_{2j} = \underbrace{\boldsymbol{\Phi}^{R_jS_m}_{R_2S_m}}_{\mathbf{G}^{(m)}_{2j}} \boldsymbol{\Gamma}^*_{R_2} \tilde{\boldsymbol{\Psi}}^*_{S_uR_2}, \tag{6.50b}$$

and $\boldsymbol{\Gamma}_{R_2} = \mathbf{P}\boldsymbol{\beta}_{R_2}\mathbf{P}$ and $\tilde{\boldsymbol{\Psi}}_{S_uR_2} = \mathbf{P}\tilde{\boldsymbol{\Phi}}_{S_uR_2}\mathbf{P}$. Further more, it can be shown that $\boldsymbol{\eta}^{(\mu)}_{R_jS_m}$ is an AWGN vector with zero-mean and covariance matrix

$$\mathbb{E}\left\{\boldsymbol{\eta}^{(\mu)}_{R_iS_m} \boldsymbol{\eta}^{(\mu')H}_{R_jS_m}\right\} = N_0 \underbrace{\left[\mathbf{G}_{1i}\mathbf{G}^H_{1j} + \mathbf{G}_{2i}\mathbf{G}^H_{2j} + \boldsymbol{\Phi}^{R_iS_m}_{R_jS_m}\right]}_{\boldsymbol{\Omega}^{(m)}_{ij}} \delta(\mu - \mu'). \tag{6.51}$$

To facilitate further processing, the samples in (6.49a) and (6.49b) are transformed to the

frequency domain by means of K-point FFT operation as

$$\mathcal{W}_{R_jS_m}^{(1)} = \sum_{u=1}^{2} \mathcal{N}_{1j}^{(m,u)} \mathcal{F}_u^{(1)} + \mathcal{N}_{2j}^{(m,u)} \mathcal{F}_u^{(2)*} + \mathcal{Z}_{R_jS_m}^{(1)} \tag{6.52a}$$

$$\mathcal{W}_{R_jS_m}^{(2)} = \sum_{u=1}^{2} \mathcal{N}_{1j}^{(m,u)} \mathcal{F}_u^{(2)} + \mathcal{N}_{2j}^{(m,u)} \mathcal{F}_u^{(1)*} + \mathcal{Z}_{R_jS_m}^{(2)}, \tag{6.52b}$$

where $\mathcal{N}_{ij}^{(m,u)} = \mathcal{G}_K \mathbf{H}_{ij}^{(m,u)} \mathcal{G}_K^H$, $\mathcal{F}_u^{(\mu)} = \mathcal{G}_K \mathbf{d}_u^{(\mu)}$, and $\mathcal{Z}_{R_jS_m}^{(\mu)} = \mathcal{G}_K \boldsymbol{\eta}_{R_jS_m}^{(\mu)}$ Arranging the frequency domain samples as

$$\underbrace{\begin{bmatrix} \mathcal{W}_{R_1S_m}^{(1)} \\ \mathcal{W}_{R_2S_m}^{(1)} \\ \mathcal{W}_{R_1S_m}^{(2)*} \\ \mathcal{W}_{R_2S_m}^{(2)*} \end{bmatrix}}_{\mathcal{V}_{S_m}} = \sum_{u=1}^{2} \underbrace{\begin{bmatrix} \mathcal{N}_{11}^{(m,u)} & \mathcal{N}_{21}^{(m,u)} \\ \mathcal{N}_{12}^{(m,u)} & \mathcal{N}_{22}^{(m,u)} \\ \mathcal{N}_{21}^{(m,u)*} & \mathcal{N}_{11}^{(m,u)*} \\ \mathcal{N}_{22}^{(m,u)*} & \mathcal{N}_{12}^{(m,u)*} \end{bmatrix}}_{\mathcal{H}^{(m,u)}} \underbrace{\begin{bmatrix} \mathcal{F}_u^{(1)} \\ \mathcal{F}_u^{(2)*} \end{bmatrix}}_{\mathcal{D}_u} + \underbrace{\begin{bmatrix} \mathcal{Z}_{R_1S_m}^{(1)} \\ \mathcal{Z}_{R_2S_m}^{(1)} \\ \mathcal{Z}_{R_1S_m}^{(2)*} \\ \mathcal{Z}_{R_2S_m}^{(2)*} \end{bmatrix}}_{\mathcal{W}_{S_m}} \tag{6.53}$$

the noise vector $\mathcal{Z}_{S_m}$ can be shown to be an AWGN vector with zero-mean and covariance matrix

$$\mathbb{E}\{\mathcal{Z}_{S_m} \mathcal{Z}_{S_m}^H\} = N_0 \underbrace{\begin{bmatrix} \Xi_{11}^{(m)} & \Xi_{12}^{(m)} & \mathbf{0} & \mathbf{0} \\ \Xi_{21}^{(m)} & \Xi_{22}^{(m)} & \mathbf{0} & \mathbf{0} \\ \mathbf{0} & \mathbf{0} & \Xi_{11}^{(m)*} & \Xi_{12}^{(m)*} \\ \mathbf{0} & \mathbf{0} & \Xi_{21}^{(m)*} & \Xi_{22}^{(m)*} \end{bmatrix}}_{\Xi^{(m)}} \tag{6.54}$$

where $\Xi_{ij}^{(m)} = \mathcal{G}_K \Omega_{ij}^{(m)} \mathcal{G}_K^H$.

Since S_m knows its own signals, and assuming perfect CSI, it subtracts its own signals as

$$\begin{aligned} \tilde{\mathcal{W}}_{S_m} &= \mathcal{W}_{S_m} - \mathcal{N}^{(m,m)} \mathcal{F}_m \\ &= \mathcal{N}^{(m,u)} \mathcal{F}_u + \mathcal{Z}_{S_m}, \quad m,u = 1,2 \text{ and } m \neq u. \end{aligned} \tag{6.55}$$

Finally, S_m performs joint equalization to the other source's signals using the linear MMSE equalizer

$$\mathcal{H}_{S_m} = \mathcal{N}^{(m,u)H} \left[\mathcal{N}^{(m,u)} \mathcal{N}^{(m,u)H} + N_0 \boldsymbol{\Omega}_{S_m} \right]^{-1}, \tag{6.56}$$

as $\{_u = [\{_u^{(1)T} \ \{_u^{(1)H}]^T$ before transforming the frequency-equalized signals to the time-domain as $\mathbf{z}_u^{(\mu)} = \mathcal{G}_K^H \{_u^{(\mu)}$ where symbol-by-symbol detection takes place.

Table 6.3: TWR D-STBC SC-FDE vs. OFDM Complexity

	IFFT	FFT	Integrator	Frequency Shifter	Resampler.
SR-OFDM	4	8	0	8	8
MR-OFDM	4	$N_{\text{TWR-D-STBC}}$	0	$N_{\text{TWR-D-STBC}}$	$N_{\text{TWR-D-STBC}}$
SR-SC-FDE	4	4	8	8	8
MR-SC-FDE	4	4	$N_{\text{TWR-D-STBC}}$	$N_{\text{TWR-D-STBC}}$	$N_{\text{TWR-D-STBC}}$

6.4 Receiver Implementation

In this section we illustrate the receivers's implementation for TWR-D-STBC SC-FDE systems, since the other two systems are subsystems of this one. The received samples at any node and for any signal in the system can be written in general form as

$$v_{XY,k}^{(\mu)} = \int P_{XY,k}^{*}(t)\, v_{Y}^{(\mu)}(t)\, dt. \tag{6.57}$$

Substitute (6.5) into (6.57) yields

$$v_{XY,k}^{(\mu)} = \int_{p=1}^{N_{XY}} \frac{H_{XY,p}^{*}}{1+a_{XY,p}} \left(\int_{kT_s+\tau_{XY,p}}^{(k+1)T_s+\tau_{XY,p}} v_{XY,p}^{(\mu)} \right) \frac{t}{1+a_{XY,p}} dt, \tag{6.58}$$

where $v_{XY,p}^{(\mu)}(t) = v_{Y}^{(\mu)}(t)\, e^{-j2\pi f_c t a_{XY,p}}$. This means that the received samples are generated at each node Y basically by three steps

1. Frequency shift by each Doppler factor: $v_{XY,p}^{(\mu)}(t) = v_{Y}^{(\mu)}(t)\, e^{-j2\pi f_c t a_{XY,p}}$.
2. Resampling by each Doppler factor: $v_{XY,p}^{(\mu)}\left(\frac{t}{1+a_{XY,p}}\right)$, and
3. Integration: $\int_{kT_s+\tau_{XY,p}}^{(k+1)T_s+\tau_{XY,p}} v_{XY,p}^{(\mu)}\left(\frac{t}{1+a_{XY,p}}\right) dt$.

Since multiple branches are used at each node, and resampling is the central theme, this pre-processing technique is called MR. So, the number of SC-branches, where each performs frequency shifting, resampling, and integrations, in the MR receivers at node Y is $N_{WY} + N_{ZY}$ where W and Z are the transmitting nodes.

A similar implementation is done for the Single Resampling (SR) technique, except that one resampling factor is used at each received node. Thus the received samples are approximated as

$$v^{(\mu)}_{\mathrm{SR},XY,k} = \sum_{p=1}^{N_{XY}} \frac{H^{*}_{XY,p}}{1+a_Y} \left[\int_{kT_s+\tau_{XY,p}}^{(k+1)T_s+\tau_{XY,p}} v^{(\mu)}_{\mathrm{SR},Y} \right) \frac{t}{1+a_Y} \Bigg[\, dt, \tag{6.59}$$

where a_Y is the SR factor at node Y, and $v^{(\mu)}_{\mathrm{SR},Y} = v^{(\mu)}_{Y}(t)\, e^{-j2\pi f_c t a_Y}$. In this case, there is only one branch of frequency shifter, resampler and integrator.

In TWR SC-FDE systems two FFT/IFFT pairs are needed in the system, one pair at each source. The number of SC-branches in the pre-processors vary depending on whether MR or SR pre-processors are used. In MR pre-processing a total of $N_{\mathrm{TWR}} = \sum_{m=1}^{2} N_{S_m R} + N_{R S_m}$ SC-branches are needed. On the other hand, in SR pre-processing one SC-branch is needed at each node, a total of 3 branches. For the corresponding OFDM systems, three IFFT blocks are required one at each transmitting node for modulation, and N_{TWR} OFDM-branches (where each branch performs frequency shifting, resampling, and FFT [8]) for MR-OFDM and three OFDM-branches for SR-OFDM. The complexity comparison is shown in Table 6.1.

In D-STBC SC-FDE two FFT/IFFT pairs are deployed at D only. Two pairs are used to facilitate parallel processing, where each signal is processed twice: once for each relay. The number of SC-branches required in the system for MR-SC-FDE is $N_{\text{D-STBC}} = \sum_{j=1}^{2} N_{S R_j} + N_{R_j D}$ and four SC-branches for SR-SC-FDE: one at each relay and two at D, again for parallel processing. For the corresponding OFDM systems, three IFFT blocks are required, one at each transmitting node, $N_{\text{D-STBC}}$ OFDM-branches for MR-OFDM and four OFDM-branches for SR-OFDM. The complexity comparison is shown in Table 6.2.

Finally, in TWR-D-STBC SC-FDE systems four FFT/IFFT pairs are required in the system, two at each destination. The number of SC-branches for MR is $N_{\text{TWR-D-STBC}} = \sum_{m=1}^{2} \sum_{j=1}^{2} N_{S_m R_j} + N_{R_j S_m}$, while the number of SC-branches for SR is eight: two at each node. This is because each node is accessed by two transmitting nodes, and to process each received signal for both transmitting node simultaneously, two SC-branches are used at each node. For the corresponding OFDM system, four IFFT block are required in the system, one at each node of OFDM modulation. The number of OFDM-branches in MR is $N_{\text{TWR-D-STBC}}$, while it is eight for the SR receivers. The complexity comparison is shown in Table 6.3.

6.5 Numerical Results

In this section the performance in terms of average bit error rate (ABER) is shown for the presented systems. The parameters used are: binary phase shift keying (BSPK) over the bandwidth 30 34 KHz. The channel parameters are shown in Figs. 6.1 and 6.2, where each path is labeled by its own Doppler scaling factor. We also assume that the reciprocal channel parameters remain the same except for the Doppler scaling factor where the sign is reversed. The x axis shows the signal-to-noise ratio (SNR) $\frac{P_T}{N_0}$, where P_T is the total available power in the systems, which is divided uniformly to all transmitting nodes.

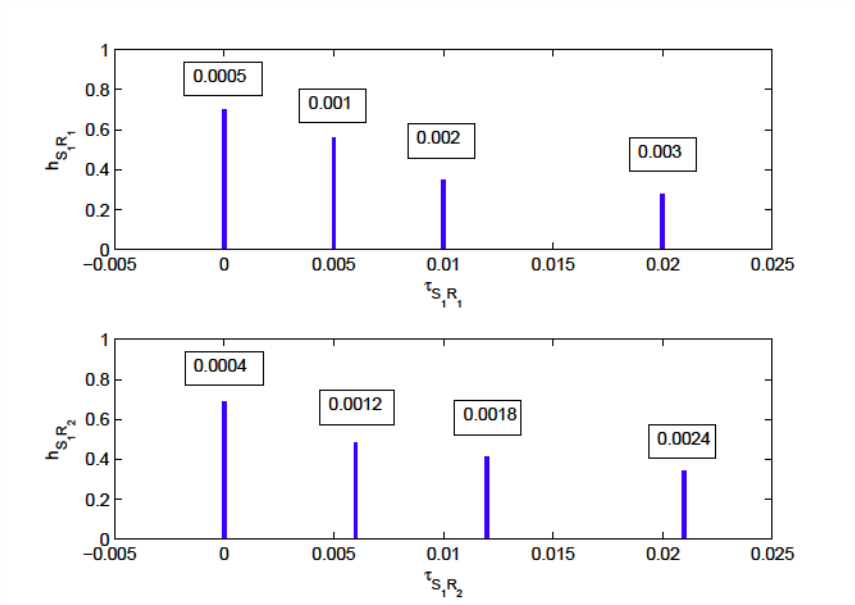

Figure 6.1: The $S_1 \simeq R_1, R_2$ channels' parameters.

In Figs. 6.3 and 6.4 the uncoded ABER vs. SNR is shown for SR/MR-TWR-SC-FDE at S_1 through R_1 and R_2, respectively, for $K = 512$. Also the corresponding curves for OFDM are shown. The SR factor at R_j is taken as the arithmetic average of the Doppler scaling factors of the strongest paths. Specifically, at R_j it is taken as $a_{R_j} = \frac{a_{S_1R_j}(1)+a_{S_2R_j}(1)}{2}$. The justification behind this is that in [53] it was shown that the optimal SR factor is approximately equals the Doppler scaling factor of the dominant path, and if the paths have similar strengths then it is approximated as the the average of the Doppler scaling factors. We have used both results: we have one dominant path from each transmitting node, but the dominant paths of the transmitting nodes are of comparable strengths. At S_m the SR factor is taken as $a_{S_m} = a_{R_jS_m}(1)$. First we observe that MR-SC-FDE outperforms SR-SC-FDE. However this comes at the expense

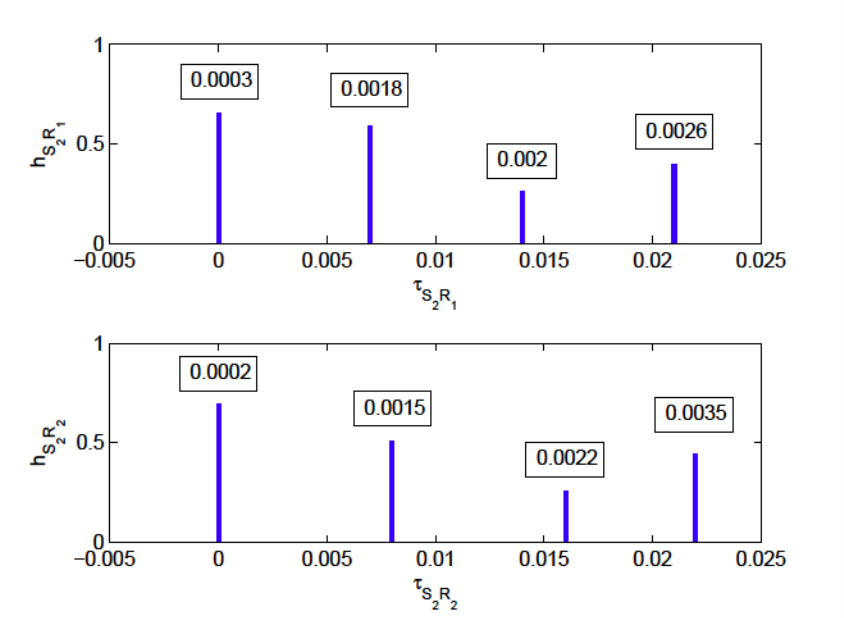

Figure 6.2: The $S_2 \simeq R_1, R_2$ channels' parameters.

of more hardware complexity, where while both uses two FFT/IFFT pairs one pair at each destination, MR receivers require eight SC-branches comparing to three SC-branches for SR receivers. Second, we observe that SC-FDE is superior to OFDM and more resilient to Doppler scaling factors resulting from the relative motion between transceivers. Interestingly enough, this comes at even lower hardware complexity. See Table 6.1. In terms of bandwidth efficiency, two signals are transmitted over two time slots, which results in bandwidth efficiency of one.

In Fig. 6.5 the uncoded ABER vs SNR is shown for MR/SR-D-STBC SC-FDE system for $K = 512$ at S_1. The corresponding curve for OFDM is shown for comparison purposes. In this case, the SR factor at R_j is taken as $a_{R_j} = a_{SR_j}(1)$, while it is taken at $D = S_1$ as $a_D = \frac{a_{R_1D}(1)+a_{R_2D}(1)}{2}$. As it is the case in TWR, MR-SC-FDE is better than SR-SC-FDE in combating time variation resulting from relative motion, and SC-FDE is proven once again from the curves to be more resilient that OFDM over UWA channels. The complexity of both systems are shown in Table 6.2. In terms of bandwidth efficiency, in this system two signals are transmitted over four time slots, resulting in bandwidth efficiency of one half. However, this reduction is compromised for better ABER performance. For example, in both systems TWR and D-STBC we have used the same channel parameters and in both systems we have three transmitting nodes, and thus the total used power is the same in both systems. However, an uncoded ABER of 10^{-4} at S_1 is achieved at SNR of about 28 dB and 25 dB in MR-TWR systems through R_1 and R_2, respectively, while it is achieve at SNR of about 17.5 dB in MR-D-STBC

systems.

In Fig. 6.6 the uncoded ABER vs. SNR is shown for SR/MR-TWR-D-STBC SC-FDE system for $K = 512$ at S_1. For SR factor at R_j is taken as $a_{R_j} = \frac{a_{S_1R_j}(1)+a_{S_2R_j}(1)}{2}$ while at S_m it is taken as $a_{S_m} = \frac{a_{R_1S_m}(1)+a_{R_2S_m}(1)}{2}$. The same conclusions can be drawn from these curves, and the complexity is shown in Table 6.3. However, as we can see, SR receivers' performance deteriorates severely in these systems. This is due to the fact that the interference at the relays is more serious, and is propagated effectively to the destination and hence contributes to the performance loss. In this case the bandwidth efficiency is one, while there is some diversity gain. In particular, an uncoded ABER of 10^{-4} is achieved at SNR of about 22 dB for MR receivers. This means that TWR-D-STBC has better performance at the same bandwidth efficiency as TWR systems, while inferior performance of about 5.5 dB compared to D-STBC with double the bandwidth efficiency. Taking into account the bandwidth efficiency and diversity gain together, TWR-D-STBC systems are good options.

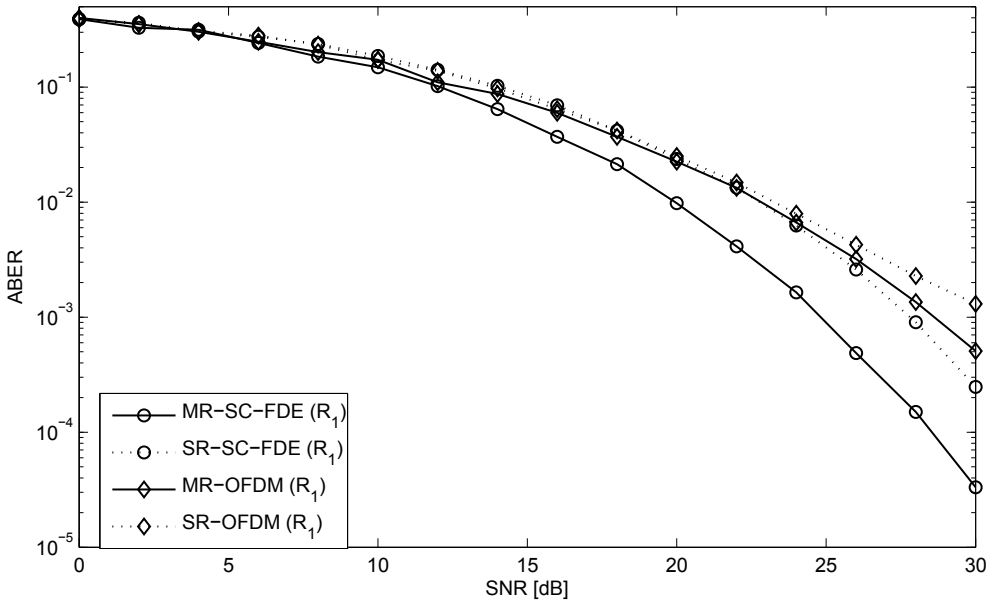

Figure 6.3: ABER of TWR SC-FDE at S_1 through R_1 for $K = 512$.

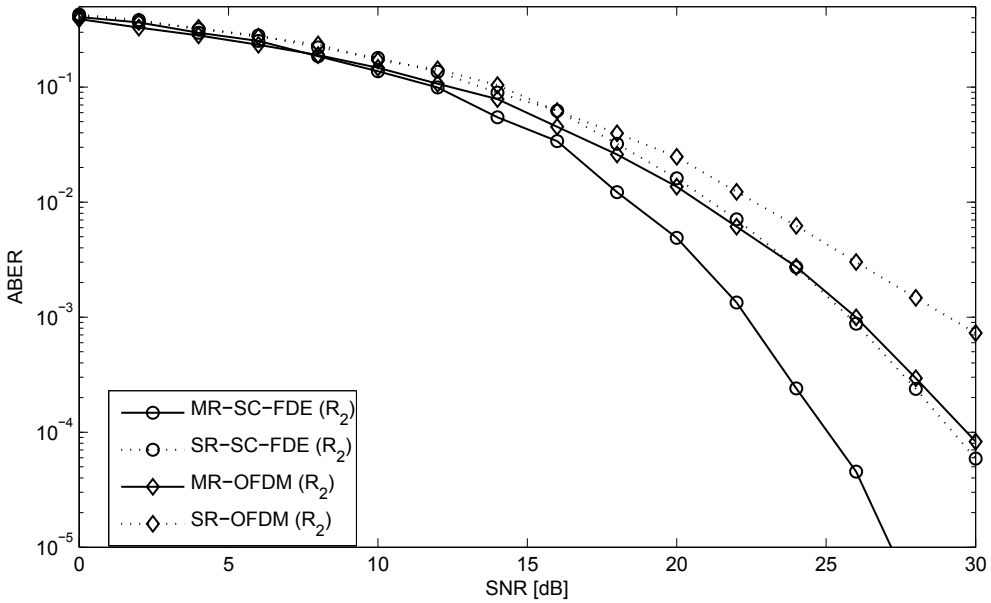

Figure 6.4: ABER of TWR SC-FDE at S_1 through R_2 for $K = 512$.

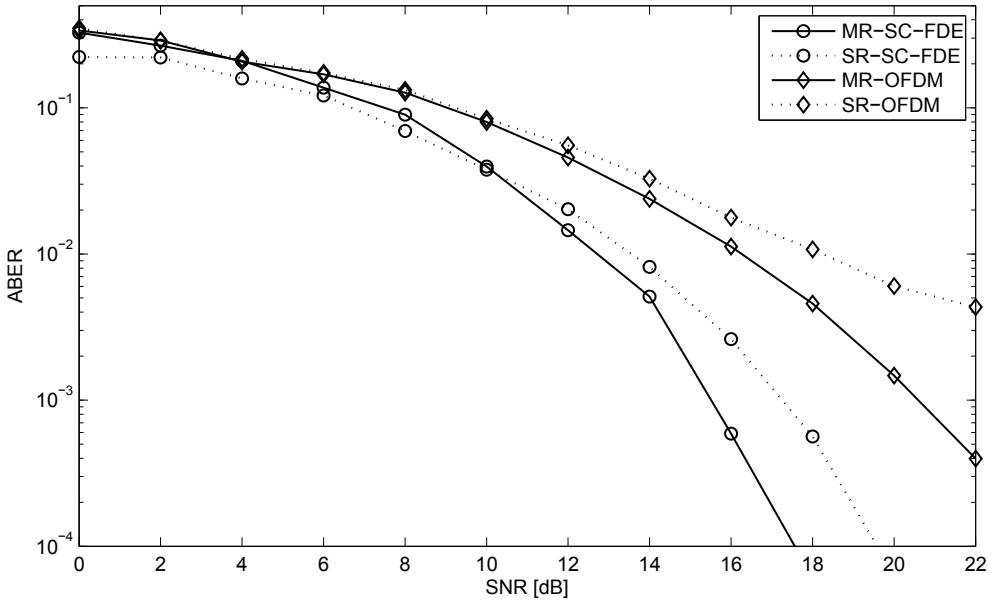

Figure 6.5: ABER of D-STBC SC-FDE for $K = 512$.

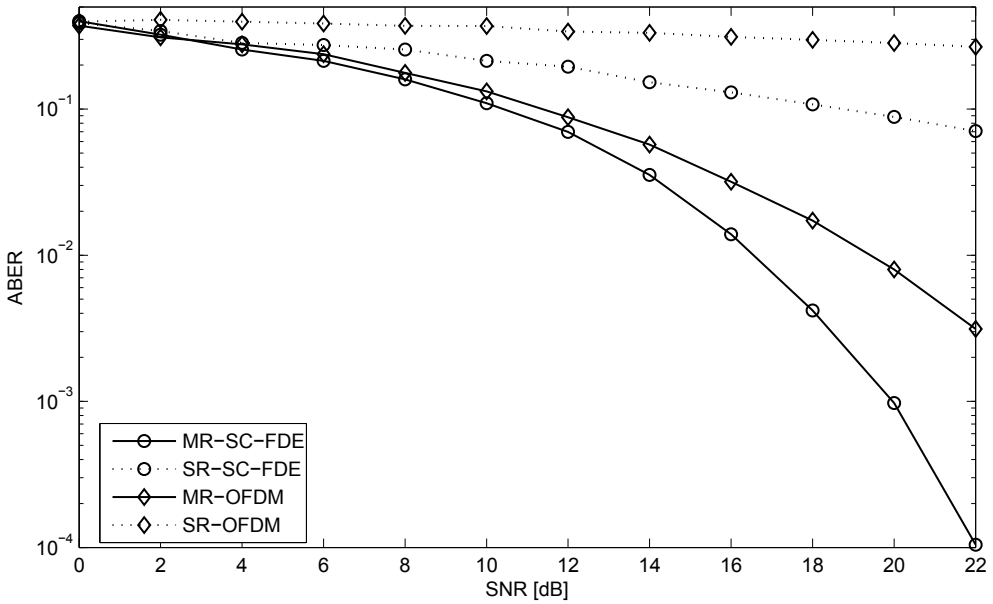

Figure 6.6: ABER of D-STBC SC-FDE for $K = 512$.

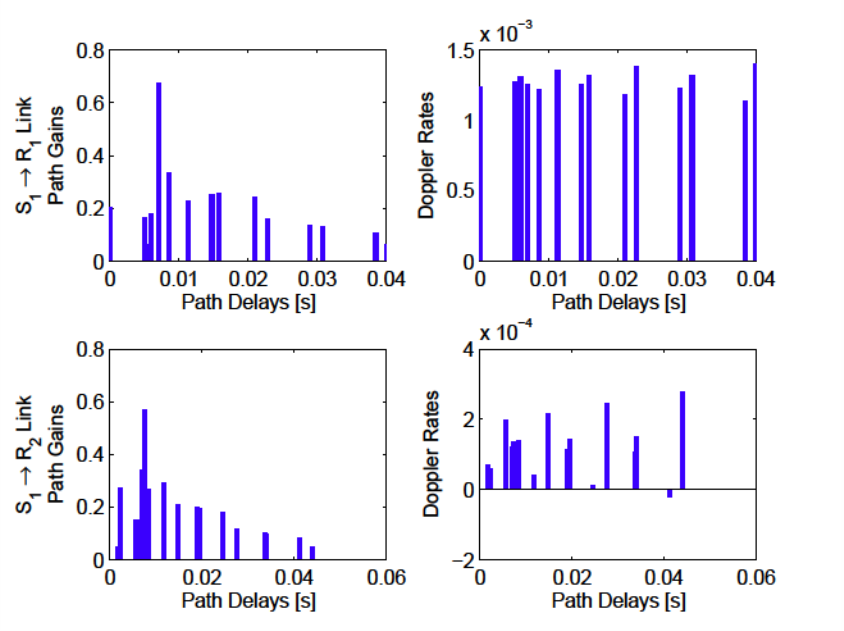

Figure 6.7: Bellhop-generated channels between $S_1 \simeq R_1, R_2$.

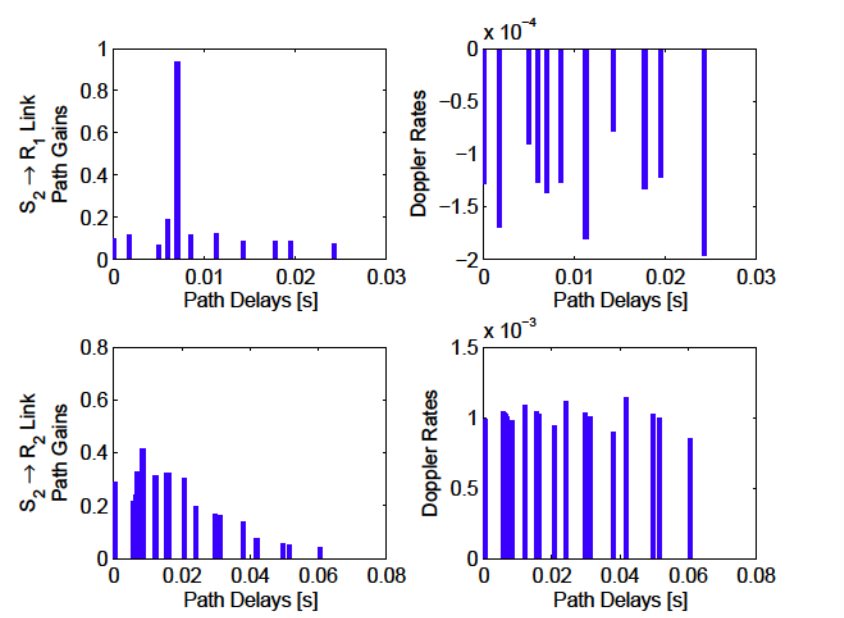

Figure 6.8: Bellhop-generated channels between $S_2 \simeq R_1, R_2$.

In the following we illustrate the performance of the aforementioned systems over UWA channels generated as described in Section 2.1.2 for $K = 256$. The depth of the nodes are given as following: S_1 and S_2 at 35m, R_1 at 30 m, and R_2 at 40m. The horizontal range between S_1 and S_2 is set to six Km, and the distance between S_1 and the relays R_1 and R_2 is set to 2.5Km and 3.5km respectively. The speed vectors are given as: for S_1 it is $[1 \;\; 0.7]^T$, for R_1 relative to

S_1 it is $[\ \ 1\ \ 0.3]^T$, for R_2 relative to S_1 it is $[0.8\ \ 0.5]^T$, and for S_2 it is $[0.8\ \ 0.4]^T$. Since S_1 and S_2 are on the opposite sides, when one of the relays move toward/away from one source, it will move away/toward the other source. Hence the speed vector of the relays relative to S_2 will be the same as relative to S_1 with the sign of ν_r (the first entry) be reversed.

In Figs. 6.7 and 6.7 the channel parameters between different nodes are depicted, where the left hand figures depict the channel magnitudes vs. paths' delays and the right hand figures depict the Doppler scaling factor vs. paths' delays. In Figs. 6.10 and 6.10 the ABER vs. SNR is shown for MR/SR-TWR systems. In Fig. 6.11 the ABER vs. SNR is shown for MR/SR-D-STBC system. Finally, in Fig. 6.13 the ABER vs. SNR is shown for MR/SR-D-STBC system. The corresponding OFDM systems were depicted also for comparison purposes. For the SR factor, it is selected as in the fixed channel case, since as it appears from Figs. 6.7 and 6.7 there is one dominant path in each link. The same observations as previously can be made, where MR technique outperforms its SR counterpart at more hardware complexity cost, while SC-FDE signaling is superior to OFDM. Finally, TWR-D-STBC in MR-SC-FDE systems serve a good compromise between the bandwidth efficiency and performance, where it has better bandwidth efficiency than D-STBC with some performance loss, while it has better performance than TWR (see Fig. 6.13) while both have the same bandwidth efficiency.

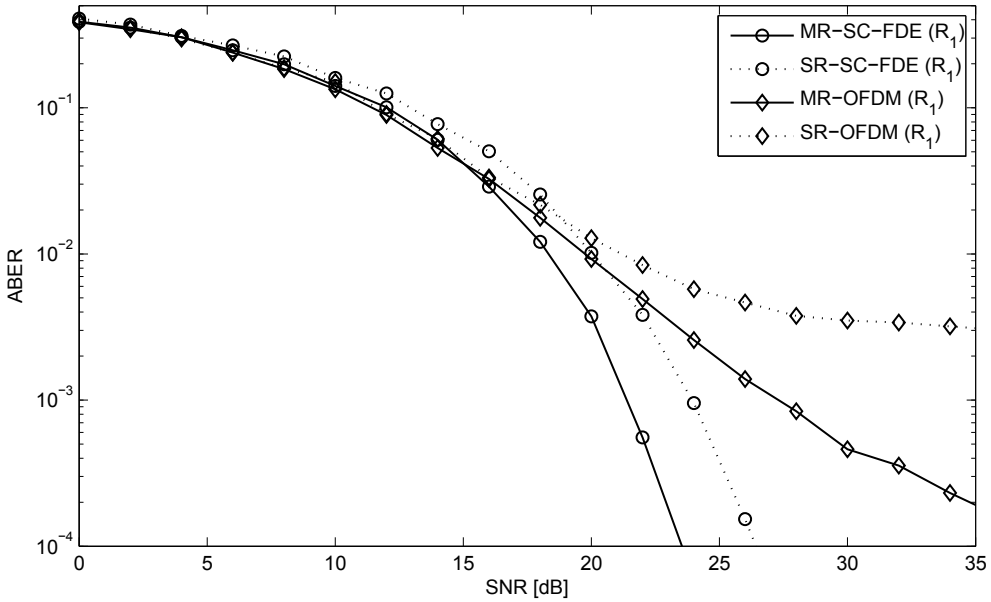

Figure 6.9: ABER of TWR-SC-FDE and OFDM systems at S_1 through R_1 for the channel parameters depicted in Figs. 6.7 and 6.8 for $K = 256$.

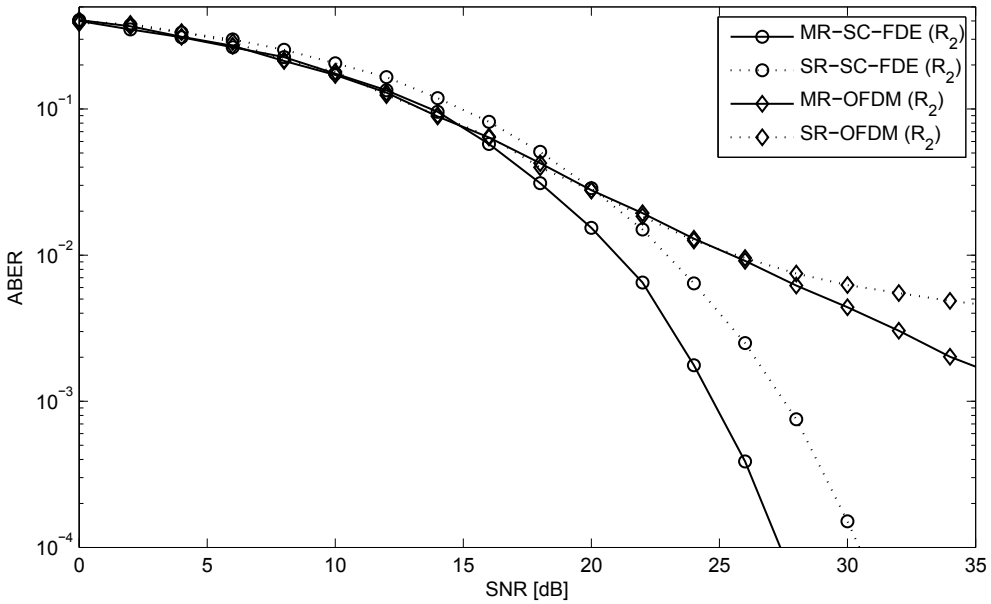

Figure 6.10: ABER of TWR-SC-FDE and OFDM systems at S_1 through R_2 for the channel parameters depicted in Figs. 6.7 and 6.8 for $K = 256$.

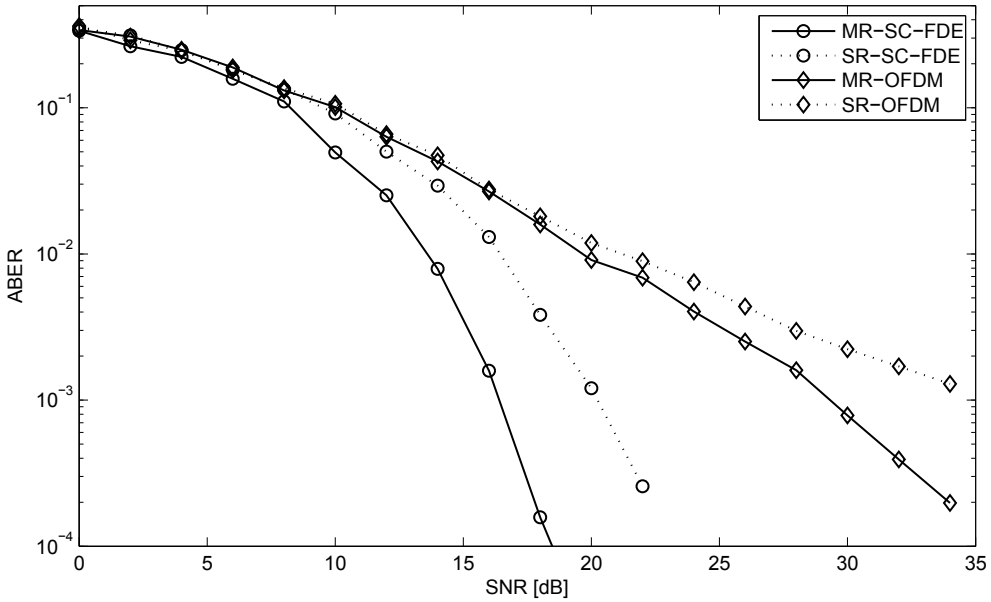

Figure 6.11: ABER of D-STBC-SC-FDE and OFDM systems at S_1 for the channel parameters depicted in Figs. 6.7 and 6.8 for $K = 256$.

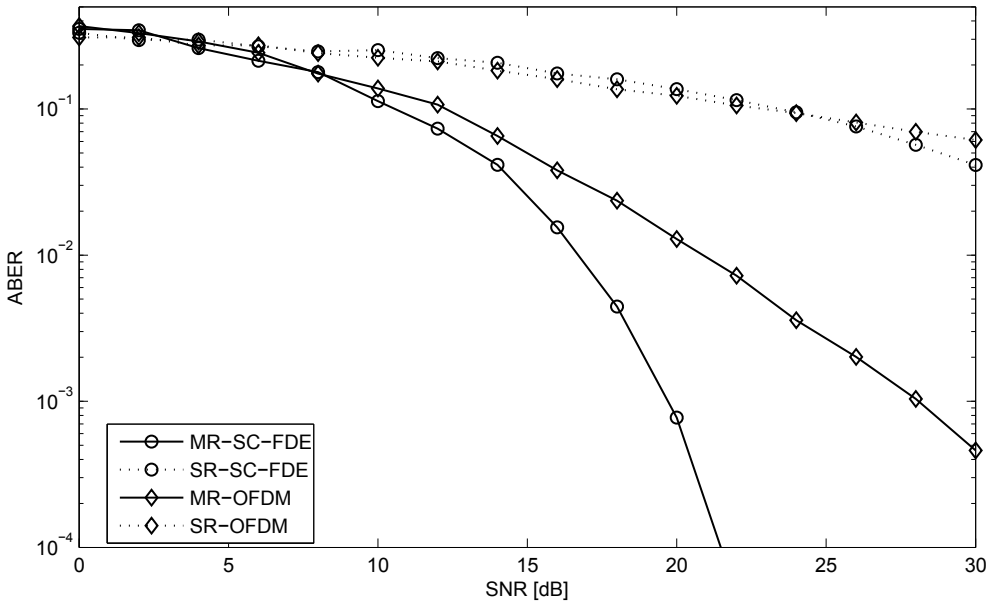

Figure 6.12: ABER of TWR-D-STBC-SC-FDE and OFDM systems at S_1 for the channel parameters depicted in Figs. 6.7 and 6.8 for $K = 256$.

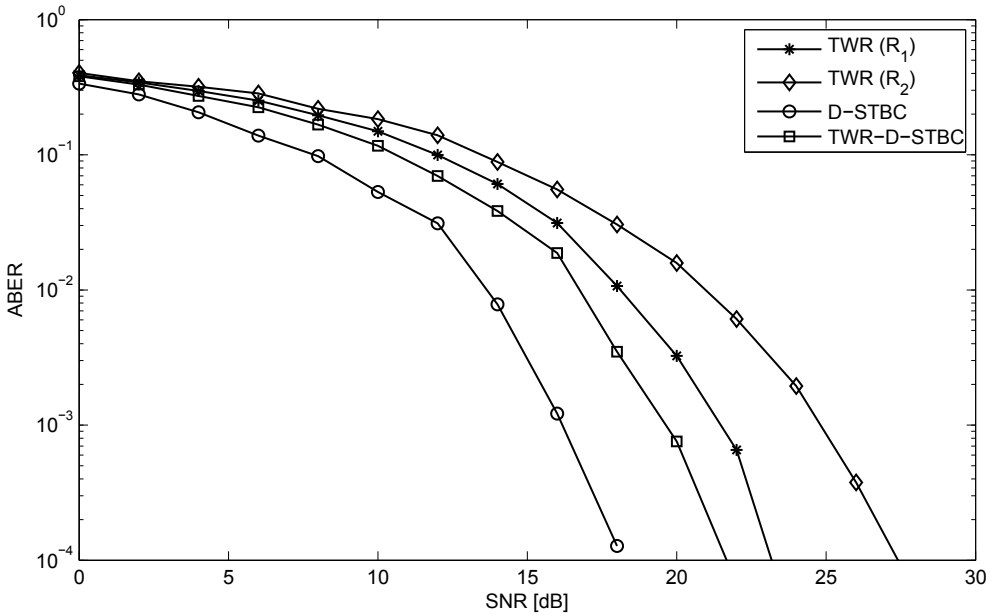

Figure 6.13: ABER comparison at S_1 between all scenarios considered for SC-FDE, namely: TWR, D-STBC, and TWR-D-STBC when MR is used for the channel parameters depicted in Figs. 6.7 and 6.8 for $K = 256$.

6.6 Conclusions

In this chapter we made a similar propositions and performance study for SC-FDE systems as those done for relay-assisted OFDM systems. In particular, we prose the use of TWR, D-STBC or a combination of both schemes when SC signaling is used at the transmitted and FDE is used at the receiver. Again, SR or MR pre-processing was used at each node to handle the effect of time variation. The effect of ISI is handled by using MMSE in the frequency domain at the destinations. A comprehensive comparison study was given for both SC-FDE and acOFDM systems for all schemes. The numerical results for uncoded ABER over artificial and Bellhop generated UWA channels, revealed similar conclusions to those of OFDM systems, where MR consistently outperformed SR, and, under total power constraint and uniform power distribution among the transmitting node, TWR-D-STBC outperformed TWR at the same bandwidth efficiency, while is outperformed by D-STBC with better bandwidth efficiency. Also, it was revealed that, SC-FDE is more Doppler-resilient than OFDM systems, which makes it a strong candidate for transmission over UWA channels.

Chapter 7

Conclusions and Future Work

7.1 Concluding Remarks

In this thesis we first studied P2P SC-FDE systems over path-specific Doppler UWA channels, and derived the corresponding ML receiver. It was shown that a pre-processing stage called MR pre-processing is necessary to minimize the effect of time variation in the time domain. This pre-processor consists of multiple branches where each branch corresponds to a path, and performs frequency shifting and resampling by its Doppler scaling factor, followed by an integration. The output of this pre-processor is still time varying, but it is minimized in a manner such that the power of the ICI coefficients in the frequency domain will be concentrated around the main diagonal. Beside this residual time variation at the output of the MR pre-processor, the samples will be contaminated by ISI, and thus a further stage of equalization is required. Ideally, this equalizer would be the MLSD, which finds the most probably sequence. To avoid the complexity associated with this optimum equalizer, we proposed the use of an MMSE equalizer in the frequency domain, where the samples are first transformed to the frequency domain by means of K-point FFT operation, and after being jointly equalized, they were transformed back to the time domain by means of K-point IFFT operation. This sequence of operations which substituted the MLSD, namely: FFT operation, MMSE FDE and IFFT operation enabled us to simplified the detection process to become symbol-by-symbol instead of joint detection. Also, a suboptimal pre-processor is proposed to further reduce the complexity of the receiver.

Then we considered MAC-SC-FDE systems over user-specific Doppler UWA channels in an attempt to increase the bandwidth efficiency of the system given the scarcity of bandwidth available in UWA channels, where multiple single-antenna users communicate with a multiple-

antenna receiver over the same bandwidth bandwidth at the same time. Similar derivations were done for this system, and showed that each antenna element must have a MR pre-processor, where each pre-processor consists of multiple branches and each branch corresponds to a user, where frequency shifting and resampling is done by the Doppler scaling factor of that user followed by integration. The output of the different pre-processors are then combined in the time domain before being transformed to the frequency domain, where joint MMSE equalization is done. Finally, the equalized symbols of each user is transformed back to the time domain where the symbols of each user were detected separately. A comprehensive study of the the performance and complexity of SC-FDE and OFDM systems were given.

Next we proposed the use of relay-assisted systems for both OFDM and SC-FDE systems in a way to achieve better bandwidth efficiency and/or reliability using the increased DoF offered by the existence of one or more relays. In particular, we considered TWR, as opposed to mere MAC, as a way to enhance the bandwidth efficiency, while D-STBC was considered, as opposed to collocated antennas, as away to enhance the reliability. Also, a combination of both was considered to enhance both the bandwidth efficiency and reliability at the same time. A comprehensive study of the ABER, complexity and bandwidth efficiency of all systems were studied, where it was shown that MR receivers always have better performance than SR counterparts at higher complexity cost, MR-SC-FDE outperforms MR-OFDM with less complexity in uncoded systems, and TWR-D-STBC offers a good balance between the bandwidth efficiency and performance. All the above makes SC-FDE a viable option in UWA communication and an alternative to OFDM.

7.2 Future Work

Inspired by what has been accomplished in this thesis, we believe there are still many open related problems that should be tackled. We list below some of these problems.

1. It has been demonstrated throughout the thesis that MR resampling outperforms its SR counterpart. The performance of both schemes has been assessed through simulations. Although we have used software that mimics real-life situations and we derived the optimal detector mathematically for both schemes, it would be interesting to analytically find the reason for the superiority of MR resampling. It is intuitive that MR should perform better because it is adapted to the various Doppler scalars that the signal undergoes,

whereas SR uses one approximated factor. Nonetheless, it would still be useful to derive the ABER performance analytically.

2. In this thesis, it is assumed that receive CSI is only available. It is interesting to consider the case when transmit CSI is available, that is when the transmitter has access to the CSI prior to transmission. In this case, resampling can be done at the transmitter. This is particularly significant in user-specific Doppler models, because resampling at the transmitter will equalize the Doppler scaling effect of the channel, rendering the received signal ICI-free at the receiver side, even if two or more nodes access the receiver simultaneously, as in multi-user MIMO, TWR and D-STBC systems. Nonetheless, transmit resampling with other Doppler scaling models is interesting to investigate, where a combination of transmit resampling and receive resampling can be used to further enhance the performance.

3. We propose the use of the available spectrum by many nodes at the same time to enhance the bandwidth efficiency, while fixing the data rate. Another way of enhancing the bandwidth efficiency is by using what so-called bit loading or adaptive modulation. Using OFDM signaling is advantageous in this respect, where the total data rate can be maximized by assigning different modulation schemes for different subchannels depending on their quality. Also, power loading can be used to control the effect of ICI.

4. Addressing system imperfections is of interest, because real systems have to estimate the channels in efficient and reliable ways. Sparse channel estimation for cascaded channels in an interesting compliment to our work, to see the effect of channel estimation error on the system performance.

REFERENCES

[1] M. Stojanovic, *Wiley Encyclopedia of Telecommunications*. A John Wiley & Sons Publication, 2003, vol. 1, ch. Acoustic (Underwater) Communications.

[2] N. Soreide, C. Woody, and S. Holt, ``Overview of ocean based buoys and drifters: present applications and future needs," in *OCEANS, 2001. MTS/IEEE Conference and Exhibition*, vol. 4, 2001, pp. 2470--2472 vol.4.

[3] A. Quazi and W. Konrad, ``Underwater acoustic communications," *Communications Magazine, IEEE*, vol. 20, no. 2, pp. 24--30, March 1982.

[4] M. Stojanovic, ``Underwater acoustic communications: Design considerations on the physical layer," in *Wireless on Demand Network Systems and Services, 2008. WONS 2008. Fifth Annual Conference on*, Jan 2008, pp. 1--10.

[5] I. F. Akyildiz, D. Pompili, and T. Melodia, ``Underwater acoustic sensor networks: research challenges," *Ad Hoc Networks*, vol. 3, no. 3, pp. 257 -- 279, 2005.

[6] B. Sharif, J. Neasham, O. Hinton, and A. Adams, ``A computationally efficient Doppler compensation system for underwater acoustic communications," *IEEE J. Oceanic Eng.*, vol. 25, no. 1, pp. 52--61, Jan. 2000.

[7] B. Li, S. Zhou, M. Stojanovic, L. Freitag, and P. Willett, ``Multicarrier communication over underwater acoustic channels with nonuniform Doppler shifts," *IEEE J. Oceanic Eng.*, vol. 33, no. 2, pp. 198--209, Apr. 2008.

[8] K. Tu, T. M. Duman, M. Stojanovic, and J. G. Proakis, ``Multiple-resampling receiver design for OFDM over Doppler-distorted underwater acoustic channels," *IEEE J. Oceanic Eng.*, vol. 38, no. 2, pp. 333--346, Apr. 2013.

[9] M. Stojanovic and J. Preisig, ``Underwater acoustic communication channels: Propagation models and statistical characterization," *IEEE Commun. Mag.*, vol. 47, no. 1, pp. 84--89, Jan. 2009.

[10] M. Stojanovic, ``On the relationship between capacity and distance in an underwater acoustic channel," in *ACM SIGMOBILE Mobile Comp. Commun. Rev*, vol. 11, no. 4, Oct.. 2007, pp. 34--43.

[11] J. Preisig, ``Acoustic propagation considerations for underwater acoustic communications network development," in *ACM SIGMOBILE Mobile Comp. Commun. Rev*, vol. 11, no. 4, Oct.. 2007, pp. 2--10.

[12] A. Singer, J. Nelson, and S. Kozat, ``Signal processing for underwater acoustic communications," *IEEE Commun. Mag.*, vol. 47, no. 1, pp. 90--96, Jan. 2009.

[13] ``U.S. National Oceanic and Atmospheric Administration," http://www.noaa.gov, [Online; accessed 2014].

[14] D. Kilfoyle and A. Baggeroer, ``The state of the art in underwater acoustic telemetry," *IEEE J. Oceanic Eng.*, vol. 25, no. 1, pp. 4--27, Jan. 2000.

[15] T. Eggen, A. Baggeroer, and J. Preisig, ``Communication over Doppler spread channels. Part I: Channel and receiver presentation," *IEEE J. Oceanic Eng.*, vol. 25, no. 1, pp. 62--71, Jan. 2000.

[16] R. Headrick and L. Freitag, ``Growth of underwater communication technology in the U.S. Navy," *IEEE Commun. Mag.*, vol. 47, no. 1, pp. 80--82, Jan. 2009.

[17] M. Stojanovic, ``Recent advances in high-speed underwater acoustic communications," *IEEE J. Oceanic Eng.*, vol. 21, no. 2, pp. 125--136, Apr. 1996.

[18] S. Climent, A. Sanchez, J. V. Capella, N. Meratnia, and J. J. Serrano1, ``Underwater acoustic wireless sensor networks: Advances and future trends in physical, mac and routing layers," *Sensors*, vol. 14.

[19] J. Catipovic, ``Performance limitations in underwater acoustic telemetry," *IEEE J. Oceanic Eng.*, vol. 15, no. 3, pp. 205--216, Jul. 1990.

[20] R. R.Coates and M. Tseng, ``Underwater acoustic communications: A second bibliography and review,'' in *Proc. Inst. Acoust*, Dec 1993.

[21] J. Catipovic, M. Deffenbaugh, L. Freitag, and D. Frye, ``An acoustic telemetry system for deep ocean mooring data acquisition and control,'' in *OCEANS '89. Proceedings*, vol. 3, Sept 1989, pp. 887--892.

[22] J. M. Stojanovic and J.Proakis, ``Phase coherent digital communications for underwater acoustic channels,'' *IEEE J. Oceanic Eng.*, vol. 19, no. 1, pp. 100--111, Jan. 1994.

[23] S. Roy, T. Duman, V. McDonald, and J. Proakis, ``High-rate communication for underwater acoustic channels using multiple transmitters and space-time coding: Receiver structures and experimental results,'' *IEEE J. Oceanic Eng.*, vol. 23, no. 3, pp. 663--688, Jul. 2007.

[24] D. Kilfoyle, J. Preisig, and A. Baggeroer, ``Spatial modulation experiments in the underwater acoustic channel,'' *IEEE J. Oceanic Eng.*, vol. 30, no. 2, pp. 406--415, 2005.

[25] M. Vajapeyam, U. Mitra, J. Preisig, and M. Stojanovic, ``Distributed space-time cooperative schemes for underwater acoustic communications,'' in *OCEANS 2006 - Asia Pacific*, May 2006, pp. 1--8.

[26] H. Song, P. Roux, W. Hodgkiss, W. Kuperman, T. Akal, and M. Stevenson, ``Multiple-input-multiple-output coherent time reversal communications in a shallow-water acoustic channel,'' *IEEE J. Select. Areas Commun.*, vol. 31, no. 1, pp. 170--178, 2006.

[27] H. Song, W. Hodgkiss, W. Kuperman, T. Akal, and M. Stevenson, ``Multiuser communications using passive time reversal,'' *IEEE J. Select. Areas Commun.*, vol. 32, no. 4, pp. 915--926, 2007.

[28] M. Vajapeyam, S. Vedantam, U. Mitra, J. Preisig, and M. Stojanovic, ``Distributed space-time cooperative schemes for underwater acoustic communications,'' *IEEE J. Oceanic Eng.*, vol. 33, no. 4, pp. 489 --501, Oct. 2008.

[29] J. Bingham, ``Multicarrier modulation for data transmission: an idea whose time has come,'' *IEEE Commun. Mag.*, vol. 28, no. 5, pp. 5--14, May 1990.

[30] B. R. S. A. R. S. Bahai and M. Ergen, *Multi-Carrier Digital Communications: Theory and Applications of OFDM*. New York: New York: Kluwer Academic/Plenum Publishers, 1999.

[31] T. Wang, J. Proakis, and J. Zeidler, ``Techniques for suppression of intercarrier interference in OFDM systems," in *Proc. IEEE WCNC*, March 2005, pp. 39--44.

[32] L. Rugini, P. Banelli, and G. Leus, ``Simple equalization of time-varying channels for OFDM," *IEEE Commun. Lett.*, vol. 9, no. 7, pp. 619--621, Jul. 2005.

[33] X. Huang and H.-C. Wu, ``Robust and efficient intercarrier interference mitigation for OFDM systems in time-varying fading channels," *IEEE Trans. Veh. Commun.*, vol. 56, no. 5, pp. 2517--2528, Sept. 2007.

[34] W. Chen, X. Lei, Y. Xiao, and S. Li, ``Iterative ICI cancellation and signal detection of OFDM system on fast time-varying channel with nonintegral-delay," in *Proc. ICCCAS*, July 2009, pp. 32--37.

[35] K. Tu, D. Fertonani, T. Duman, M. Stojanovic, J. Proakis, and P. Hursky, ``Mitigation of intercarrier interference for OFDM over time-varying underwater acoustic channels," *IEEE J. Oceanic Eng.*, vol. 37, no. 2, pp. 156--171, Apr. 2011.

[36] B. Li, J. Huang, S. Zhou, K. Ball, M. Stojanovic, L. Freitag, and P. Willett, ``Further results on high-rate MIMO-OFDM underwater acoustic communications," in *OCEANS 2008*, Sept 2008, pp. 1--6.

[37] P. Carrascosa and M. Stojanovic, ``Adaptive MIMO detection of OFDM signals in an underwater acoustic channel," in *OCEANS 2008*, Sept 2008, pp. 1--7.

[38] B. Li, J. Huang, S. Zhou, K. Ball, M. Stojanovic, L. Freitag, and P. Willett, ``MIMO-OFDM for high-rate underwater acoustic communications," *IEEE J. Oceanic Eng.*, vol. 34, no. 4, pp. 634--644, Oct. 2009.

[39] M. Stojanovic, ``MIMO-OFDM over underwater acoustic channels," in *Signals, Systems and Computers, 2009 Conference Record of the Forty-Third Asilomar Conference on*, Nov 2009, pp. 605--609.

[40] ------, ``Low complexity OFDM detector for underwater acoustic channels," in *OCEANS 2006*, Sept 2006, pp. 1--6.

[41] S. Yerramalli, M. Stojanovic, and U. Mitra, ``Partial FFT demodulation: A detection method for highly Doppler distorted OFDM systems," *IEEE Trans. Signal Processing*, vol. 60, no. 11, pp. 5906--5918, Nov. 2012.

[42] A. Radosevic, R. Ahmed, T. Duman, J. Proakis, and M. Stojanovic, ``Adaptive OFDM modulation for underwater acoustic communications: Design considerations and experimental results," vol. 39, no. 2, pp. 357--370, Apr. 2014.

[43] F. Pancaldi, G. Vitetta, R. Kalbasi, N. Al-Dhahir, M. Uysal, and H. Mheidat, ``Single-carrier frequency domain equalization," *IEEE Commun. Mag.*, vol. 25, no. 5, pp. 37--56, Sept. 2008.

[44] D. Falconer, S. Ariyavisitakul, A. Benyamin-Seeyar, and B. Eidson, ``Frequency domain equalization for single-carrier broadband wireless systems," *IEEE Commun. Mag.*, vol. 40, no. 4, pp. 58--66, Apr. 2002.

[45] T. Walzman and M. Schwartz, ``Automatic equalization using the discrete frequency domain," *IEEE Trans. Inform. Theory*, vol. 19, no. 1, pp. 59--68, 1973.

[46] J. Zhang, Y. Zheng, and C. Xiao, ``Frequency-domain equalization for single carrier MIMO underwater acoustic communications," in *OCEANS 2008*, 2008, pp. 1--6.

[47] ------, ``Frequency-domain turbo equalization for MIMO underwater acoustic communications," in *OCEANS 2009 - EUROPE*, May 2009, pp. 1--5.

[48] J. Zhang and Y. Zheng, ``Frequency-domain turbo equalization with soft successive interference cancellation for single carrier mimo underwater acoustic communications," *IEEE Trans. Wireless Commun.*, vol. 10, no. 9, pp. 2872 --2882, Sept 2011.

[49] L. Wang, J. Tao, C. Xiao, and T. C. Yang, ``Frequency-domain turbo detection for LDPC-coded single-carrier MIMO underwater acoustic communications," in *OCEANS 2010*, Sept 2010, pp. 1--5.

[50] M. Xia, D. Rouseff, J. Ritcey, X. Zou, C. Polprasert, and W. Xu, ``Underwater acoustic communication in a highly refractive environment using SC-FDE," *IEEE J. Oceanic Eng.*, vol. 39, no. 3, pp. 491--499, Jul. 2014.

[51] R. Iltis, ``Iterative joint decoding and sparse channel estimation for single-carrier modulation," in *Proc. IEEE ICASSP*, Mar. 2008, pp. 2689--2692.

[52] S. Yerramalli and U. Mitra, ``On optimal resampling for OFDM signaling in doubly-selective underwater acoustic channels," in *OCEANS 2008*, Sept 2008, pp. 1--6.

[53] ------, ``Optimal resampling of OFDM signals for multiscale, multilag underwater acoustic channels," *IEEE J. Oceanic Eng.*, vol. 36, no. 1, pp. 126--138, Jan 2011.

[54] J. Huang, S. Zhou, J. Huang, C. Berger, and P. Willett, ``Progressive inter-carrier interference equalization for OFDM transmission over time-varying underwater acoustic channels," *IEEE Journal of Selected Topics in Signal Processing*, vol. 5, no. 8, pp. 1524--1536, Dec. 2011.

[55] Z. Wang, S. Zhou, J. Catipovic, and J. Huang, ``Factor-graph-based joint IBI/ICI mitigation for OFDM in underwater acoustic multipath channels with long-separated clusters," vol. 37, no. 4, pp. 680--694, Oct. 2012.

[56] S. Mason, C. Berger, S. Zhou, and P. Willett, ``Detection, synchronization, and doppler scale estimation with multicarrier waveforms in underwater acoustic communication," vol. 26, no. 9, pp. 1638--1649, Jan. 2008.

[57] Z. Wang, S. Zhou, J. Preisig, K. Pattipati, and P. Willett, ``Clustered adaptation for estimation of time-varying underwater acoustic channels," *IEEE Trans. Signal Processing*, vol. 60, no. 6, pp. 3079 --3091, Jun. 2012.

[58] S. Mason, C. Berger, S. Zhou, K. Ball, L. Freitag, and P. Willett, ``An OFDM design for underwater acoustic channels with Doppler spread," in *Digital Signal Processing Workshop and 5th IEEE Signal Processing Education Workshop, 2009. DSP/SPE 2009. IEEE 13th*, Jan 2009, pp. 138--143.

[59] J. Proakis, *Digital Communications*, 4th ed. McGraw-Hill, 2000.

[60] S. Haykin, *Adaptive Filter Theory*, 4th ed. Upper Saddle River, NJ: Prentice Hall, 2002.

[61] A. V. Openhein, R. W. Schafer, and J. R. Buck, *Discrete-Time Signal Processing*, 2nd ed. Prentince Hall, 1998.

[62] A. Radosevic, J. G. Proakis, , and M. Stojanovic, ``Statistical characterization and capacity of shallow water acoustic channels," in *Proc. IEEE OCEANS Conf.*, May 2009, pp. 30--33.

[63] H. Sari, G. Karam, and I. Jeanclaude, ``Transmission techniques for digital terrestrial tv broadcasting," *IEEE Commun. Mag.*, vol. 33, no. 2, pp. 100 --109, Feb. 1995.

[64] Y. Han, S. H. Ting, C. K. Ho, and W. H. Chin, ``Performance bounds for two-way amplify-and-forward relaying," *IEEE Trans. Wireless Commun.*, vol. 8, no. 1, pp. 432--439, Jan. 2009.

[65] H. Guo, J. Ge, and H. Ding, ``Symbol error probability of two-way amplify-and-forward relaying," *IEEE Commun. Lett.*, vol. 15, no. 1, pp. 22--24, Jan. 2011.

[66] F.-K. Gong, J.-K. Zhang, and J.-H. Ge, ``Asymptotic SEP analysis of two-way relaying networks with distributed alamouti codes," *IEEE Trans. Veh. Commun.*, vol. 61, no. 8, pp. 3777--3783, Oct. 2012.

[67] S. Alamouti, ``A simple transmit diversity technique for wireless communications," *IEEE J. Select. Areas Commun.*, vol. 16, no. 8, pp. 1451--1458, 1998.

[68] V. Tarokh, H. Jafarkhani, and A. Calderbank, ``Space-time block coding for wireless communications: performance results," *IEEE J. Select. Areas Commun.*, vol. 17, no. 3, pp. 451--460, 1999.

[69] H. Eghbali, S. Muhaidat, and N. Al-Dhahir, ``A novel receiver design for single-carrier frequency domain equalization in broadband wireless networks with amplify-and-forward relaying," *IEEE Trans. Wireless Commun.*, vol. 10, no. 3, pp. 721--727, Mar. 2011.